EUROPEAN COMMISSION
DIRECTORATE-GENERAL
Joint Research Centre

EUR 22510 EN

Institute for Energy

Assessment of Dissimilar Weld Integrity: Final Report of the NESC-III Project

NESC
Network for Evaluating Structural Components

Mission of the Institute for Energy

The Institute for Energy provides scientific and technical support for the conception, development, implementation and monitoring of community policies related to energy. Special emphasis is given to the security of energy supply and to sustainable and safe energy production.

European Commission

Directorate-General Joint Research Centre (DG JRC)
http://www.jrc.ec.europa.eu/

Institute for Energy, Petten (the Netherlands)
http://ie.jrc.ec.europa.eu/

Contact details:
N.G. Taylor
Tel. +31 224 565202
E-mail: nigel.taylor@ec.europa.eu

EUR 22510 EN
ISSN 1018-5593
Luxembourg: Office for Official Publications of the European Communities

Printed in Italy

EUROPEAN COMMISSION
DIRECTORATE-GENERAL
Joint Research Centre

EUR 22510 EN

Institute for Energy

Assessment of Dissimilar Weld Integrity: Final Report of the NESC-III Project

Editors
N. Taylor European Commission Joint Research Centre, Institute for Energy, The Netherlands
C. Faidy EDF SEPTEN, Lyon, France
P. Gilles AREVA NP SAS, Paris, France

NESC
Network for Evaluating Structural Components

CONTENTS

EXECUTIVE SUMMARY

Dissimilar metal welds are a common feature of light water reactors in connections between ferritic components and austenitic piping systems. Inspection difficulties, variability of material properties and residual stresses all combine to create problems for structural integrity assessment. NESC-III was organised by the Network for Evaluating Structural Components (NESC) as a complementary activity to the European Commission sponsored ADIMEW project, with the following objectives:

- Quantify the accuracy of structural integrity assessment procedures for defect-containing, dissimilar metal welds in aged PWR Class 1 piping.
- Utilise results of the ADIMEW large-scale test to determine the actual behaviour of a defect in a DMW of industrial scale.
- Address critical issues including: inspection performance, laboratory-scale fracture testing on welds and potential benefits of advanced fracture modelling.
- Use the results to promote best practice and the harmonisation of international standards.

Five Task Groups (TGs) were set up:

- TG1 (Non-Destructive Inspection) focussed on the performance of inspection techniques, based on a blind round robin trial (RRT) using a specially manufactured mock-up.
- TG2 (Materials Characterisation) re-analysed the ADIMEW data and performed some supplementary tests.
- TG3 (Stress and Fracture Analysis) organised a series of pre- and post-test analyses of the ADIMEW test.
- TG5 (Evaluation) evaluated the project data and produced the final report.
- TG6 (Residual Stresses) organised a series of round robin exercises to assess the reliability of finite element calculations of residual stress distributions.

NESC-III relied on in-kind i.e. un-funded, contributions. Altogether twenty-one organisations participated in the project, which ran from 2000 to 2006. The main conclusions are as follows:

- The ADIMEW test is confirmed as an important benchmark for verifying flaw assessment methods for dissimilar metal welds. It demonstrated that a real size structure with a circumferential defect in the buttering close to the fusion line can sustain bending displacements and loads above the limit level without cleavage or unstable tearing. The crack growth mechanism corresponded to that found in the earlier BIMET tests i.e. initial deviation towards the fusion line followed by extensive stable ductile tearing in the buttering along the fusion line. Stability assessment for such tearing is considered critical to any integrity or leak-before-break assessment. The post-test analyses have shown that in the maximum applied moment in the ADIMEW was probably close to the instability limit, enhancing its usefulness for verification of calculation methods.
- Determination of a representative J-R curve for the defect location and expected crack propagation path along the buttering interface emerged as a key challenge. Despite the extensive labora-

tory testing programme conducted in ADIMEW and its subsequent analysis, there remains uncertainty over the crack initiation toughness. The test data available provide some evidence that J- or CTOD-R-curve for cracks propagating very close to the fusion line is lower than that of the bulk buttering material, as would be suggested theoretically by high level of stress concentration (constraint) due to the yield-strength mismatch at this location. Recommendations for future fracture testing include: a preference for the C(T) rather than the SE(B) geometry; use of specimens with pre-cracks either on the fusion line or well (>2 mm) into the buttering, as results from "intermediate" crack positions can prove difficult to interpret; pre-cracking should be done with side grooves; specimen dimensions should be as large as possible (if necessary used weld build-up) to maximise ductile growth. With respect to the latter, CTOD rather than load line displacement measurements allow for a larger range of valid crack growth measurement.

- In characterising the residual stresses present in the ADIMEW weld, the different measurement techniques proved complementary. The neutron diffraction data provided a 3-D mapping of the strains and stresses, although the thickness of the weld and its crystallographic texture meant that only the hoop direction data is fully reliable. The surface hole drilling measurements proved susceptible to machining effects and need to be treated with caution if they are used to infer through-section profiles. In this respect the cut-compliance method proved useful in explaining apparent discrepancies between the surface and ND data, but it is limited to one directional component. The computational round robins to predict the residual stresses demonstrated that full weld process simulations produced distributions in reasonable agreement with the ND measurements. The simulation of creep effects during the PWHT proved critical, and it is recommended that creep properties should be clearly defined at the beginning of future exercises of this type. Simplified calculations based on thermal mismatch alone were found to underestimate stresses at some locations.

- The application of FAD methods confirmed that basic option 1 (which uses the lowest yield strength properties i.e. of the 316L(N) pipe) is highly conservative. More realistic predictions require incorporation of better estimates of the crack driving force and limit load, for instance from FE analysis, and allowance for mismatch effects. Incorporating the measured weld residual stress profiles further reduced the predicted initiation load (or, equivalently, the critical defect size). However FE weld simulation models show that the axial weld residual stresses are small at 300˚C. Furthermore their effect can be neglected for crack tearing analysis (although their role in driving sub-critical crack growth processes remains important).

- The usefulness of elasto-plastic FE cracked body models for best-estimate approaches with the J-integral or CTOD parameters was demonstrated. The overall mock-up behaviour could be simulated to a good degree of accuracy, although the fact that the calculated crack tip moment values for a given average ram displacement overestimates that measured experimentally by 4 to 8% indicates that the models were slightly too stiff. The narrow load range for initiation of crack extension was predicted,. At initiation the analyses show that the 316L parent pipe is subjected to extensive yielding. The small mixed mode character of the field at the inclined crack appears to have minor influence when assessing the fracture initiation load.

- The implicit assumption of load rather than displacement controlled conditions in the tearing and stability analyses resulted in rather low estimates of the amount of stable crack extension (2.5

mm), an order of magnitude below that observed in the ADIMEW test. Furthermore the uncertainty about the tearing modulus of the J-R curve and the lack of valid experimental data for crack growth for more than a few mm was reflected in the variability of the instability load estimates. The FE cracked-body approach requires combining results from a series of meshes of different crack depths together with a representative J-R curve. For 3-D models this requires considerable effort as well as *a priori* assumptions about the direction of likely growth over the crack front. Simplified 2-D sub-models were shown to provide an efficient alternative.

- Local approach models provided capable of accurately predicting the crack path for up to 5 mm of growth. Further verification of these damage models was limited by difficulties in simulating the tearing process close to the interface, where the hydrostatic stresses are very high. The difficulties encountered in simulating the overall piping system response to a high degree of accuracy, in particular the over-estimation of the ram forces and hence the applied moment response, did not impact the moment-CMOD behaviour, which was well reproduced in the numerical analysis.

- The detection performance achieved in the ISI round robin trial was relative good, with 5 out of the 9 teams detecting all the defects larger than the detection target for the austenitic weld and 6 of the 8 teams for the Inconel weld. There no evidence that the detection performance for artificial defects types such as PISC type A defects was better than that for more realistic defect types. The sizing accuracy for through wall extent and length however showed a significant scatter for both welds.

- In view of the fact that many of the inspection teams used similar detection and sizing techniques yet obtained different results, it is recommended that the entire inspection system, including the equipment, inspection procedure and personnel, should verified by inspection qualification methodologies on appropriate test specimens and defects prior to an on-site inspection to demonstrate that it is capable of meeting the specified inspection objectives.

- The project has shown that careful application of available flaw assessment techniques in combination with the improved awareness of the likely tearing behaviour for circumferential cracks at the buttering interface can provide reliable predictions of crack initiation and stability loads for this type of dissimilar weld. Areas recommended for further investigations include:
  - assessment of the consequences of low tearing resistance resistance in the buttering close to the fusion line for evaluation of leak-before-break behaviour;
  - development and standardisation of robust experimental methods to accurately measure fracture toughness properties in heterogeneous regions of dissimilar metal welds, and verification of their suitability for assessment of component integrity;
  - clarification of the effect of long-term ageing on the fracture and tearing properties for buttering cracks;
  - application of local approach models to better understand the margins for ductile tearing instability under operation conditions involving both applied pressure and displacements.
  - further analysis of the inspection blind trial data to investigate the influence of factors such as the quality and training of the inspectors; the scanner and equipment; and the data processing equipment and software, on performance and on the influence of the different defect types.

ABBREVIATIONS AND SYMBOLS

ACPD	Alternating Current Potential Drop
ADIMEW	Assessment of Aged Piping Dissimilar Metal Weld Integrity (EC FP5 Project)
ASTM	American Society for Testing and Materials
BIMET	Structural Integrity of Bi-Metallic Components (EC FP4 Project)
BMW	Bi-Metallic Weld
BS	British Standard
°C	Degree Celsius
CC	Cut-Compliance technique for residual stress measurement
CGHAZ	Coarse Grained Heat Affected Zone
CMOA	Crack Mouth Opening Angle
CMOD	Crack Mouth Opening Displacement
CRR	Computational Round Robin
C(T)	Compact Tension
CTOD	Crack tip opening displacement
DISWEC	Evaluation of Techniques for Assessing Corrosion Cracking in Dissimilar Metal Welds (EC FP4 Project)
DMW	Dissimilar Metal Weld
EAC	Environmentally Assisted Cracking
EAM	Engineering Assessment Method
EC	European Commission
EDM	Electro-Discharge Machining
EMAT	Electro Magnetic Acoustic Transducer
ENIQ	European Network on Inspection and Qualification
FAD	Failure Assessment Diagram
FE	Finite Element
FP	Framework Programme (of the European Commission)
FPB	Four Point Bending
HAZ	Heat Affected Zone
HFR	High Flux Reactor, Petten, The Netherlands
LCNDF	Large Component Neutron Diffraction Facility
LOF	Lack Of Fusion
LOP	Lack Of Penetration
LWR	Light Water Reactor
ND	Neutron diffraction technique for residual stress measurement
NDE	Non-Destructive Evaluation
NDT	Non-Destructive Testing
NESC	Network for Evaluating Structural Components
NPP	Nuclear Power Plant
OA	Operating Agent
PISC	Programme for the Inspection of Steel Components
PWHT	Post Weld Heat Treatment
PWR	Pressurised Water Reactor
RL	Reference Laboratory
RMS	Root Mean Square
RRT	Round Robin Trial
SCC	Stress Corrosion Cracking
SE(B)	Single Edge Bend
SNR	Signal to Noise Ratio

TC	Thermocouple
TG	Task Group
TRL	transmitting - receiving: longitudinal wave
UT	Ultrasonic Testing
UTS	ultimate tensile strength
a	crack depth
Δa	increment of crack growth
ε	strain
G_{fr}	Tearing parameter in the CEA J_i-G_{fr} model
K_j	crack tip stress intensity or crack driving force
K_{Ic}	fracture toughness
J	J-integral
J_i	J-integral at initiation of crack growth
$J_{0.2}$	J-integral as defined from the 0.2 mm offset blunting line following the French GFR procedure
$J_{0.2BL}$	J-integral as defined from the 0.2 mm offset blunting line following ASTM testing procedure
σ	stress
σ_y	yield strength
σ_f	flow stress
M	moment
$R_{p0.2\%}$	yield strength

1 INTRODUCTION

1.1 DISSIMILAR WELD INTEGRITY ASSESSMENT ISSUES

Various forms of cracking have been observed in dissimilar metal welds between piping components in nuclear power plant. Mixed mode loading, inspection difficulties, variability of material properties, residual stresses and conservatism of current engineering methods all combine to create problems for structural integrity assessment. These factors have also made dissimilar welds a natural area of interest for the NESC network, in particular to study a large-scale benchmark test designed to validate the integrated, multi-disciplinary approach to structural integrity assessment.

Dissimilar welds are a common feature of pressurised water and boiling water reactors in connections between ferritic components and austenitic piping systems. Those in safety critical locations include the connections from the reactor pressure vessel, steam generator and pressuriser of the primary circuit (safe end welds) and vessel penetrations, for instance for the control rod drive mechanism and instrumentation. These welds are typically fabricated following special manufacturing procedures to ensure a good resistance of the joint, using either austenitic steels or nickel-base alloys as consumables. First, high strength austenitic steel is selected for the joint, then the ferritic end is buttered with several layers of a type of austenitic steel close to the selected weld metal. Post weld heat treatment (PWHT) is applied to reduce residual stresses in the heat-affected zone (HAZ) that develops along the interface in the ferritic steel. Potential defects are more difficult to detect and size in these welds as in more classical welds because of the presence of at least three different materials, possible metallurgical embrittlement in the HAZ, or remaining residual stresses. Hydrogen cracking may appear during welding close to the fusion boundary and local high temperatures combined with residual stresses may result in subsequent stress corrosion cracking during service. Thermal ageing may reduce the material toughness close to the ferritic/buttering interface. But the main concern is the large difference of plastic behaviour between austenitic and ferritic steels that causes strain concentration along the interface, therefore creates a source of damage.

Recent operating experience (e.g. V.C. Summer, Ringhals, Biblis and various EDF plants) has shown that these welds can be susceptible to various forms of external cracking. When such cracking is detected, usually during non-destructive examination, the operator has to make an assessment of the situation depending on the extent and severity of the reported damage. Existing engineering methods may be too conservative due to the need to account for uncertainties such as:

ISI: The detection and sizing of cracks in dissimilar metal welds using ultrasound methods are difficult where a greater understanding of current capability is needed.

Materials Properties: Within the weld, there are several regions of material that have substantially different properties. These are a function of the welding procedure and the parent and consumable materials. Industrial welding of larger scale pipe will generally require high heat input and larger bead sizes and these may adversely affect the properties of heat affected zones and interface regions if not optimised and quality controlled. There is currently no generally agreed materials testing standard for dissimilar metal welds and current methods rely on large test specimens that do not always sample the most vulnerable microstructures.

Fracture Mechanics: Dissimilar welds create problems for structural assessment because the stress fields have a significant mixed mode component and there is mismatch between the tensile plasticity properties of the different materials. Both of these affect the constraint acting on a crack and its susceptibility to propagate. Whereas fracture mechanics procedures are now well established for orthogonal stress fields and homogeneous materials, there is a lack of experimental data that current approaches apply in more complex situations.

Weld Residual Stresses: quantitative description of the magnitude and distribution of residual stresses within a dissimilar metal weld of an industrial scale is lacking.

1.2 RECENT REVIEWS OF DMW ISSUES

A review of design practices and procedures used for bi-metallic weldments in LWRs and other reactor types was made in the late 1990s [1] as part of the European Commission's Working Group on Codes and Standards. The study included a review of experimental and service performance of relevant weld types. The potential for common European procedures was assessed as follows:

i) in general bi-metallic weldments are used in similar locations in the different designs of PWR and (in general) use similar materials;

ii) the experience to date suggests that failures are very few and where these occur are influenced by environmental/metallurgical aspects;

iii) a general consensus may be possible on the use of specific austenitic nickel based filler metals, welding procedures and on the consequences of pre and post weld heat treatments for specific material grades and conditions;

iv) inspection of transition joints is difficult particularly for volumetric and ultrasonic inspection and routine in-service procedures are likely to be restricted to surface examination;

v) design code procedures do not at present specifically cover bi-metallic weldments and the designer is left to local practice in deciding its treatment in design in relation to homogeneous welds. It may be possible to prepare simple guidelines for designers using as a basis the common practices in the design and construction companies and taking account of available research and development experience. The procedures would need to cover damage mechanisms associated with primary and secondary stresses and include assessments against progressive deformation and fatigue. These could in fact be formulated on the basis of the present treatment of homogeneous welds;

vi) recognising the importance of experimental data there is a need to initiate collaborative activities in this area in support of the above. This would be particularly useful within Europe with the development of the EPR design.

Details of dissimilar metals weld production and inspection requirements have been discussed in a recent IAEA TEC DOC [2], although integrity assessment is not specifically addressed. State-of-the-art approaches to residual stress simulation and stress corrosion crack growth for the safe-end weld of the V.C. Summer plant are described in [3], as part of the investigations following the leakage incident in 2000. Williams et al [4] have also considered the implications for leak-before-break behaviour. For EDF plant, Devaux et al [5] have considered defect assessment, concluding that a

fully circumferential crack of 8 mm depth, located in the buttering at 200 μm from the interface, will remain stable under a LOCA condition corresponding to the failure of a primary pipe.

The situation with respect to Russian-design WWER plants has been reviewed as part of the NESC-III project [6]. These are light water cooled and moderated PWRs and can be described as an East European variant of the PWR plants. The "WWER family" plants are commonly grouped into three generations: the WWER-440 - V-230 type and V-213 type and the WWER-1000 - V-320 type. The type WWER-440/V-230 was built first and the WWER-1000/V-320 was built last. All WWER plants include dissimilar metal welds located in safety critical areas at locations are similar to those in PWRs. They connect austenitic stainless steel piping and ferritic steel components as well as stainless steel auxiliary pipelines and ferritic steel pipelines. The most important WWER-440 dissimilar metal welds are located between reactor pressure vessel nozzles and main coolant lines and between the pressurizer and the surge lines. In WWER-1000s the most important dissimilar metal welds are located between Emergency Core Cooling Systems piping and ferritic steel nozzles. The principal details of the design and fabrication of WWER and PWR dissimilar metal welds are comparable. The material used for the buttering in WWER plants has a higher Ni-content in comparison to the stainless steel buttering used in PWR plants, but less Ni-content in comparison to the Ni-base alloy buttering. Up to now operating experience and in-service inspections have not evidenced any degradation or flaws. Integrity assessment for WWER DMWs is done in accordance with the estimation of the remaining lifetime of the components important to safety and evaluation of the Leak-Before-Break (LBB) concept. Several tests were performed as part of PHARE and TACIS projects [7,8,9]. In particular, samples from the weld between the safe ends of RPV nozzles and MCL and from the pressurizer nozzle to the surge line from the Greifswald NPP (Germany) were investigated. Assessment of fracture toughness, hardness and microstructure indicated acceptable mechanical properties; these findings support the applicability of LBB arguments. Current activities to assure dissimilar metal welds integrity are directed to the improvement of capability and reliability of non-destructive examination systems, through the implementation of in-service inspection qualification and optimisation.

1.3 THE NESC NETWORK

The Network for Evaluating Structural Components (NESC) was launched in 1992 to promote and manage collaborative international projects that focus on the validation of the entire process of structural integrity assessment. NESC has worked over the last 10 years to:

- create an international network to undertake collaborative projects capable of validating the entire structural integrity process;
- support development of best practices and the harmonisation of standards;
- improve codes and standards for structural integrity assessment and to transfer the technology to industrial applications.

The network [10] brings together some 30 operators, manufacturers, regulators, service companies and R&D organisations in large-scale experimental projects. It is operated by the European Commission's Joint Research Centre (JRC) as part of a family of European networks [11]. The Network Steering Committee is the overall decision-making body in which the key Network partners are represented. It elects a Chairman for a two year-term. The day-to-day coordination of the activities

is done by the Institute for Energy of European Commission's Joint Research Centre, within the framework of the SAFELIFE internal project. Its role as operating agent is to support the Steering Committee and the organisation of the network and its projects. The JRC also contributes its own R&D expertise for experimental and analytical work.

The network projects are generally focussed on large-scale experimental activities capable of being benchmarks. A strong multi-disciplinary element is aimed for, combining various aspects of structural integrity assessment, in particular inspection, materials characterisation, fracture mechanics and instrumentation. Each project has a manager, normally nominated by the organisation performing the large-scale test. He is assisted by an operating agent project responsible.

Four projects (including now NESC-III) have been completed and one is currently running, as indicated in Table 1.1. The set of coordinated experimental and analytical studies making up each project are funded primarily through so-called "in-kind" contributions, whereby participating organisations contribute work and are then entitled to have access to the contributions of others to any given project. Members have also benefited from the shared cost actions (SCA's) of the European Commission's Research Framework Programmes. In many cases these small dedicated research projects have been pilot or seed projects for subsequent larger Network supported actions.

The NESC Steering Committee foresees the continuation of its work as part of an integrated, networked effort in the area of plant life assessment, capable of working at European level to produce and exploit R&D in support of the safe and competitive operation of nuclear power plants, recognising that the majority of reactors have now been operating for longer than 20 years and their continuing safe operation needs to be supported by effective lifetime management tools.

Table 1.1: *NESC Network Projects*

Project	Benchmark Test(s)	Duration
NESC-I spinning cylinder presurised [12]	Spinning cylinder pressurised thermal shock (PTS) test performed by AEA Technology in March 1997 (main test sponsor HSE)	1993-2001
NESC-II Brittle crack initiation, propagation and arrest of shallow cracks in a clad vessel under PTS loading [13]	Two PTS tests on cylinders with shallow cracks performed by MPA Stuttgart in 2000/2001 (main test sponsor BMFT)	1999-2003
NESC-III Integrity of dissimilar metal welds	Large-scale test on a dissimilar weld pipe assembly (performed by EDF, as part of ADIMEW)	2001-2006
NESC-IV [14] Investigation of the transferability of Master Curve technology to shallow flaws in reactor pressure vessel applications	Biaxial bend tests on large cruciform-type test pieces with surface-breaking semi-elliptic defects and uniaxial bend tests on beams with simulated sub-surface flaws (performed by ORNL as part of the HSST programme)	2001-2006
NESC-TF Thermal Fatigue [15]	Database of thermal fatigue data for operating components and mock-ups	2003→ 2006

2 EURATOM RESEARCH ON DMWS

Issues concerning DMWs in nuclear plant have been addressed in several recent Euratom research projects: DISWEC (Evaluation of Techniques for Assessing Corrosion Cracking in Dissimilar Metal Welds), BIMET (Structural Integrity of Bi-Metallic Components) and ADIMEW (Assessment of Aged Piping Dissimilar Metal Weld Integrity). The main findings are summarised in the sections below.

2.1 DISWEC

Because of their metallurgy dissimilar metal welds are particularly prone to localised corrosion and especially environmentally assisted cracking (EAC). Despite this potential EAC susceptibility and the occurrence of environmental cracking in practice, only very limited data on crack initiation and propagation rates are available in the literature. Analysis suggests that this may be due in part to the fact that the test techniques in this area are not well developed or standardised. The main objective of DISWEC was therefore to identify and evaluate techniques suitable for assessing environmentally assisted cracking of dissimilar metal welds [16]. The experimental work comprised two phases, the first being a comparison of a variety of screening test techniques designed to investigate the susceptibility of the various dissimilar metal weld constituent materials and local microstructural regions to corrosion cracking. Having established the regions of the dissimilar metal weld most sensitive to corrosion cracking, a second series of experimental techniques were performed targeted specifically at generating quantitative data on crack growth rates. A review was also undertaken of worldwide experience of environmental cracking in dissimilar metal welds in operating nuclear plant, as well as a review of available experimental data. The testing programmes were performed on specimens cut from a specially prepared weldment between A533B pressure vessel steel and 316L austenitic stainless steel, made using alloy 82 weld metal. The weld specification was typical of a DMW found in the nuclear industry. The tests were performed in a simulated light water reactor environment but to accelerate test timescales, the water chemistry was enhanced to favour EAC conditions, by increasing sulphate and oxygen levels compared to operating plant.

The major outputs of DISWEC were a review of plant experience with dissimilar metal welds and of laboratory DMW corrosion cracking data, results of screening tests assessed for their suitability for reproducing stress corrosion cracking (SCC) in dissimilar metal welds in operating nuclear plant, identification of test techniques suitable for quantifying crack growth in DMWs in nuclear coolant environments and crack growth data for a specific transition weld in high temperature pressurised water under off-chemistry conditions.

2.2 BIMET

The BIMET project (Structural Integrity of Bi-Metallic Components) was a three-year collaborative research (1997-2000) project carried out for the European Commission under the Euratom Fourth Framework Programme [17-19]. The objective was to contribute to the development and verification of analysis methods to describe the behaviour of an external circumferential defect at the surface of a bimetallic weld.

Five DMW specimens were manufactured, of which two have been tested in 4-point bending after crack insertion, the remaining three being used for the experimental determination of welding residual stresses and for the generation of material property data for input to the analysis procedures. The geometry studied was a pipe assembly of 152.4 mm (6") mean diameter containing

a bi-metallic girth weld joining A508 ferritic steel and 304 type stainless steel sections (Figure 2.1). A circumferential surface breaking defect with a straight front was inserted into the pipe in the 309L austenitic buttering layer immediately adjacent to the ferritic base material. Type 308L austenitic steel was used for the remaining layers of buttering and as the weld filler material. Experimental programmes were performed to characterise the material properties and the residual stresses. Fracture toughness tests at 25°C revealed fully ductile fracture behaviour for the majority of weld regions. Unstable crack growth without much ductile tearing was occasionally observed in the fusion boundary area.

Two tests were successfully completed under four-point bending loads at room temperature (Figure 2.2, Figure 2.3). In both tests at initiation the crack deviated from the initial notch direction and ran in the buttering following a plane perpendicular to the pipe surface. BIMET-01 pipe, with an initial notch depth (at an angle of 25°) of 13.6 mm, produced 2.4 mm of stable, ductile tearing. In BIMET-02 the maximum initial notch depth was 9.2 mm at 25° and the test produced up to 8.4 mm of stable ductile tearing (at a much higher applied displacement). When the crack tip reached the bimetallic interface the path deviated and ran parallel to the interface principally on the austenitic side (Figure 2.4).

A range of analysis methodologies, including engineering flaw assessment methods, crack-tip FE models and a local approach method were applied to predict the critical load for initiation of the defect. The results demonstrated the complementary benefits of applying both finite element analyses and engineering assessment methods (EAMs). e.g. using FE to establishing stress intensity factor solutions and yield load solutions with greater accuracy than is possible by reference to handbook solutions alone. With these methods a modest effect of residual stress on crack initiation was identified, which accounted for an approximate 6% load reduction in the predicted initiation load.

For the EAMs applied to components under elastic–plastic loading such as the BIMET welds, the plastic yield load is the most important parameter in failure assessment. This requires accurate yield load solutions (either from handbooks or supporting FEA), as well as accurate values of the material yield strength. In the present case, it proved important to have yield strength values for all the relevant material zones. The BIMET analyses also underlined the important point that in heterogeneous structures the cracked zone is not necessarily the one that controls the global yield load.

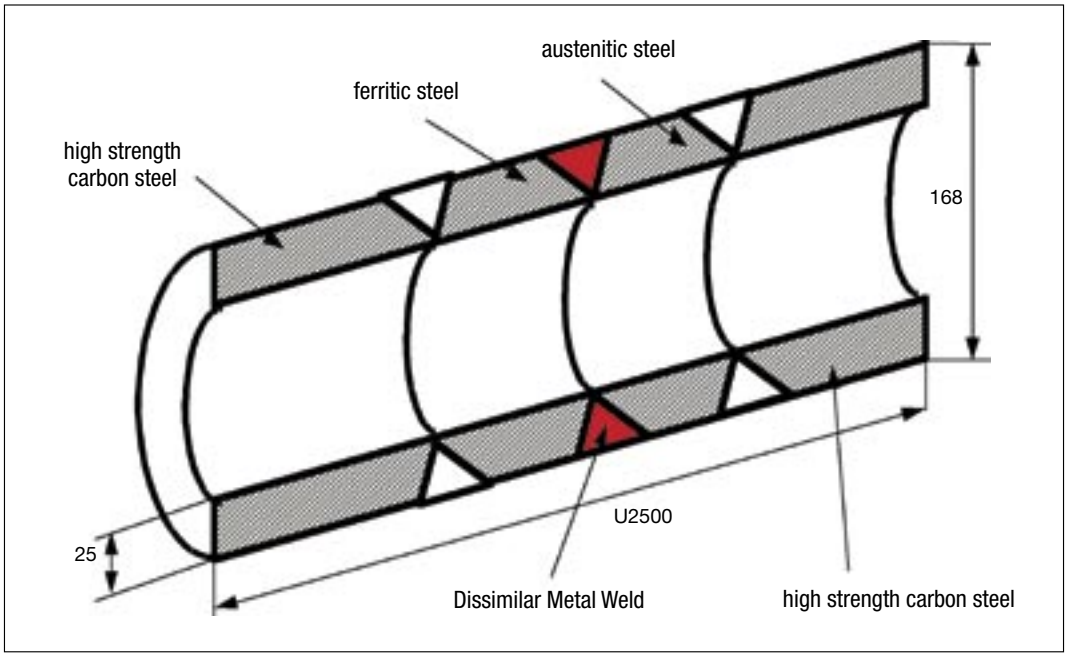

Figure 2.1: *Schematic of the mock-up used in the BIMET project*

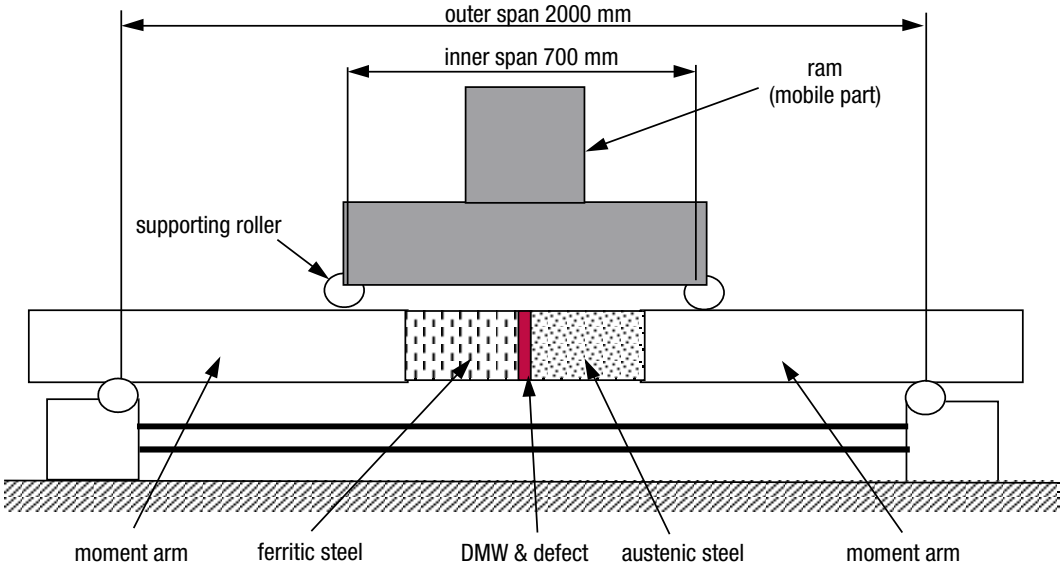

Figure 2.2: *Loading arrangement for the BIMET tests*

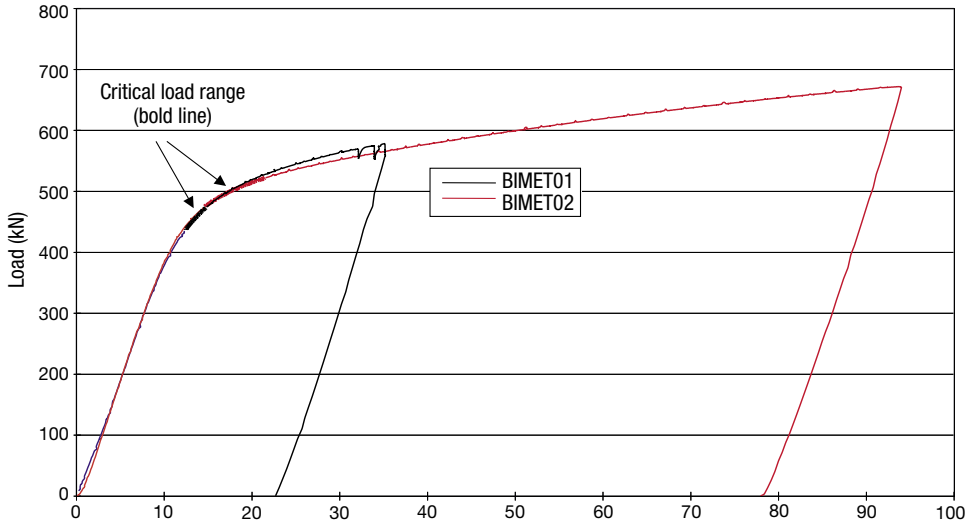

Figure 2.3: *Load-displacement records from the two BIMET tests*

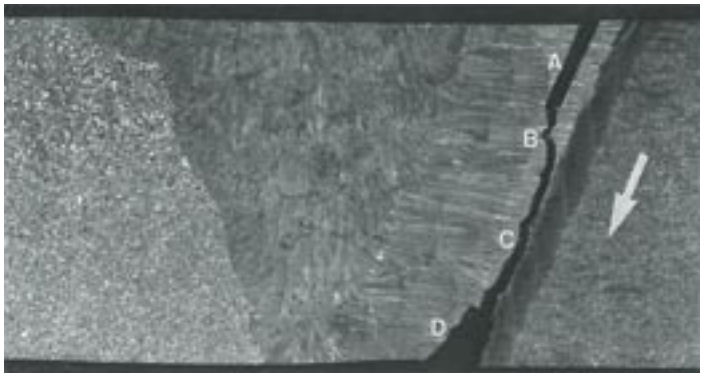

Figure 2.4: *Post-test cross-section from the BIMET-02 mock-up: location A is the implanted notch, B-C is the crack extension during the test and C-D is where the pipe was split open after the test for destructive examination*

Based on comparison with FE predictions, the effect of residual stresses is likely to be overestimated in the case of EAMs.

Problem definition sheets for the two BIMET tests are available in Annex 1 of this report. These provide details of the components, the material characteristics and test results and are intended to allow the tests to be used as calculation benchmarks by interested organisations.

2.3 ADIMEW

Following the success of BIMET, the ADIMEW project [20-24] was set up to examine the performance of a single benchmark 4-point bend pipe test, conducted on a nominal 16" piping assembly at 300°C and containing a ferritic to stainless steel (Figure 2.5, Figure 2.6). A notch-like defect with a tip of radius 0.2 mm was inserted at the ferritic steel/buttering layer interface, to simulate plant experience of damage at the worst-case location for a crack in such components. A second DMW mock-up was also manufactured for the experimental determination of welding residual stresses and for the generation of material property data for input to the analysis procedures. A range of analysis methodologies, including conventional flaw assessment methods, J approaches and Local Approach methods were applied to predict the critical load for initiation of the defect, the extent of crack growth and the path followed by the crack through the weld up to the maximum load. Consideration was also given to measurement of the welding residual stresses. The ADIMEW test was successfully executed in July 2003. The results of the fractographic investigation of the test piece were available in October 2003 and the post-test analyses were completed in December 2003. Since the ADIMEW test provided the central focus of NESC-III, the following sections on the mock-up fabrication and the test are included here for reference purposes.

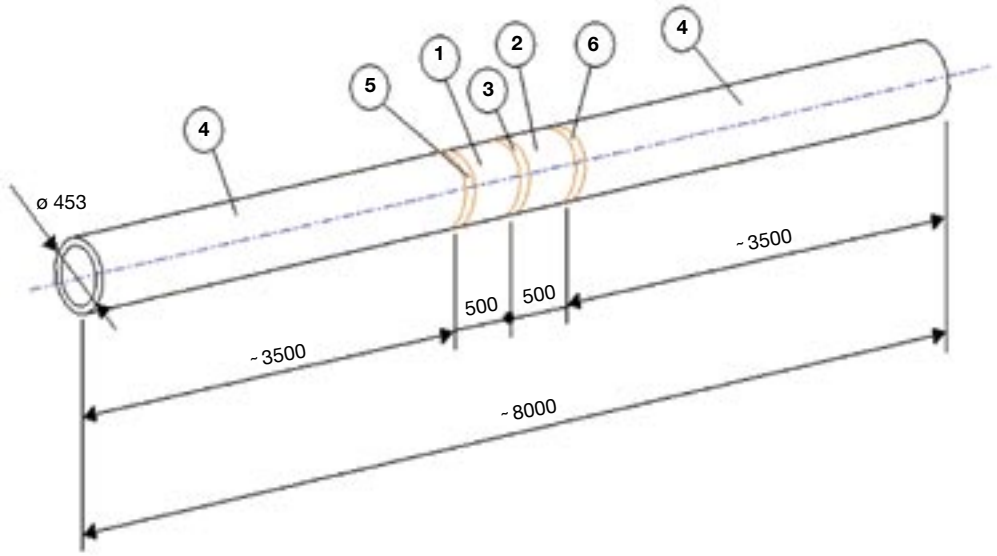

1. Austenitic base metal; 2. Ferritic base metal; 3. Dissimilar metal weld; 4. Prolongation arms; 5. Weld connecting austenitic base metal to prolongation arm; 6. Weld connecting ferritic base metal to prolongation arm

Figure 2.5: *Schematics of the ADIMEW mock-up*

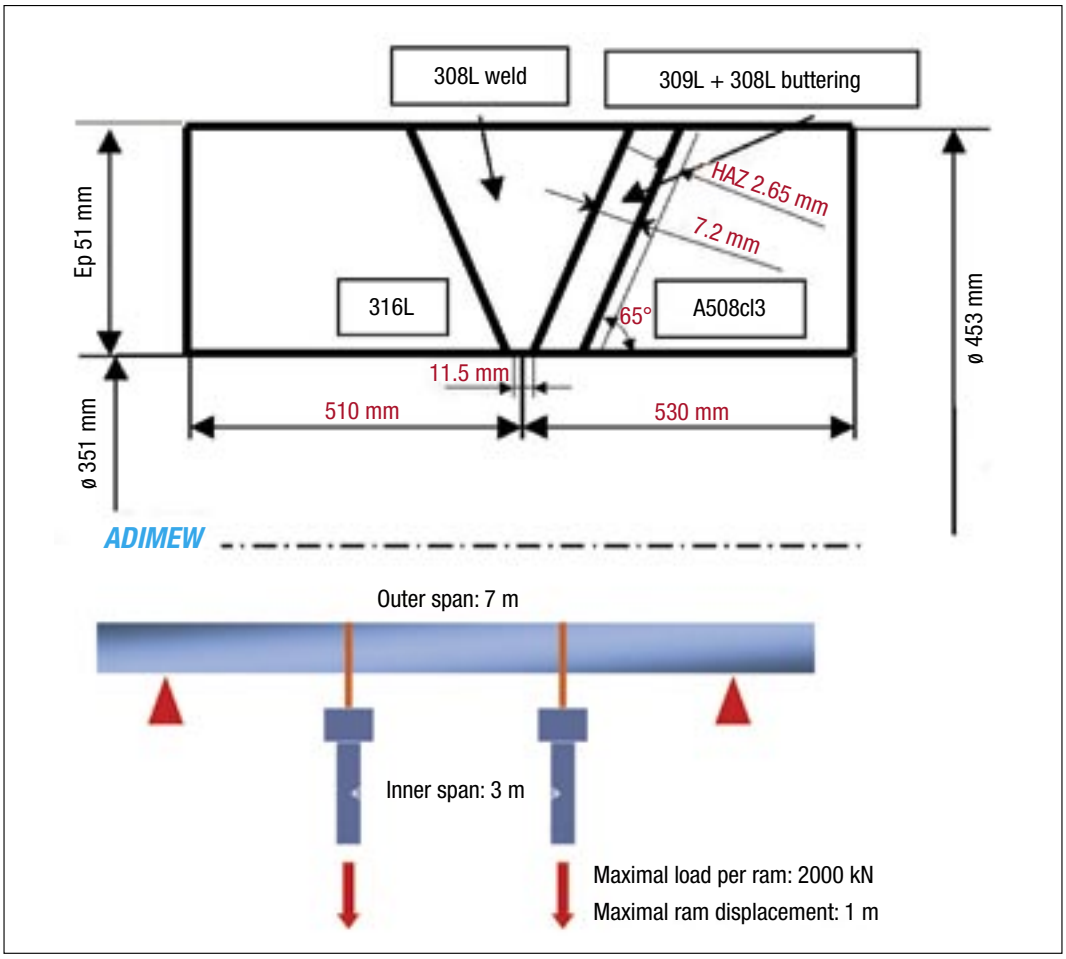

Figure 2.6: *The location of the ADIMEW defect and testing principle*

2.3.1 Mock-Up Fabrication

Two identical mock-ups were produced:

- AD01, for the residual stress measurements and the materials properties investigations, and
- AD02, for the actual ADIMEW bend test.

2.3.1.1 Material specifications

The ferritic pipe material was an ASTM A508 Class 3 low carbon steel. The austenitic pipe material was an ASTM 316L. The weld filler material was AWS E308L stainless steel (electrode type

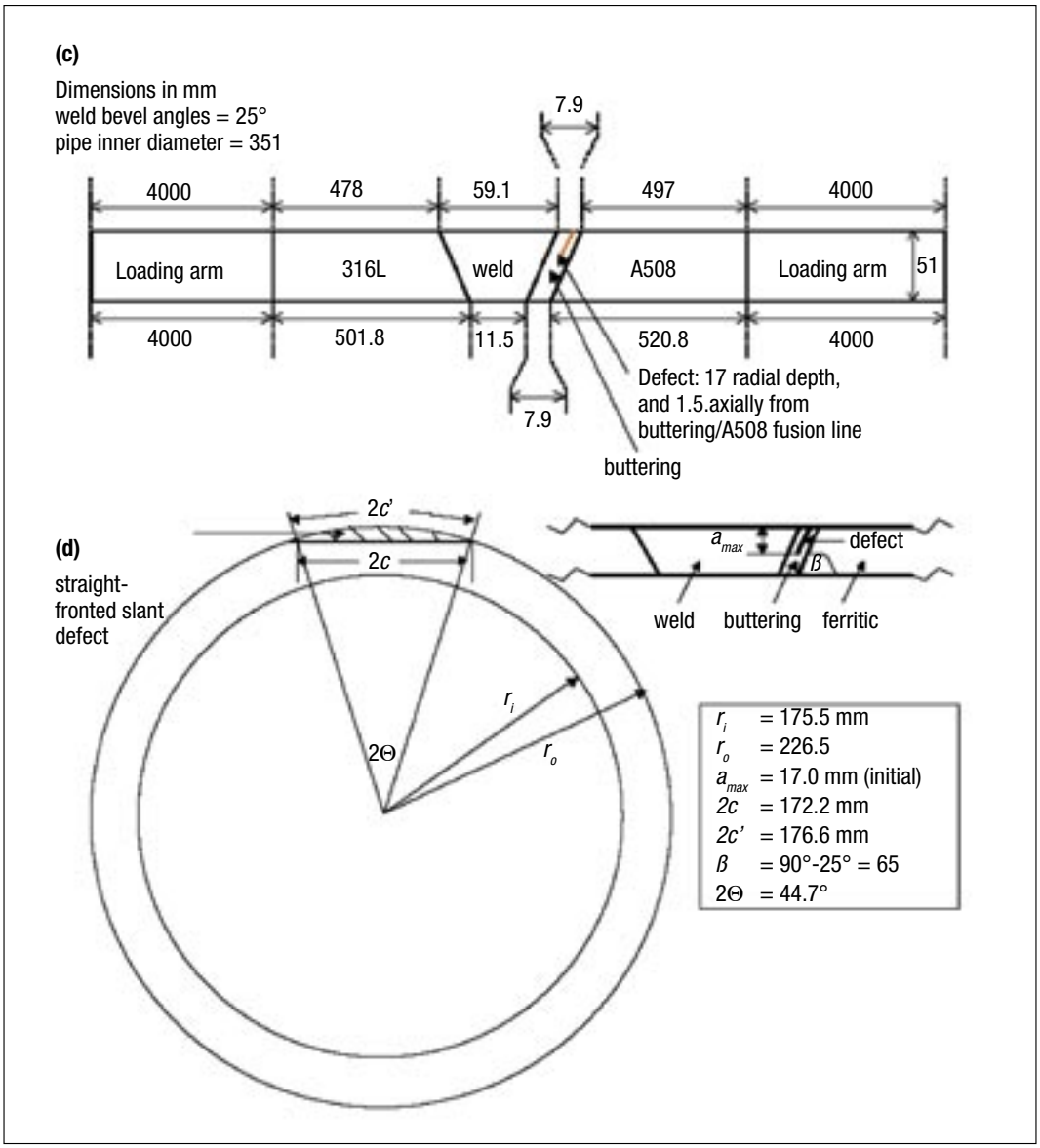

Figure 2.7: *Schematic of the ADIMEW mock-up at the cross section containing the defect*

used was ESAB-OK61.30N 308L). For the buttering, two different materials were used: an AWS E308L stainless steel and an AWS E309L stainless steel, which is richer in Cr and Ni than E308L. The electrodes used were ESAB-OK61.30N and SOUDOCROM L309LQ5. The nominal chemical composition of these materials is summarised in Table 2.1.

Table 2.1: *Composition of the materials used in the ADIMEW weld (weight %)*

Steel	C	Mn	Cr	Mo	Ni	Si	Cu	Al	V	P	S	N
A508 Cl.3	0.15-0.25	1.2-1.5	0.025-0.15	0.15-0.6	0.4-1	0.15-0.4	0.04-0.06	0.027	0.001-0.05	0.005-0.025	0.003-0.025	–
316L	0.03	–	16-18	2-3	10-14	0.75	–	–	–	0.045	0.03	0.1
Weld filler 309L	0.03	1.8	19	–	9.7	0.45	–	–	–	–	–	–
Butter 309L	0.03	1.8	23.4	–	13	0.6	–	–	–	–	–	–

2.3.1.2 Welding Procedure

The procedure started with the ferritic pipe in its as-received state, with an external diameter of 473 mm, a thickness of 69 mm and a length of 530 mm. One side of the pipe was machined to a slope of 25°. The welding procedure was performed in five stages:

Stage 1 - Buttering
First a so-called butter layer was deposited on the ferritic part using austenitic electrodes. In both cases (AD01 and AD02) the pipe was pre-heated using an electric resistance heater. The pipe was supported on a rotating table completely unrestrained in an upright position that facilitated buttering deposition. The buttering consisted of four layers of weld passes to give a total thickness of 12mm (the number of weld passes was 70). The number of passes for the first two buttering layers can be seen on the etched cross-section of specimen AD01 shown in Figure 2.8. The welding parameters for each specimen are listed in Table 2.2. After buttering and prior to welding, the pipe was heated in an electric resistance furnace for 4 hours at 400°C. This process is not a stress relief heat treatment, but a requirement of the French RCC-M code [25]. It was then allowed to cool down freely to room temperature.

Stage 2 - Buttering Machining
The pipe was machined down to give an external diameter of 467 mm and a wall thickness of 64 mm. The face of the buttering was itself machined back to a give a thickness of 7.2 mm.

Stage 3 - Welding
The two pipes were assembled and tacked together with spot welds. The austenitic pipe had an external diameter of 467mm, a thickness of 73mm and was about 510mm long. As in the case of the ferritic pipe, it is assumed that the austenitic pipe in the as-received state was completely stress free, having one end machined to a slope of 25°. During welding the assembly was supported on rollers, approximately 25cm from the weld centreline, in order to be completely unrestrained. The welding parameters are listed in Table 2.2. The bead sequence for AD02 is illustrated in Figure 2.9. Not all weld passes are visible since the external and internal surfaces of the mock-up were subsequently machined (see Step 5 below). After welding the assembly was allowed to cool down to room temperature.

Stage 4 - Post Weld Heat Treatment

The full PWHT heating, soak (nominally 6 hours at 600ºC) and cooling sequence is illustrated in Figure 2.10.

Stage 5 - Final Machining

After completion of the PWHT the assembly was machined down to its final dimensions: external diameter was 453 mm and wall thickness 51 mm.

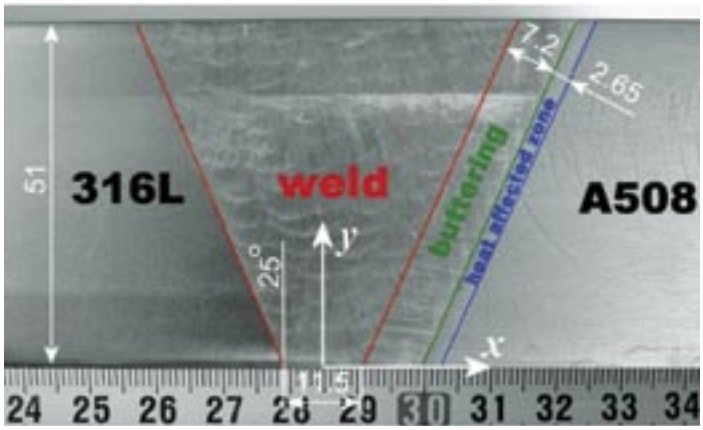

Figure 2.8: *Longitudinal cross-section of the ADIMEW AD01 dissimilar metal pipe weld, showing geometry details and materials involved*

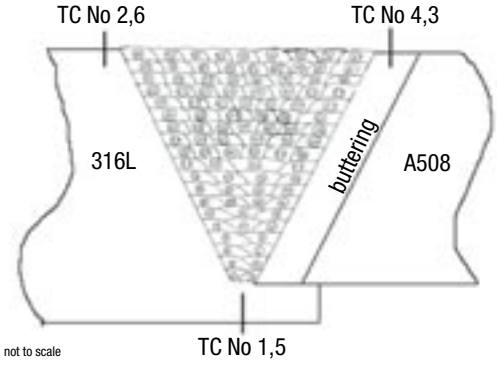

Figure 2.9: *Bead sequence for ADIMEW mock-up AD02*

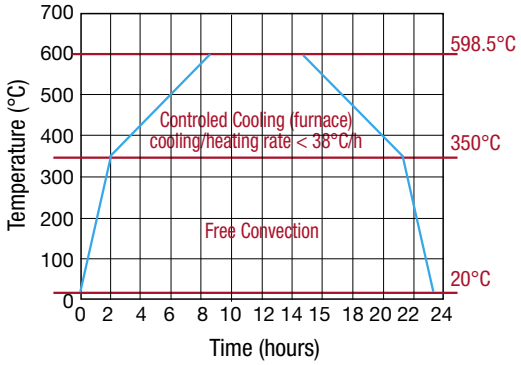

Figure 2.10: *The applied post weld heat treatment for ADIMEW mock-up AD02*

Table 2.2: *Welding parameters for the ADIMEW mock-ups*

Welding Parameters	**AD01**	**AD01**
welding machine	MESSER G400.1	
Buttering		
number of weld pass layers	4	
total number of weld passes	70	
pre-heating temperature (°C)	151	152
inter-pass temperature (°C)	215	199
Welding Current (A)	135-145 (1st layer)	145 (1st layer)
	135 (2nd layer)	130-135 (2nd layer)
	180 (3rd and 4th layer)	
arc voltage (V)	24	
electrode type/diameter (mm)	Soudometal-SOUDOCROM L309L Q5 / 4 (1st layer)	
	ESAB OK 61.30N 308L / 4 (2nd layer)	
	ESAB OK 61.30N 308L / 5 (3rd and 4th layer)	
electrode travel speed (cm/min)	20	
post-heating period (minutes)	255	260
post-heating temperature (°C)	298-342	258-352
Weld Fill		
number of weld pass layers	18	19
total number of weld passes	91	97
pre-heating temperature (°C) inter-pass temperature (°C)	20	
	97	74
Welding Current (A)	135 (for 4mm electrodes)	140 (for 4mm electrodes)
arc voltage (V)	185 (for 5mm electrodes)	195 (for 5mm electrodes)
	24	
electrode type/diameter (mm)	ESAB OK 61.30N 308L / 4 mm	
	ESAB OK 61.30N 308L / 5 mm	
electrode travel speed (cm/min)	20	
PWHT		
maximum heating rate (°C/h)	40	38
heating period (minutes)	368	363
heating temperature (°C)	595-606	595-602
maximum cooling rate (°C/h)	38	37

2.3.1.3 Defect Insertion

The final stage in the preparation AD01 for the bend test involved the insertion of a simulated crack-like defect. The project group specified this to be a partial circumferential defect with a maximum depth of third of the wall thickness i.e. 17 mm depth, located in the first buttering layer at a constant distance of 2 mm from the fusion line. The defect was produced by means of electro-discharge machining, producing a notch tip radius of approximately 0.2 mm.

2.3.2 The ADIMEW Test

The test consisted in a four-point bending test (inner span 3 m, outer span 7 m) on the mock-up assembly, which consisted of the DMW weld described above, together with ferritic pipe extension arms (Figure 2.11). The load was applied via two bending 4 m long bending arms, and the force application points were accurately known. Steel collars were used to transmit the load; the outer collars were connected to wheels, which could roll on flat horizontal surfaces, while inner collars were directly connected to the rams, through crank-arms equipped with knee-joints (Figure 2.12). All the collars, wheels and crank-arms were designed to remain completely elastic. Because of the differences in mechanical properties of the pipe sections to either side of the defect, the pipe was offset on the rig in an effort to ensure equal forces on the two rams.

Since the test was to be performed at normal operating conditions (metal temperature of 300°C), an external and internal heating system was applied. Thermocouples were used to establish thermal map of the mock-up. The load and displacement of each ram were measured as well as deflection and rotations. For detection of crack initiation, an alternating current potential drop (ACPD) method was applied around the crack together with other sensors that measured the crack mouth opening displacement (CMOD) and crack mouth opening angle (CMOA). Measurements of the displacement of the collars relative to the pipe, rotations of crank-arms, and rotations of the wheels were also made.

For the central part of the mock-up to reach a stable temperature of 300°C, heating was required for 49 hours. During the two-hour test the temperature increased slightly by about 2.5°C. The temperature field around the defect area was homogeneous (±1.5°C), but decreased rapidly outside this zone (125°C 1 metre away, and 50°C 2 metres away from the defect). The two extension arm welds remained below 200°C. The temperature profile in the defect area shows a thermal gradient of only 23°C caused by convection. It was assumed that this had no major influence on the mechanical behaviour of the test piece. The test itself was performed under constant displacement of the loading rams. Figure 2.13 shows the ram displacement data. It is seen that Ram 1 on the austenitic side took more load. This problem was caused by the fact that Ram 1 was slightly ahead of Ram 2, by an amount that reached 2.8mm, but remained below 5% of the average displacement. Overall, the signal-to-noise ratio of the whole experiment was good and the deformation of the crank-arms remained negligible.

The moment vs. displacement curve (Figure 2.14) is calculated using the formula:

$$M(x) = \frac{L-l}{2}.\left[F_1 - \frac{F_2 - F_1}{L} \cdot x\right]$$

where L is the outer span, l the inner span, and x the distance from the defect plane ot the centre-line. Given the offset of 285 mm in the test, the bending moment is given by:

$$M \approx 0.9208 \cdot F_1 + 1.0791 \cdot F_2$$

The test measurement showed that deformation was concentrated to austenitic stainless steel section. The full instrumentation data from the ADIMEW test is available in an Excel spreadsheet (see Annex 2).

Several methods were used to determine when crack initiation occurred:

a) Plotting the ACPD signal against the average CMOD, and determining the instant of the first change of slope, indicates initiation occurred at about 0.83 mm of CMOD (Figure 2.15).

b) From the CMOD vs. average ram displacement data, small accelerations of CMOD were observed after each partial unloading phase (Figure 2.16). If these are treated as crack tip events, it implies initiation occurred at around 120 mm of average ram displacement, corresponding to a CMOD value of 0.72 mm.

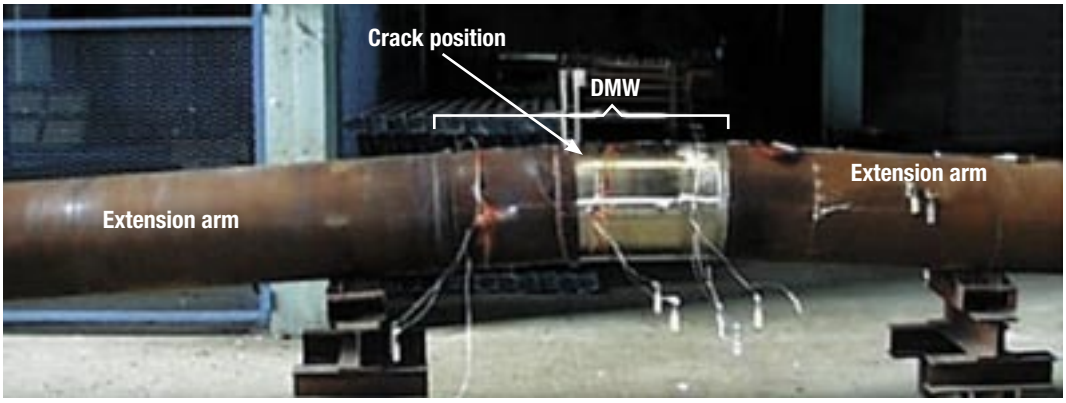

Figure 2.11: *The mock-up after the test, showing that substantial bending occured*

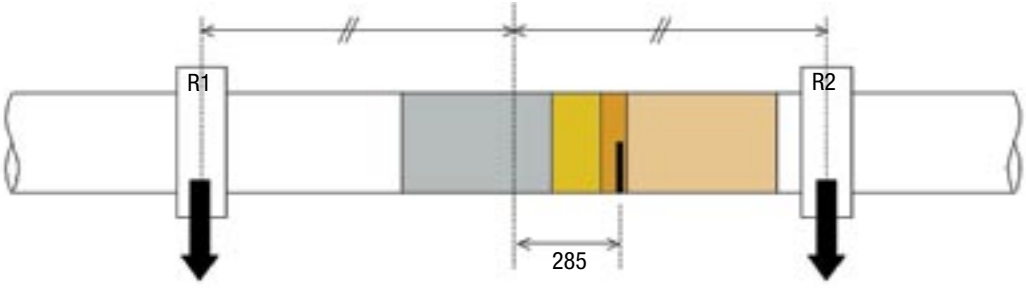

Figure 2.12: *Schematic of the test mock-up and indication of the offset (unit: mm – drawing not to scale)*

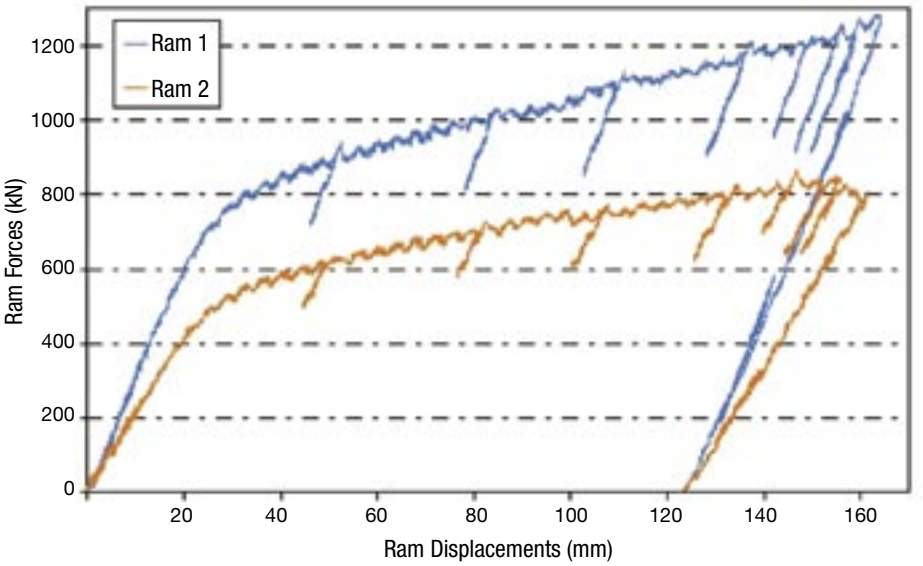

Figure 2.13: *ADIMEW test - ram forces vs. displacements*

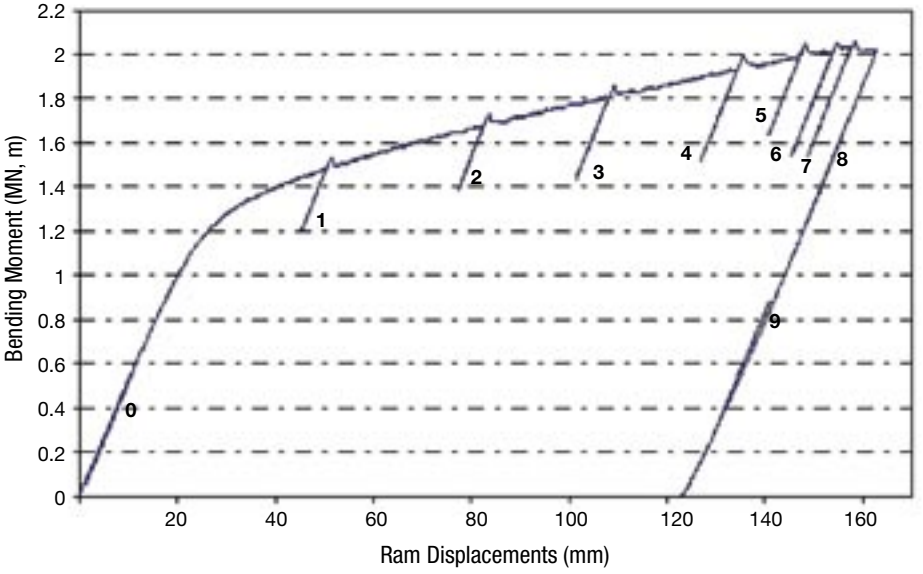

Figure 2.14: *ADIMEW test - bending moment vs. displacement curve*

c) An unloading compliance technique was applied during the test to provide information about the crack initiation and extent of subsequent growth. The elastic slope of bending moment vs. CMOD during successive unloadings was found to first increase, before then decreasing. The first phase (increase of the slope) is thought to correspond to plasticity development and hardening. Taking the maximum slope as a reference, an estimate of the crack growth just before each unloading phase can be obtained; these results showed that crack initiation occurred between 0.42 mm and 0.59 mm of CMOD, with a maximum estimated crack growth of around 16 mm.

d) A so-called mixed approach was also applied. First, a correlation function between the ACPD signal and the crack growth was estimated using the compliance method. By plotting the resulting crack growth data with CMOD, an initiation value of 0.62 mm was derived.

e) Lastly the CMOA values were also considered. CMOA was determined by plotting the pseudo-rotation centre against the test duration (Figure 2.17). The pseudo-rotation centre is the position of the plastic knee-joint at the beginning of the test. The decrease of the pseudo-rotation centre observed in Figure 2.17 gives an approximation of crack initiation time as well as information on different crack propagation phases. Plotting CMOA against CMOD gives a clear indication of change in behaviour; the first phase corresponding to crack opening without propagation, and the second phase (occurring around 1 mm) indicating crack propagation (Figure 2.18).

Table 2.3 provides a summary of the results obtained using these different methods. The "mixed method" is considered to provide the best estimates of initial moment/displacement. The values from the AC-PD and CMOA approaches give higher values which are considered less reliable.

After the test a comprehensive destructive examination was carried out. The defect itself was carefully sectioned. These confirmed that notch had been inserted in the desired position, parallel to the interface, 17 mm deep and 2 mm away from the fusion line. Figure 2.19 shows the defect after having been split open in the laboratory. There is extensive through-thickness crack propagation and no circumferential crack propagation (the crack propagated only within the depth of the material). The maximum propagation depth was around 28 mm. SEM examination of the fracture surface confirmed that the growth was fully ductile. The crack path was first towards the fusion and then along buttering side of the interface as shown in Figure 2.20. This behaviour is very similar to that observed in the BIMET tests e.g. Figure 2.4 above.

Table 2.3: *Summary of the crack initiation values*

Measurement Method	CMOD (mm)	Average ram displacement (mm)	Bending moment (MN. m)	Force on ram 1 (kN)	Force on ram 2 (kN)
AC PD	0.83	126	1.91	1144	795
CMOD	0.72	115	1.86	1123	769
Compliance	0.42~0.59	78~103	1.70~1.79	1026~1078	703~744
Mixed approach	0.62	110	1.82	1100	750
CMOA	1.00	135	1.96	1179	810

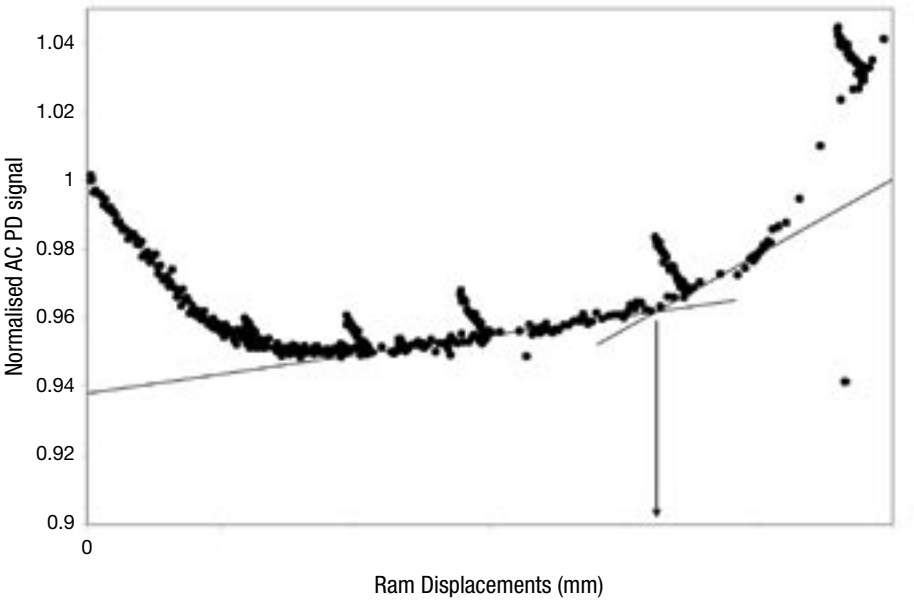

Figure 2.15: *ADIMEW test - determination of CMOD at initiation based on the AC potential drop data at the centre of the defect*

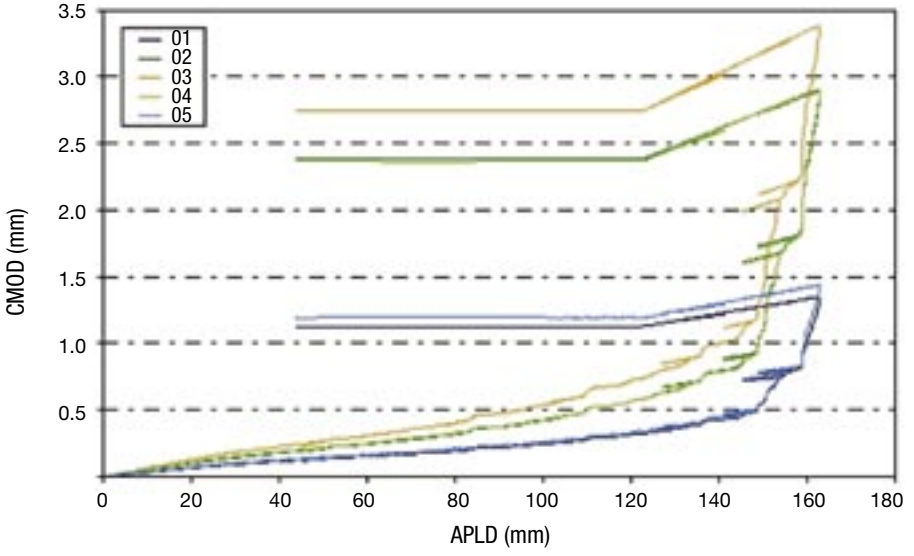

Figure 2.16: *ADIMEW test - CMOD against average ram displacement – gauges O2 and O3 were at the centre of the defect, while O4 and O5 were at 40 mm either side*

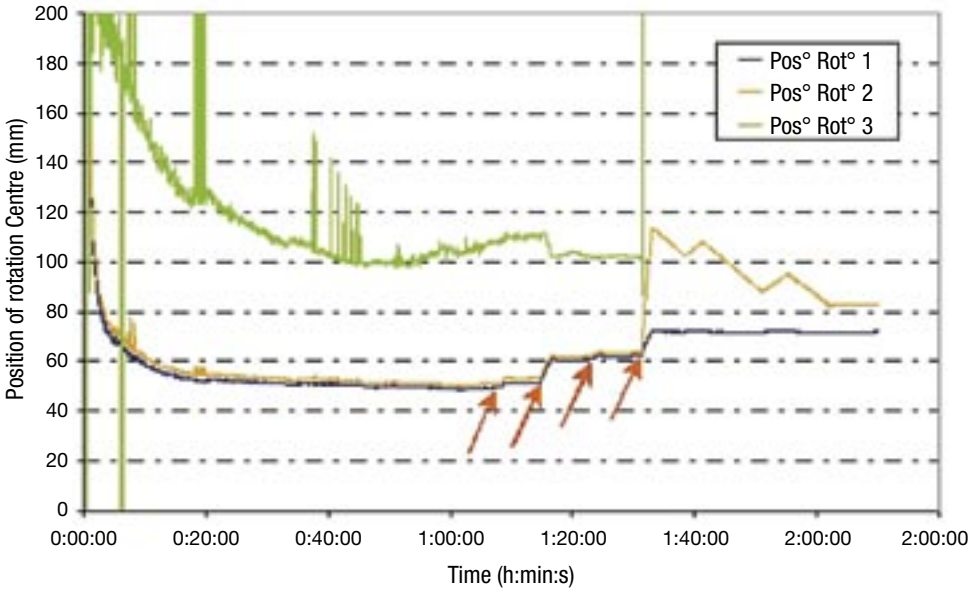

Figure 2.17: *ADIMEW test – the pseudo-rotation centre as a function of time, used to determine crack initiation and revealing also different crack propagation phases (indicated with red arrows)*

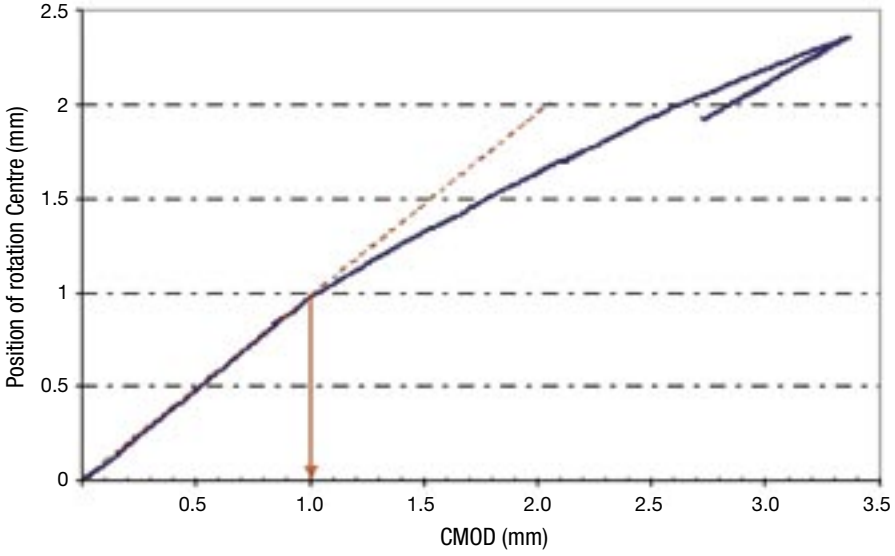

Figure 2.18: *ADIMEW test - plot of CMOA vs. CMOD revealing two distinct phases*

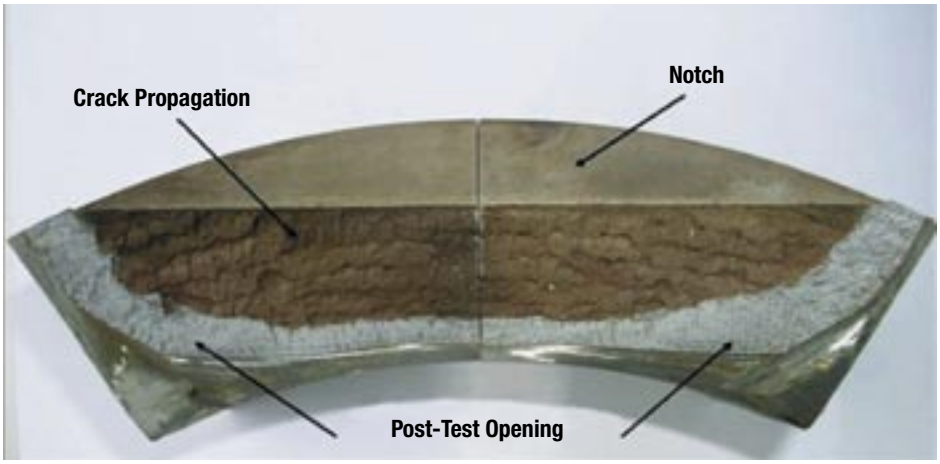

Figure 2.19: *The ADIMEW defect after having been split open after the test; the extent of crack growth is clearly evident and amounted to 28 mm at the deepest point (in the centre)*

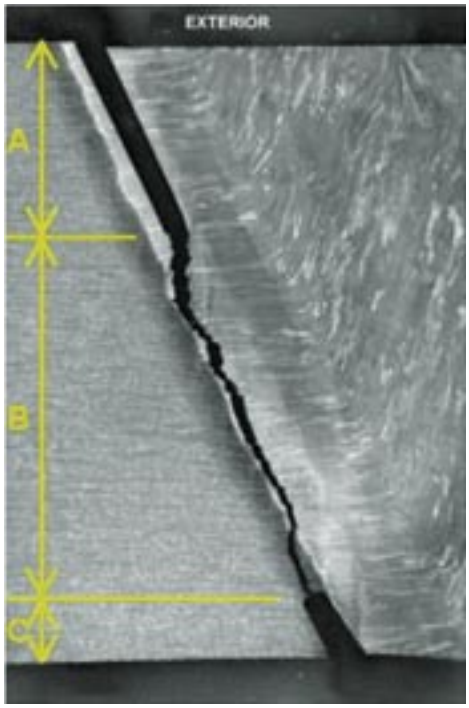

Figure 2.20: *Cross-section at the centre of the crack showing, A) the inserted notch, B) crack propagation path during the test and C) fracture path during the destructive examination*

3 THE NESC-III PROJECT

3.1 OBJECTIVES

The NESC-III project was organised as a complementary activity to the ADIMEW project, with the following objectives:

- Quantify the accuracy of structural integrity assessment procedures for defect-containing, dissimilar metal welds in aged PWR Class 1 piping.
- Utilise results of a unique large scale test (ADIMEW) to determine the actual behaviour of a defect in a DMW of industrial scale.
- Address critical issues including: inspection performance, laboratory-scale fracture testing on welds and potential benefits of advanced fracture modelling.
- Use the results to promote best practice and the harmonisation of international standards.

3.2 TECHNICAL SCOPE AND ORGANISATION

On account of the limitations to ADIMEW's budget, its tasks were concentrated on essential items relating to the test performance. NESC therefore took the opportunity to coordinate a series of complementary investigations as a network project. Five Task Groups (TGs) were set up:

Task Group 1: Non-Destructive Inspection
TG1 focussed on the performance of inspection techniques, based on a blind round robin trial (RRT) using a specially manufactured mock-up. It was intended that participating teams could benefit from experience of different defect types and from information on the capabilities of both industrial applied procedures and more advanced techniques.

Task Group 2: Materials Characterisation
For TG2 the scope for additional materials testing was limited since only a small segment of the AD01 weld remained available after the ADIMEW testing. Hence the main effort was on the analysis of the ADIMEW data and some supplementary tests: micro-hardness profiles, instrumented hardness measurements and notch tensile tests (for calibration of local approach ductile tearing models).

Task Group 3: Stress and Fracture Analysis
The main TG3 tasks concerned the analysis of the benchmark tests, considering the specific challenges associated with the BIMET and ADIMEW DMWs: material mismatch, mixed mode crack tip loading, residual stresses etc. The investigations have been performed as part of the pre- and post-test analyses of the ADIMEW test.

Task Group 5 Evaluation
TG-5's role was to evaluate the data gathered during the project and to produce a final report.

Task Group 6: Residual Stresses
TG6 focused on the reliability of finite element calculations of residual stress distributions in DMWs. This involved a series of round robin exercises, starting with a simplified approach and

leading to complex 3-D simulations of the entire welding process. To validate the results, the group had access to the ADIMEW residual stress measurements made via neutron diffraction as well as results from comprehensive temperature and strain measurements performed during welding, for which NESC-III provided additional funding.

NESC-III relied on in-kind i.e. un-funded, contributions, following the established system for NESC network projects. Furthermore an agreement was made so that specified ADIMEW documents would be released to NESC-III for information and peer review, and that ADIMEW partners would automatically be included in NESC-III, receiving the contribution-in-kind reports. Altogether twenty-one organisations participated in NESC-III, as shown in Table 3.1.

As the NESC Operating Agent, the JRC coordinated the project work as well as making technical contributions in several areas. The progress of the project was reported to the NESC Steering Committee, who also have final approval of all documents released by the network. The main milestones in the execution of the project were listed in Table 3.2. The project documentation including minutes of meetings, test results, analyses and the main reports are stored in the NESC archive and are available electronically via the JRC's DOMA site: http://odin.jrc.nl/doma.

Table 3.1: *The organisations that participated in ADIMEW and NESC-III*

Organisation	ADIMEW	NESC-III
AREVA NP SAS, France[1]	✓	✓
AREVA NP GmbH, Germany[2]		✓
Basler & Hofmann, Switzerland		✓
Bay Zoltan Foundation, Institute for Applied Logistics, Hungary		✓
Bohunice NPP, Slovakia		
CEA, France	✓	✓
CEGELEC, Germany		
EDF, France	✓	✓
European Commission, Joint Research Centre, Institute for Energy	✓	✓
GRS, Germany		✓
Inspecta Technology AB[3], Sweden		✓
Lithuanian Energy Institute, Lithuania		✓
Mat-Tec AG, Switzerland		✓
Mitsui Babcock Energy Ltd., UK		✓
NRG, The Netherlands		✓
Nuclear Research Institute Rež plc, Czech Republic		✓
Serco Assurance, UK	✓	✓
Tecnatom SA, Spain		✓
TWI Ltd., UK	✓	✓
VTT, Finland	✓	
VUJE Inc., Slovakia		✓

[1]Formerly Framatome ANP SAS; [2]Formerly Framatome ANP GmbH; [3]Formerly Det Norske Veritas Inspection AB

Table 3.2: *Milestones in the NESC-III Project*

Date		**Event/Action**
2000	October	Kick-Off Meeting, Lyon, France (in parallel with the ADIMEW Kick-Off)
2001	May	2nd Progress Meeting, Petten, The Netherlands
2002	January	Fabrication of the ADIMEW AD01 Weld Mock-Up
	February	Fabrication of the ADIMEW AD02 Weld Mock-Up
	March	3rd Progress Meeting, Renfrew, UK
	December	4th Progress Meeting, Paris, France
2003	February	Release Pre-test Problem Definition Document
	June	Start of the ISI Round Robin Trials
	July	5th Progress Meeting, Moret-sur-Laing, France
	July	ADIMEW Test (EDF Les Renardieres)
	October	ADIMEW Test Report End of the ADIMEW contract
2004	April	6th Progress Meeting, Lyon, France
	June	Completion of the ISI Round Robin Trials
	July	Start of Destructive Examination of the ISI Mock-Up
	October	7th Project Meeting, Petten, The Netherlands
	December	Preliminary performance evaluation the ISI Round Robin
2005	September	8th Project Meeting, Erlangen, Germany
		NESCDOC TG6 05-01 “TG6 Synthesis Report”
	November	NESCDOC-05-11, “TG3 Collation of the Stress and Fracture Mechanics Analyses“
2006	February	NESCDOC-05-12, “Results of the Destructive Examination of the NESC-III Mock-Up”
	June	TG1 Data Evaluation Meeting, Petten
	September	TG1 Final Report
	September	Final Report approved by the Network Steering Committee

4 IN-SERVICE INSPECTION

4.1 INTRODUCTION

A major task for NESC-III was to consider the performance of non-destructive inspection techniques for the type of dissimilar weld used in ADIMEW. This was motivated by the recognition that the inspection of dissimilar metal welds continues to be difficult. The level of performance of ultrasonic inspection in defect detection and sizing demonstrated in earlier PISC exercises [26-28] was found not to be well aligned with the needs of structural integrity analysis. Development in ultrasonic inspection methods, for example the trend towards increasing use of phased array probes, were claimed to deliver significantly improved inspection performance. Nevertheless, problems encountered in the late 1990s [29, 30] with the characterisation of defects of complex morphology, such as primary water stress corrosion cracking, again cast doubt on ultrasonic inspection effectiveness. There was therefore a need for re-assessment of the capability of ultrasonic inspection. To address this Task Group 1 was set up to organise a blind round robin trial. It was intended that participating teams could benefit from experience of different defect types and from information on the capabilities of both industrial applied procedures and more advanced techniques. This chapter provides a synthesis of the inspection trial programme and results obtained, based on the TG1 final report [31]. Following the practice of NESC inspection activities, individual organisations are not identified.

4.2 ORGANISATION OF THE TRIAL

4.2.1 Mock-Up Fabrication and Defect Insertion

From the start of the NESC-III project it was clear that a dedicated mock-up component would be required for the inspection performance trial as the ADMIWEW AD01 and AD01 welds were required for the test itself and the materials characterisation programme. Furthermore during the development of the TG1 programme a number of defects were found in Inconel 182 DMWs, in particular at the V.C. Summer [29] and Ringhals [30] plants. It was therefore decided to manufacture a new mock-up with the same pipe diameter as in ADIMEW but containing two different types of DMW - one with austenitic 308L filler (as in the ADIMEW mock-up) and one with Inconel 182 filler. The generic defect types to be inserted were decided at the TG1 kick-off meeting in June 2002. The dimensions of the mock-up are shown in Figure 4.1. The weld and materials configurations for the two welds are shown in Figure 4.2. The total weight of the assembly was 580 kg. The JRC, who procured the mock-up and acted as referee for the trial, exclusively knew the number, location, type and dimensions of the defects present.

4.2.2 The Round Robin Inspections

The following seven organisations participated in the trial, which was coordinated by the JRC:

- Tecnatom SA Spain
- VTT Finland
- CEGELEC Germany
- Mitsui Babcock Ltd UK
- Bohunice NPP Slovak Republic
- Areva ANP SAS France
- CEA France

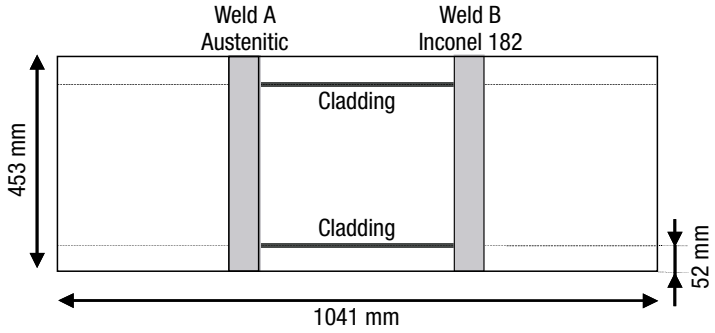

Figure 4.1: *Schematic of NESC-III inspection trial component*

ID	Description	Weld A	Weld B
#1	Ferritic base material	SA508	SA508
#2	Austenitic base material	304L	304L
#3	Buttering	309L + 308L	Inconel 182
#4	Weld filler	308L	Inconel 182
#5	Cladding material	309L	309L

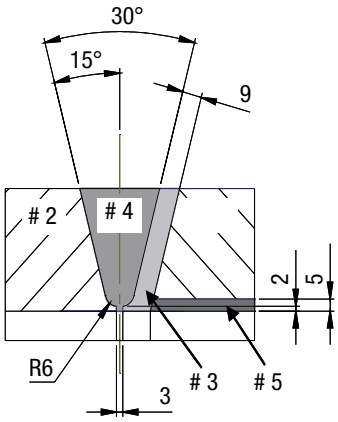

Figure 4.2: *Materials and weld configuration of welds in the NESC-III inspection trial component*

Each organisation was supplied with comprehensive documentation on the mock-up component and the inspection reporting requirements [32, 33]. For the trial the teams were asked to carry out a full volumetric inspection of the two welds, looking for the following defect types:

- **Circumferential defects:** outer surface breaking defects (weld A only); embedded defects and inner surface breaking defects
- **Axial defects:** inner surface breaking (weld B only)

The detection target for both welds was 5 mm TWE and 10 mm length; the sizing targets were ± 3 mm for TWE and +10 mm / -5 mm for length.

The mock-up was circulated to the different teams according to an agreed inspection schedule. Under the rules of the trial each team had two weeks to complete its inspection and four weeks to report its data, although in some cases the latter time-scale was relaxed. Teams could choose if they wanted to inspect only one weld or both. The component was equipped with an anti X-ray device during the exercise, so that invigilation was not deemed necessary for inspections from the external surface. However, teams could also choose to inspect the welds from the internal surface, and in these cases JRC staff invigilated the inspection.

The inspections were carried out in the period between August 2003 and June 2004. As in previous similar RRT trials (PISC III and NESC-1 [34]) inspection data were handled in a confidential way. The inspection reports were submitted to JRC, and each team was given a unique team code. A total number of 17 inspection data sets were handed in to the JRC for the two welds. Table 4.1 summarises the available inspection data sets. Only two teams inspected the component from the internal surface. The main ultrasonic techniques applied were pulse echo (TRL & shear wave), focussed probes, phased array and time-of-flight diffraction (TOFD). One team applied acoustic holography to complement standard techniques.

Table 4.1: *Summary of the inspections carried out in the NESC-III RRT*

Team code	Inspection from outside		Inspection from inside	
	Weld A	Weld B	Weld A	Weld B
AC01	Yes	–	–	–
BE01 #1	Yes	Yes	–	–
DF01	Yes	Yes	–	–
DF02	–	–	Yes	Yes
GJ01	Yes	Yes	–	–
HL01	Yes	Yes	–	–
HL02	–	–	Yes	Yes
KM01	Yes	Yes	–	–
NP01 #2	Yes	Yes	–	–

#1 procedure did not cover outer 1/3 of wall thickness the assembly
#2 procedure only covered through wall extent sizing of outer surface breaking defects

4.2.3 Destructive Examination for Defect Characterisation and Sizing

Once the inspection trials were completed, the JRC performed a destructive examination to provide definitive information on the dimensions, location and morphology of the defects [35]. A total 10 defects were present in weld A and 7 defects in weld B. The type of defects can be subdivided into the following four main categories (examples are shown in Figure 4.3):

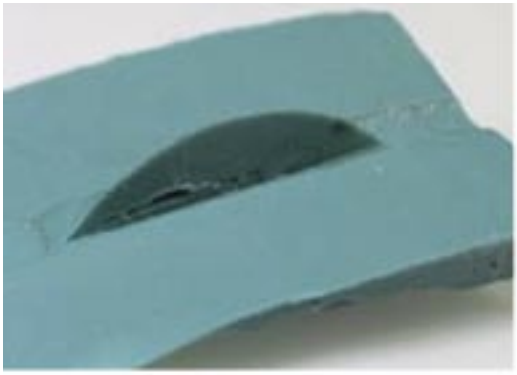

a) PISC Type A - replica[4] of EDM notch A7 in the austenitic weld, depth 5 mm, length 21.1 mm

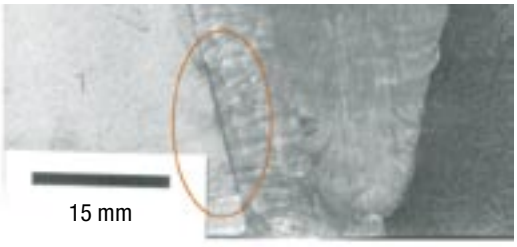

b) Sidewall lack of fusion (defect B5 in Inconel weld , TWE = 13.8 mm)

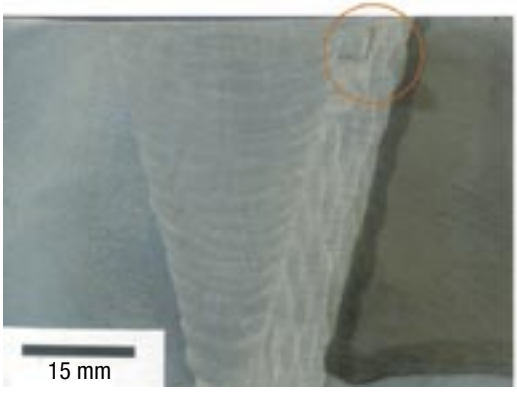

c) Technique "A" - smooth flaw technique (defect A6 in austenitic weld A, TWE = 3.8 mm)

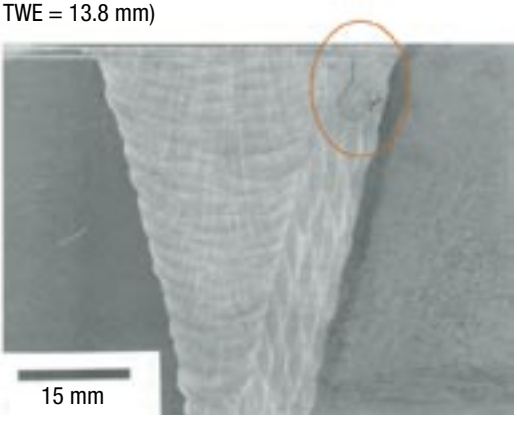

d) Technique "B" - simulated stress corrosion cracking (defect A9 in austenitic weld A, TWE = 6.8 mm)

Figure 4.3: *Examples of defects from the four manufacturing techniques used*

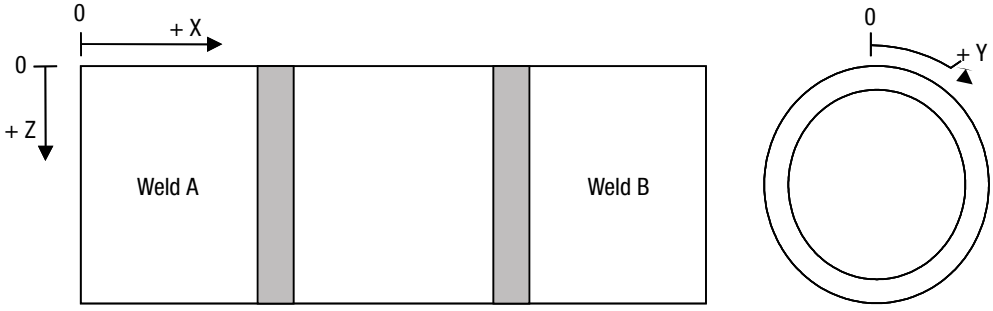

Figure 4.4: *The coordinate system used for the mock-up in the NESC-III inspection performance trial*

[4] During the post-test destructive examination the dimensions of the EDM defects could be accurately measured from rubber replicas, and were sectioned.

- PISC Type A: Sharp-edged PISC type A Notches; the defects were introduced by JRC-IE Petten by means of electro-discharging machining (EDM).
- LOF: Sidewall lack-of-fusion. introduced using the patch welding method.
- Technique "A": Smooth flaw technique (only present in weld A); this type of defect aimed to simulate inter-granular cracking and was introduced using a doped electrode technique.
- Technique "B": Simulation of intergranular stress corrosion crack, introduced by local use of a high carbon stainless steel filler metal.

The examination also took into account the results submitted by the inspection teams, so that reports of unintended indications could be assessed in order to provide information on false calls. Although two such locations were examined for both welds, no unintended defects were found. Weld A contained only circumferential defects and weld B contained both circumferential and axial defects. The final results are listed for welds A (austenitic) and B (Inconel) in Table 4.2 and Table 4.3 respectively. Figure 4.4 shows the coordinate system used.

Table 4.2: *The reference locations and coordinates of the defects in weld A (austentic)*

ID	Y pos. [deg]	Orien-tation	Tilt [deg]	Skew [deg]	Start X1 [mm]	End X2 [mm]	Start Y1 [deg]	End Y2 [deg]	Start Z1 [mm]	End Z2 [mm]	Length [mm]	TWE [mm]	Description
PISC type A													
A1	10	Circ.	0	0	318	319.5	5.6	14.4	45.6	52.1	27.0	6.5	Internal surface breaking (in weld material)
A7	264	Circ.	0	0	319.5	320.7	260.1	267	47.1	52.1	21.1	5.0	Internal surface breaking (in weld material)
Technique A													
A2	50	Circ.	0	0	319.5	319.6	48.3	51.6	48.5	52.1	10.0	3.6	Internal surface breaking (in weld material)
A4	138	Circ.	15	0	334.5	340	134.2	142.3	0.8	19.5	32.0	18.7	External - in buttering
A6	217	Circ.	15	0	338.8	339.8	213.5	219.8	1.4	5.2	25.0	3.8	External - in buttering
Technique B													
A9	331	Circ.	15	0	335.5	338	322.2	328	1.2	8	23.0	6.8	External - in buttering
A3	85	Circ.	15	0	327	333	83.4	90.7	37.2	52.2	29.0	15.0	Internal surface breaking (in buttering)
LOF													
A5	188	Circ.	15	0	332	333.7	187.2	188.8	41.5	47	5.0	5.5	LOF from triple point
A8	298	Circ.	15	0	334	336.5	297.3	301.9	29.1	38.5	18.0	9.4	LOF buttering/ferritic
A10	282	Circ.	–	–	315	315.7	277.6	287	43.2	43.9	23	0.7	Real manufacturing (pore)

Table 4.3: *The reference locations and coordinates of the defects in weld B (Inconel)*

ID	Y pos. [deg]	Orien-tation	Tilt [deg]	Skew [deg]	Start X1 [mm]	End X2 [mm]	Start Y1 [deg]	End Y2 [deg]	Start Z1 [mm]	End Z2 [mm]	Length [mm]	TWE [mm]	Description
PISC type A													
B2	80	Axial	0	90	700	730	79.7	80.3	44	52.2	30.0	8.2	Internal surface breaking (in weld material)
B4	155	Axial	0	90	706.5	721.5	154.9	155.2	49.2	52.1	15.0	2.9	Internal surface breaking (in weld material)
B6	265	Circ.	0	0	714	716	260.9	269.1	43.9	52.2	25.1	8.3	Internal surface breaking (in weld material)
Technique B													
B3	115	Axial	0	90	707.5	722	115.3	117.9	34.3	52.3	14.5	18.0	Internal surface breaking (in weld material)
B7	318	Axial	0	90	710	720	315.7	317.2	46.6	51.6	6.0	5.0	Internal surface breaking (in buttering)
LOF													
B1	25	Circ.	15	0	699	701	23.4	28.3	40.5	47.4	15.0	6.9	LOF from triple point
B5	194	Circ.	15	0	697.9	701.6	190.3	199.8	33.7	47.5	29.0	13.8	LOF from triple point

4.3 ANALYSIS AND EVALUATION OF THE RESULTS OF THE TRIAL

4.3.1 Inspection Performance

Detection performance

Detection performance was generally good for austenitic weld where five of the nine teams detected all the defects larger than the detection target (Figure 4.5). For the Inconel weld six of the eight teams detected all defects larger than the detection target (Figure 4.6). In the austenitic weld the 5 top teams demonstrated the robustness of their techniques by detecting 2 to 3 of the 4 defects smaller than the target size, whereas in the Inconel weld only one team reported the one defect smaller than the target size.

In general the detection performance was similar for the austenitic and Inconel welds, with average flaw detection frequencies[5] of 0.88 and 0.85 respectively. For the Inconel weld one team NP01 missed all defects. The team inspected only for circumferential defects, which meant that they missed 3 out of 3 defects larger than the detection target. The reported data suggests that the team found some indications in the vicinity of the defects, but all these were outside the agreed tolerances.

[5] Flaw Detection Frequency (FDF) is the number of defects detected by a team divided by the total number of defects in the volume inspected.

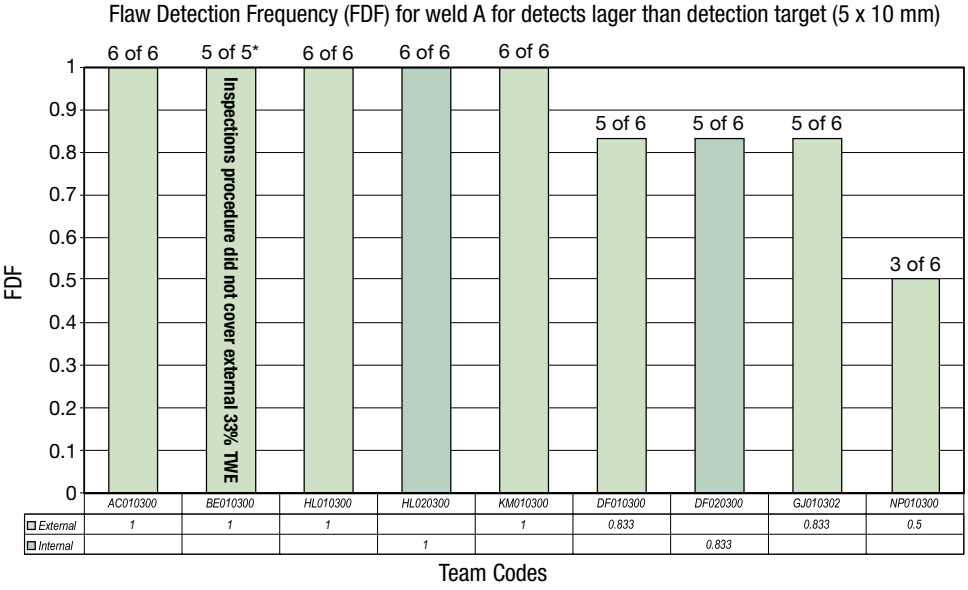

Figure 4.5: *Detection performance (FDF) in the austenitic weld for defects larger than the agreed defection target of 5 mm TWE and 10 mm length*

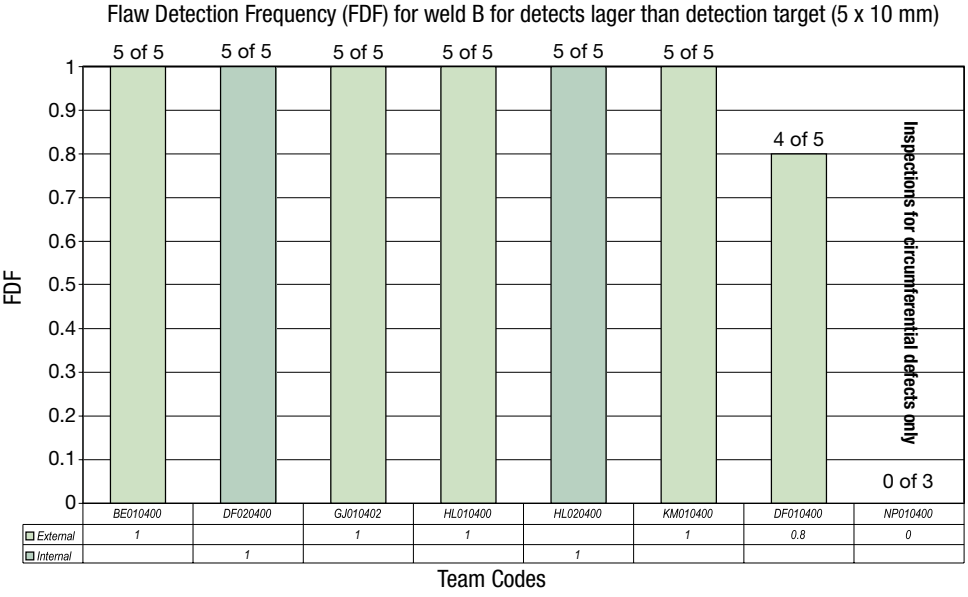

Figure 4.6: *Detection performance (FDF) in the Inconel weld for defects larger than the agreed defection target of 5 mm TWE and 10 mm length*

The ultrasonic techniques used for detection included pulse echo using single crystal and twin crystal probes in either shear wave mode or longitudinal mode, focussed probes and phased arrays; and techniques in tandem. The trial results, however, did not provide any evidence that the procedure or technique used had a significant influence on detection capability.

False calls

Only two teams (BE01 and KM01) reported false calls larger than the detection target in the austenitic weld. These were also the only teams that reported false calls in the Inconel weld. Detection rate is plotted versus false call rate for the austenitic and Inconel welds in Figure 4.7 and Figure 4.8 respectively. Here the y-axis (FDF) relates to the safety of an inspection and the x-axis (FCRD) relates to the potential cost of unnecessary repairs; for optimum performance a team's result should lie in the upper left corner (FDF > 0.8 and FCRD < 0.2). On this basis the general detection performance is considered good for 7 of the 9 teams in the case of the austenitic weld and for 5 of the 8 teams in the case of the Inconel weld. For the austenitic weld 3 teams detected all defects and had no false calls, for the Inconel weld 4 teams achieved the same excellent performance.

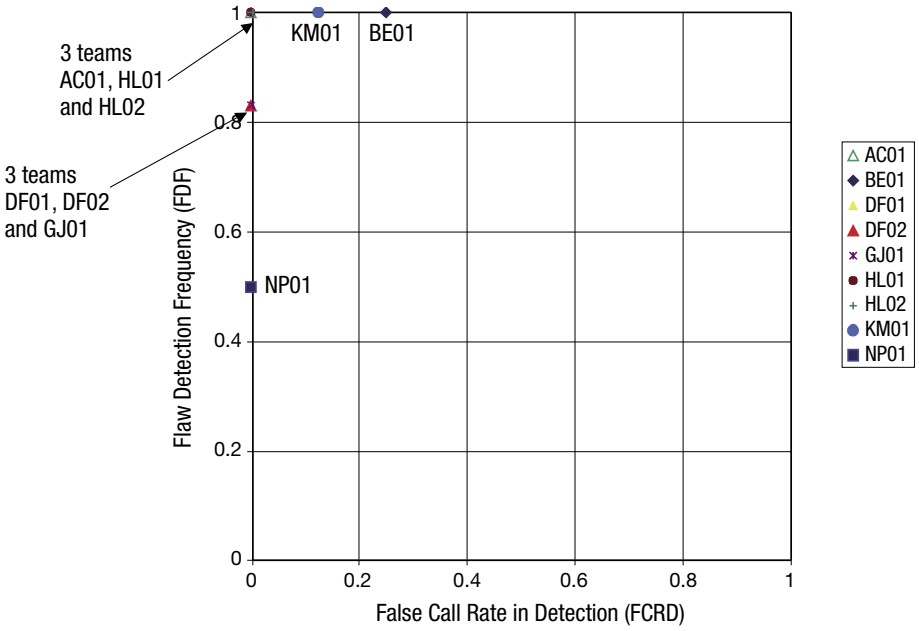

Figure 4.7: *Detection Frequency (safety) versus False Call Rate in Detection (efficiency) for the austenitic weld*

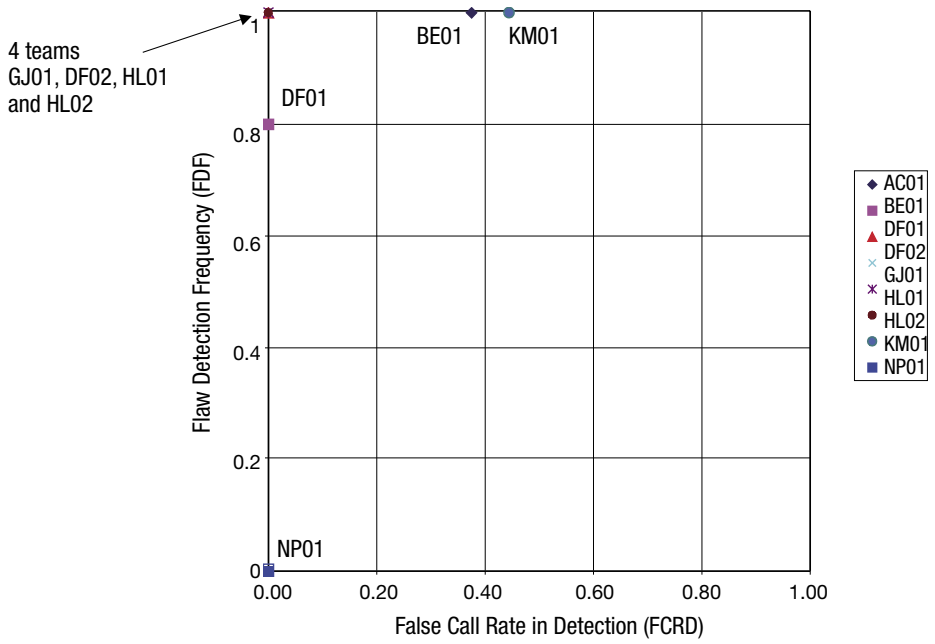

Figure 4.8: *Detection Frequency (safety) versus False Call Rate in Detection (efficiency) for the Inconel weld*

TWE sizing

In general there was a large scatter in the TWE sizing results for both welds. For the austenitic weld only two of nine teams had a RMS[6] error in the through-wall extent of 3 mm or less (Figure 4.9), of these only one team (GJ01) had sized all defects within the target of ±3 mm (Figure 4.10). For the Inconel weld none of the seven teams managed to size all defect within the target of ±3 mm. (Figure 4.11), and six of seven teams had at least one serious undersizing above 5 mm. The average RMS TWE sizing error was larger for the Inconel weld (5.2 mm) than for the austenitic weld (4.2 mm). In both welds there was a tendency for the teams to undersize the larger defects and oversize the smaller defects. These results from the internal inspections did not show any improvement in TWE sizing for either the austenitic or the Inconel weld when compared to those from the external inspections.

Length sizing:

Figure 4.12 and Figure 4.13 show the length sizing performance for the austenitic and Inconel welds respectively. For the austenitic weld five out of nine teams obtained a RMS error of 5 mm or less. One of the remaining four teams obtained less favourable results with a RMS error of 14.3 mm, which was caused by their strong tendency to overestimate the length. For the Inconel weld only one team (GJ01) achieved an RMS error in length sizing of 5 mm or less.

[6]Root mean square error (RMS) = $\sqrt{\sum (u_i - v_i)^2 / n}$, where u_i is the reference defect TWE v_i is the measured flaw TWE and n is the number of measurements.

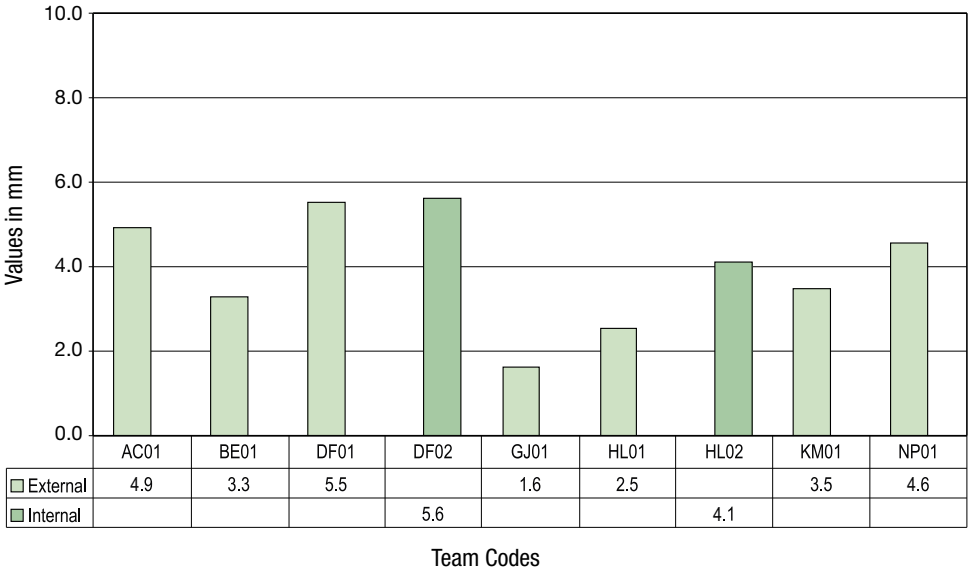

Figure 4.9: *RMS errors in through wall extent sizing for all defects larger than the detection target for the austenitic weld*

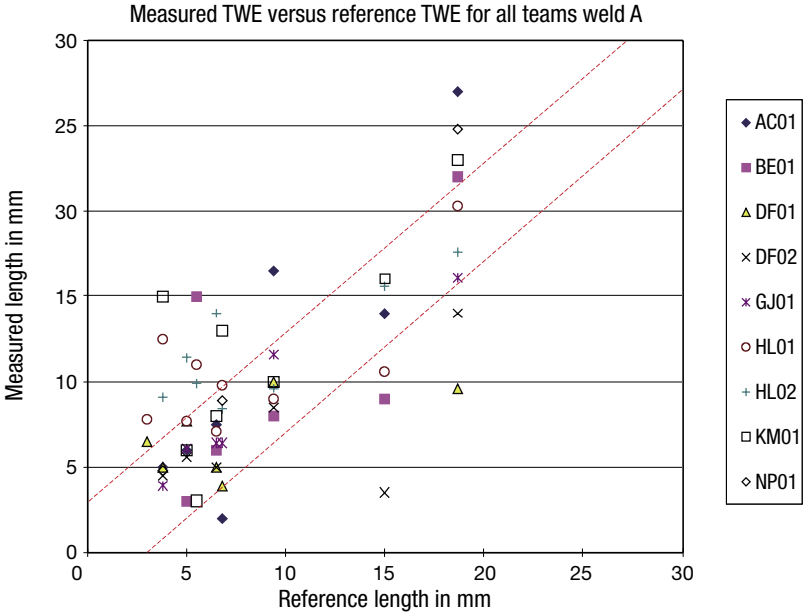

Figure 4.10: *Through wall extent sizing for all defects in the austenitic weld, showing the ±3 mm performance target*

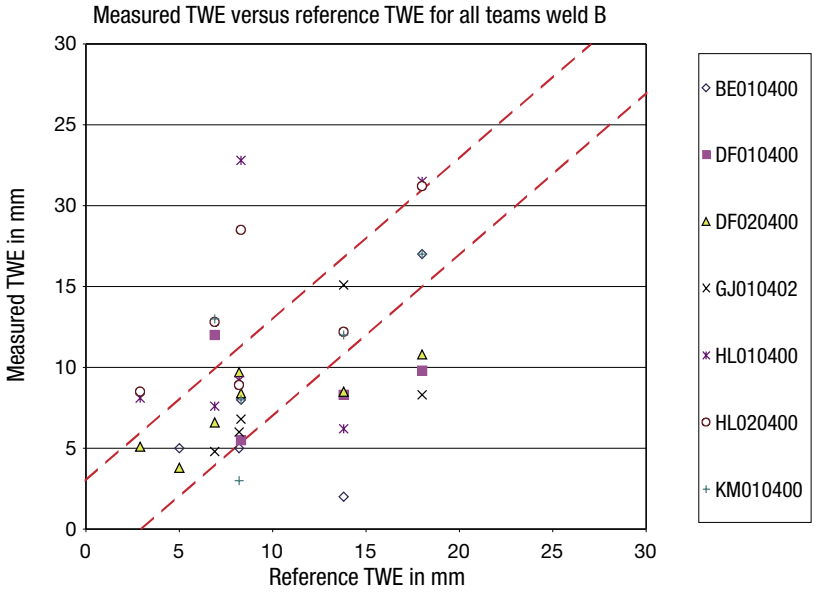

Figure 4.11: *Through wall extent sizing for all defects in the Inconel weld, showing the ±3 mm performance target*

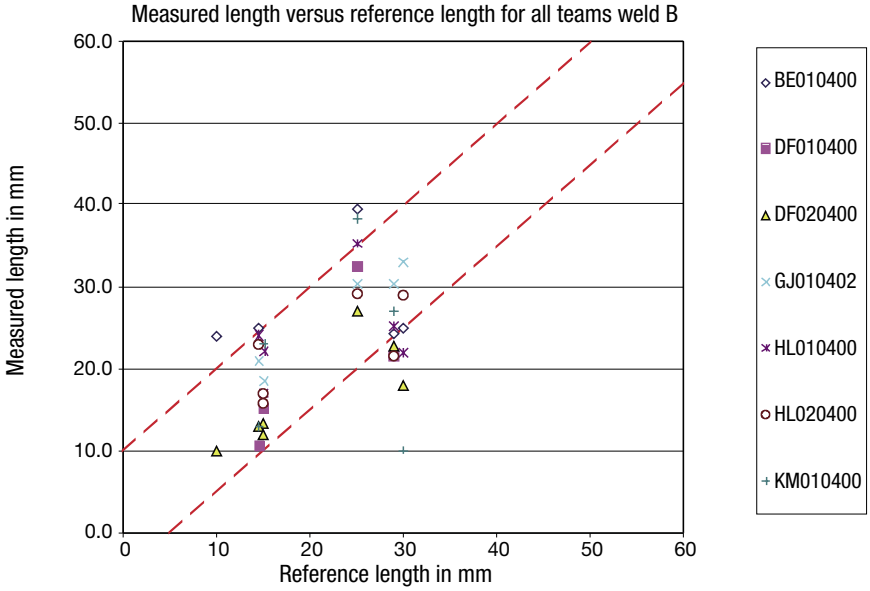

Figure 4.12: *Length sizing for all defects in the austenitic weld, showing the +10 / -5 mm performance target*

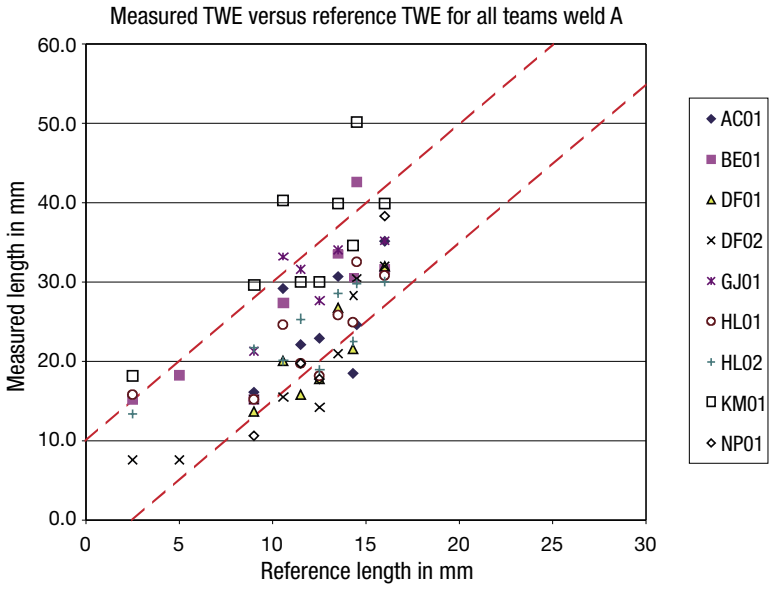

Figure 4.13: *Length sizing for all defects in the Inconel weld, showing the +10 / -5 mm performance target*

4.3.2 Factors Influencing Performance

For sizing the through-wall extent of a defect, the results have confirmed the importance of using the tip-diffracted wave from a crack tip. To some extent the variability in sizing accuracy appears to stem from the operator rather than the technique used. The same applies to length sizing, for which all the teams used amplitude drop techniques.

There were also several aspects of the trials that differed from the conditions normally encountered in on-site ISI. Firstly, access to the component was more favourable and the inspections were performed under laboratory-type conditions with easy access to both surfaces of the weld. During ISI on piping often only the external surface can be accessed. Secondly, there is the issue of surface finish since both the inner and outer surfaces were machined at the end of fabrication. A further related factor that could have had a beneficial effect on performance relates to the thickness and surface condition of the cladding on the ferritic pipe. In the present studies this was a 2-layer strip cladding machined down to a thickness of 5 mm. In the field this is not always the case and previous studies [36, 37] established that the surface finish associated with a strip-clad surface could have a profound effect on the amplitude of the ultrasonic beam entering the component. The issue of the cladding effect on the signal amplitude has also been dealt with in the ENIQ 2nd Pilot Study [38].

Another potentially beneficial factor was the length of time allowed for the inspections; this was one week for approximately 2 meter of welds. However, from information supplied by the teams

after the inspections it appears that many of the teams experienced time pressure in completing the sizing of the indications detected due to the relatively large number of defects present in the component and the effort needed to size these. In view of this it can be concluded that the length of time allocated was not a particularly beneficial factor.

The effect of the number of probes, i.e., techniques, used by a team has been evaluated, since a larger number of probes gives, in principle, more chances of obtaining a signal. However, examination of the results indicates that there is no significant difference in performance between teams that used few techniques and those that used more. Similarly, the spacing of the scan raster could, in principle, influence detection capability by giving more chances of obtaining a signal from a defect. In the present study most teams used a smaller raster (between 0.75 mm to 4 mm) than would generally be expected for on-site inspection. For sizing, it is common practice for inspectors to use small raster scans, so the sizing procedures used in the present study probably conform more to industrial practice.

4.3.3 Influence of Human Error

Mistakes were made in both sizing and detection that could be attributed to the inspection team personnel. In one case, did a team not detect any defect in the Inconel weld, even though they found indications in the vicinity of some of the defects. This is unlikely to have been due to insufficient capability of the inspection system used, since other similarly sized defects were reported with correct locations for the austenitic weld. Another team reported two defects in the Inconel weld, which were later explained by the team to have been a human error in the interpretation of the ultrasonic signals. Also some basic simple human errors were observed, such as the case of a typographical error in transferring the coordinates of a defect to the final report.

4.3.4 Best Inspection Practices

The results of the trial show that the majority of the teams achieved good detection results using a relative high sensitivity at the search stage (the same conclusion was reached in NESC-I and PISC exercises). This is therefore a best practice recommendation for good detection. It is recognised that some development studies will normally be required to set an appropriate threshold, probably close to the level of ultrasonic noise, but this will ensure that the best possible detection capability is achieved.

The sizing data indicate that the best accuracy in sizing the through-wall dimension of the defects is achieved by techniques based on obtaining and analysing signals from the crack tip. However, there was some variability in the sizing results and it appears that reliable sizing performance is a function of the use of the tip-diffracted wave, the inspectability of the material and of the inspector's capability. Adequate qualifications and proper training in applying the techniques to typical defects is also a strong requirement.

For length sizing the applied amplitude drop method together with the procedure of combining results from different techniques (transducers) sometimes result in some oversizing. In many cases

this performance is satisfactorily, but care should be taken in specifying the correct procedure for application in practice. Relative size of the defect and the width of the ultrasound beam must be taken into consideration, together with the accuracy of the scanning equipment.

4.3.5 Suitability of the Defects for ISI Qualification

There are several factors to be considered when assessing the suitability of various defect types for insertion in ISI qualification test assemblies. Principally, they must be representative ultrasonically of the type of damage to be detected, but as well it must be possible to define accurately the size and position of the test defects. This later task is usually much easier for artificial rather than realistic defects, for which destructive examination is usually required. Since destructive examination destroys the test assembly considerable expense can be involved, both in carrying out the destructive examination and, if necessary, replacing the test assembly. Another important consideration is that the insertion of an artificial defect in a test assembly does not disturb the surrounding material. In considering whether to insert artificial or realistic defects one of the main questions to be addressed is whether the artificial defects presents broadly the same level of difficulty to the detection and sizing techniques that are included in the inspection procedures.

In the present study, detection of the artificial EDM notches proved to be as difficult as for the more realistic defect types (Figure 4.14). The main difference between the defect types was that the EDM notches were smooth-sided whereas the realistic cracking had some roughness on the crack surfaces and, in some cases, even facets. This would tend to improve the detectability of the realistic cracking, although the results suggest that this was not a major influence. In addition, the EDM notches were fabricated with sharp radius tips making the ultrasonic response of the crack tip similar to that of the realistic cracking. This factor made the sizing task of similar difficulty. It is concluded therefore that the sharp radius EDM notches can be considered as suitable for use in ISI qualification test assemblies, provided that they adequately represent the damage to be detected and that the challenge to the detection and sizing techniques is of similar difficulty.

4.3.6 Extension of the Results into Practice

Good performance in the present exercise does not necessarily imply that a technique will provide reliable in-service inspection. Other factors can influence the effectiveness of an ISI, related both to conditions on-site and to the inspector. Notable amongst these are the qualifications and, particularly, the adequacy of the training of an inspector for the specific task. Both these aspects and the capability of the technique can be tested and validated in an inspection qualification exercise. The results of the NESC-III trial underline the importance of implementing such procedures.

The on-site factors that potentially reduce the effectiveness of the inspection include inspector fatigue due to long working hours and shift work, pressure to respect the allotted time schedule, concern about radioactive conditions and the tedium associated with repetitive work. None of these were considered in the NESC-III trial; however the PISC III programme [39] concluded that inspector effectiveness could vary significantly from day-to-day, particularly for manual inspec-

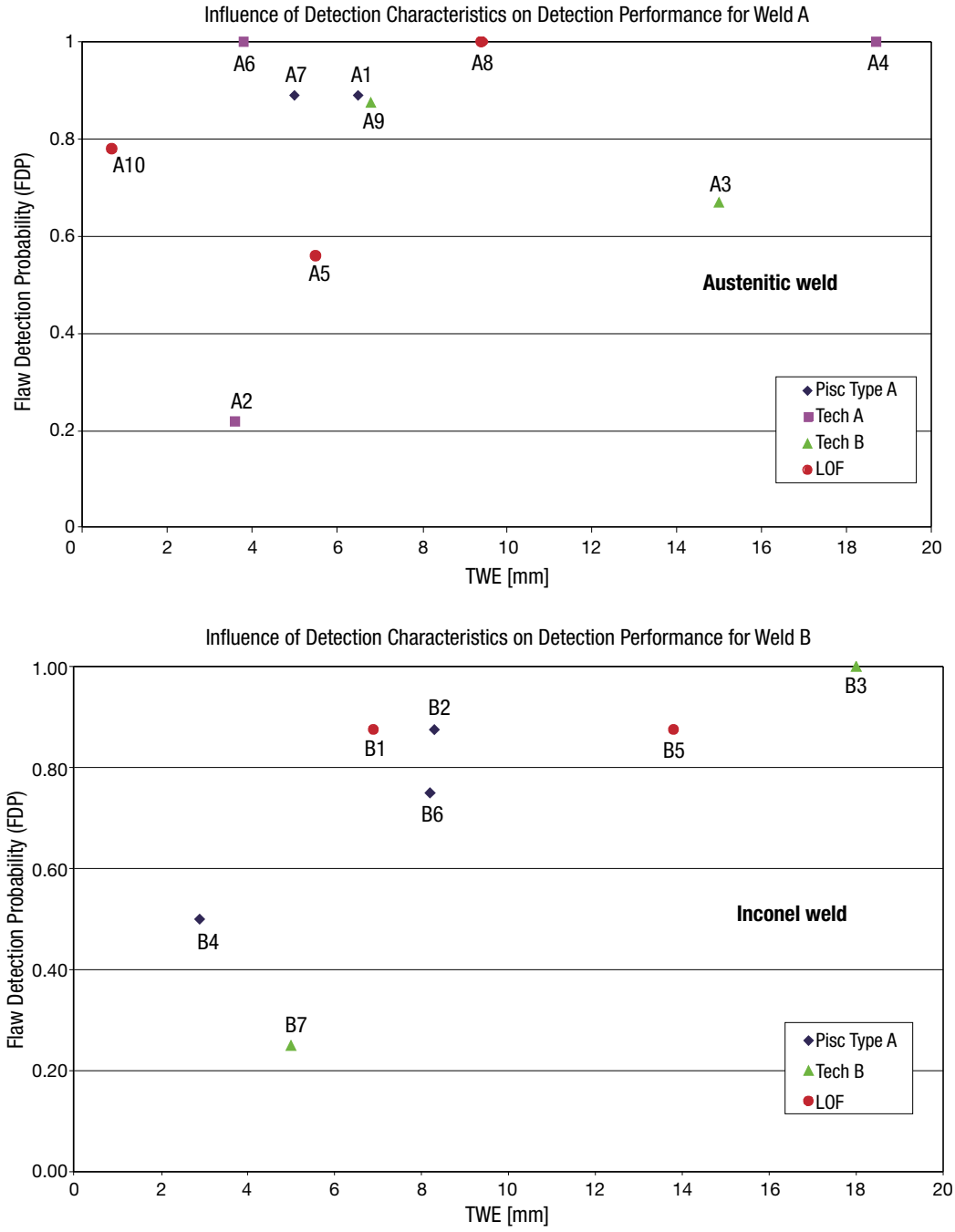

Figure 4.14: *Flaw detection frequency as a function of defects size and type*

tors, although the NESC and PISC results show clearly that human error can also occur in automated inspections. This range of errors can be controlled to some extent by the use of unambiguous inspection procedures, well-designed equipment, adequately trained inspectors, preferably having been trained for the specific application, and good supervision during the actual inspection. Preparing for and taking part in inspection qualification exercises addresses many of these aspects, but others, such as on-site supervision, need specific care when planning an ISI.

4.4 RECOMMENDATIONS

Based on the above the results the following recommendations are made with the purpose of ensuring, as far as is possible, firstly, that the capability of the entire inspection system, including equipment, inspection procedures and personnel, is adequate for the intended purpose, and secondly, that high reliability is achieved when the inspection is performed on-site.

- Special attention needs to be given to the definition of realistic inspection targets for both detection and sizing. Future round robin trials investigating inspection capabilities should also include some open test pieces in order to optimise inspection procedures in line with a normal qualification process.
- Precautions should be taken to reduce the incidence of human error as far as possible. This aim could be assisted by well-written unambiguous procedures both for data acquisition and data analysis as well as good quality control, training (including on-the-job training) of the inspection personnel. In addition it is recommended that the influence of in-service inspection conditions on the performance of the inspectors should be considered.
- In view of the observation that many of the teams used similar detection and sizing techniques yet obtained different results it is recommended that the entire inspection system, including the equipment, inspection procedure and personnel, should verified by inspection qualification methodologies on appropriate test specimens and defects prior to an on-site inspection to demonstrate that it is capable of meeting the specified inspection objectives. It is further recommended that, following completion of the NESC III project, a further analysis of the NESC III data should be made to investigate the influence of factors such as the quality and training of the inspectors; the scanner and equipment; and the data processing equipment and software, on performance and on the influence of the different defect types. In addition, such studies would analyse the procedures used by the teams that performed particularly well in order to obtain a better understanding of the techniques that could be used to achieve good results. Such studies would require the co-operation of the teams involved, but would be carried out without breaching the confidentiality observed in the round robin trials.

5 MATERIAL CHARACTERISATION

The materials characterisation activity focussed on reviewing the available ADIMEW material properties data and making recommendations regarding the testing and data analysis methods to be applied when characterizing a dissimilar metal weld. Some additional testing was performed using the limited remaining material from the ADIMEW programme, comprising hardness measurements, instrumented indentation tests and notched tensile tests.

5.1 MECHANICAL PROPERTIES

The ADIMEW partners performed an extensive testing programme using the AD01 mock-up. Emphasis was given to examination of the different material zones in the vicinity of the fusion line between the ferritic base metal (SA508) and the first buttering layer (E309L). The bulk of the tests were performed by VTT at 300 °C i.e the nominal operating temperature for these welds and that of the ADIMEW test. The results were detailed in the ADIMEW Final Report [40]. The tensile data was released to NESC-III as part of the pre-test datasheet [41].

5.1.1 Tensile properties

A series of standard tensile test experiments using 4 mm diameter cylindrical specimens were performed both at room temperature and at 300 °C covering the two base metals, the E308L weld material and the buttering. The tensile bars were taken out in the longitudinal pipe direction (corresponding to the main deformation direction during the large scale test) with the exception of the buttering specimens, which were extracted parallel to the weld fusion line. The sampling took place at four wall depth positions. Tensile strength and 0.2% proof stress data are reported in Table 5.1. The results fall within the range of typical literature values for the materials concerned.

Figure 5.1 compares the tensile properties of the various materials; in terms of yield strength the 316 L pipe has the lowest value. The nominal mismatch ratios at 300 °C are:
$M_{BU\text{-}A508} = 349/463 = 0.75$
$M_{WM\text{-}316L} = 346/213 = 1.62$

The under-matching effect for the buttering is enhanced by the presence of the hardened ferritic HAZ layer next to the fusion line. For this zone only room temperature data is available, but it indicates that the mismatch ratio is increased to 0.62. At the other side of the weld, the weld metal is over-matched with respect to the 316L pipe by 1.62.

Figure 5.2 compares the room temperature yield strength values of the ADIMEW and BIMET weld materials (see Table 5.2). It is evident that the 316L austenitic pipe used in ADIMEW has a somewhat lower yield strength than the 304L BIMET pipe. In the case of the BIMET weld, the nominal under-match for the butter layer was slightly more pronounced, with $M_{BU\text{-}SA508} = 0.62$.

Table 5.1: *Measured tensile properties at different locations of the ADIMEW dissimilar weld*

Material	Temperature T [°C]	Young's Modulus E [MPa]	Proof Stress $R_{p0.2}$ [MPa]	Tensile Strength R_m [MPa]
316L BM	20	186000	294	592
316L BM	300	139000	213	453
A508 BM	20	201000	513	671
A508 BM	300	172000	463	640
A508 CGHAZ	20	201000	677	782
E308L WM	20	194000	370	636
E308L WM	300	165000	346	441
E309L BU	20	197000	418	615
E309L BU	300	171000	349	462
BU_{FL}*	20	197000	384	615
arms	20	201000	591	711
arms	300	172000	566	679

*first buttering layer, ~0.5 mm from fusion line

Table 5.2: *Tensile properties of the materials in the BIMET dissimilar weld at RT*

Material	E modulus GPa	Yield Strength $R_{p0.2\%}$, MPa
Ferritic Pipe (SA 508)	205	584
Ferritic HAZ	210	698
Buttering (308L)	180	364
Weld (309 L)	180	373
Austenitic pipe (304L)	188	322
Arms (St 52)	191	343

With regard to the spatial variation of the tensile properties in the area immediately surrounding the defect location, two investigations were performed.

a) VTT performed tensile tests using sub-size flat specimens (1 x 2 mm cross-section) taken out parallel to the fusion line at two different though-wall depths corresponding to 1/3 and 2/3 of the wall thickness as part of ADIMEW. Figure 5.3 shows the resulting tensile strength and yield strength values at room temperature for a range of locations, starting from the ferritic base metal and crossing the other materials under consideration. Results from the tests on the 4 mm diameter specimens are also shown in this figure and demonstrate that there were no significant differences in the data from the two specimen types. The only exception was the coarse grained HAZ

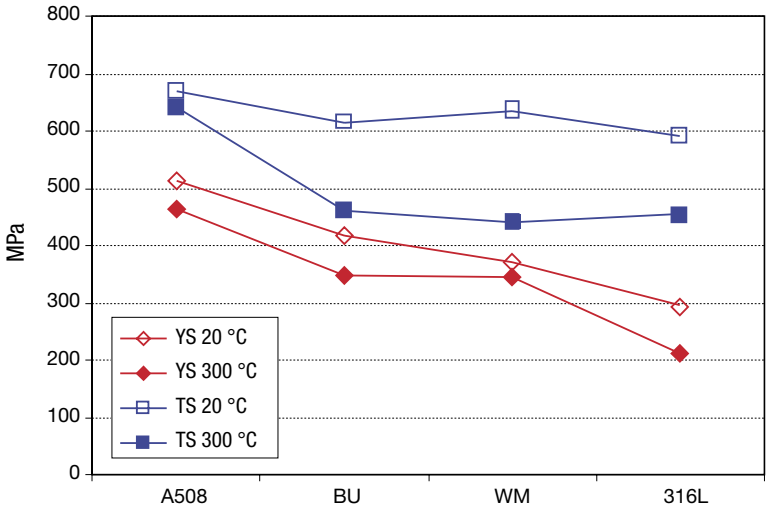

Figure 5.1: *Yield strength and ultimate tensile strength values for the pipe, buttering (BU) and weld (WM) materials*

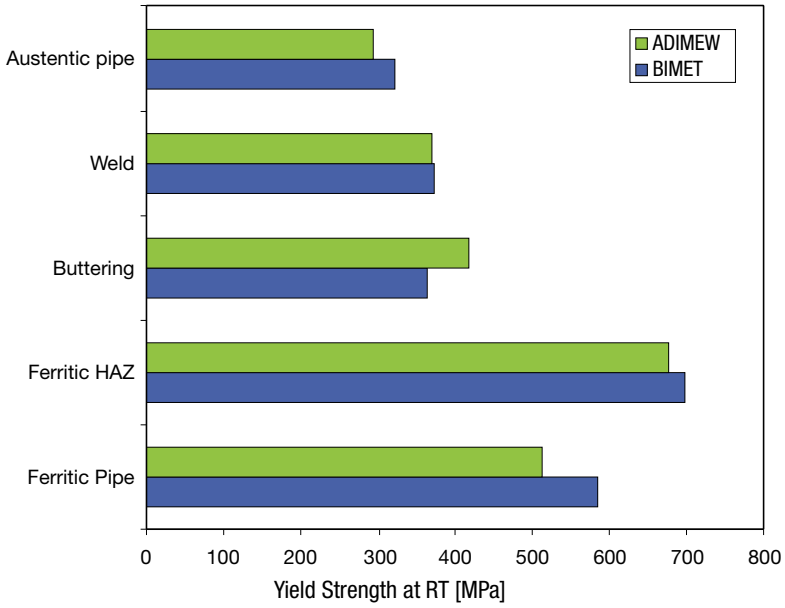

Figure 5.2: *Comparison of the room temperature yield strength properties of the materials in the ADIMEW and BIMET welds*

adjacent to the fusion line, for which the miniature tests detected considerably higher tensile and yield strength values. Also this was the only location for which a significant difference observed between the two sampling depths.

b) JRC performed two series of hardness measurements on a cross-section of the weld. The first phase looked at standard Vickers hardness measurements. The highest values were measured in the A508 HAZ close to the fusion line. This is as expected considering the presence of the coarse grained HAZ (CGHAZ) in this area. The average hardness value for the A508 base metal (203HV10) was higher than the equivalent value determined for the austenitic stainless steel 316L (152HV10), which correlated with the significant difference in tensile strength. For the weld it was found that the second buttering layer is harder than the other parts of the weld.

Micro-hardness measurements were also made in the fusion line region using a Vickers indenter and a load of 100gf. Figure 5.4 shows the profiles normal to the fusion line. A good 'relative' correspondence is noticed between this profile and the miniature tensile test data shown in Figure 5.3. The values reach a maximum in the HAZ close to the fusion line as expected. On the weld side, there is some evidence to lower hardness in the first 1 mm of buttering; however the average values for the buttering a 1.5 mm from the fusion line are only 5% less than those for the filler at the centre of the weld (Figure 5.5). These data have been used to verify the predictions of the finite element welding simulations (see §6.2.2).

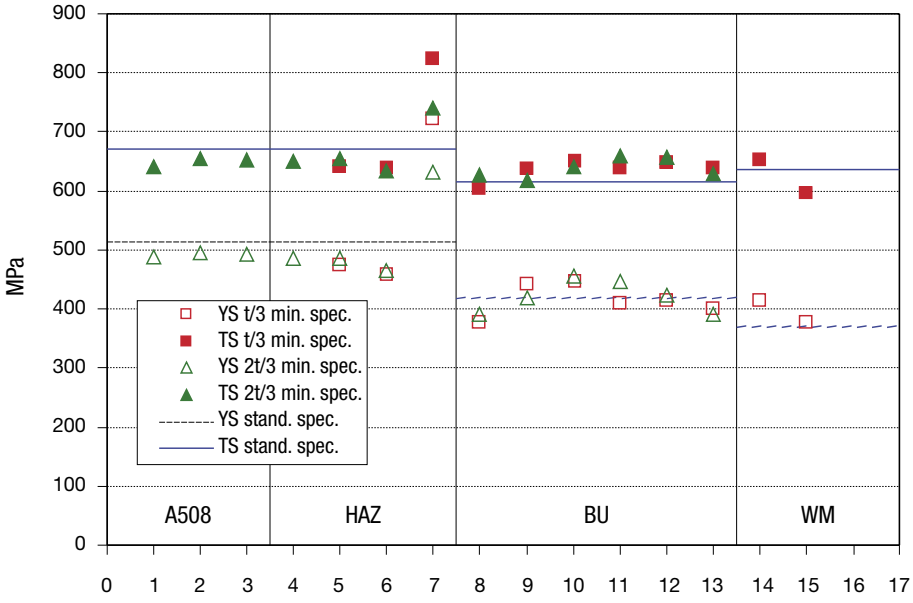

Figure 5.3: *Yield and ultimate tensile strength from room temperature miniature tensile tests, together with corresponding results from 4 mm diameter tensile tests*

5.1.2 Stress-Strain Data

The VTT tensile test data for the 4 mm diameter specimens was used to generate stress-strain curves for use in the finite element and fracture mechanics analyses. Some manipulation of the data was necessary since a lateral rather than an axial extensometer system was used in the tests. First, the uniaxial true stresses versus equivalent true strain curves were determined. The data points obtained were fitted using a Hollomon-type relation. The uniaxial stress was converted into equivalent, Bridgman corrected, true stress to arrive at the equivalent true-stress–true-strain curves. These are shown here in Figure 5.6. The advantage of the lateral stain measurement technique is that it allows the determination of stress–strain curves up to very large strain values (beyond necking). On the other hand it may result in less accurate strain measurements at the initial stage of the tensile test and in poor estimates of the elastic modulus. Consequently the E values in the data sheet were taken from standard literature sources. A control test was made for the 316L pipe base material at 300 °C using conventional axial extensometry; the resulting true stress-strain curve is in very good agreement with the ADIMEW data (Figure 5.7).

It is noted that attempts to fit power law i.e. Ramberg-Osgood, type relations proved unsatisfactory, with quite poor agreement at the initial stage of the curves. Hence a point-wise definition of the tensile curve was considered preferable, noting that if extrapolation to very high strain values is required, a linear or power law function can be used. The ADIMEW datasheet provided such piecewise data from the test results. JRC also developed a simplified representation but equally accurate of the curves for each material at 300 °C; these data are provided in tabular form in Annex 2. Strictly seen the stress – strain curves made available were sufficient for performing all the structural analyses planned within ADIMEW. Nevertheless additional experiments could be desirable to investigate the effect of the sampling location and the specimen direction could have been further explored. For example the E308L weld may show considerable anisotropy and could have been modelled by at least three different zones (top – mid – bottom) represented by three different tensile curves.

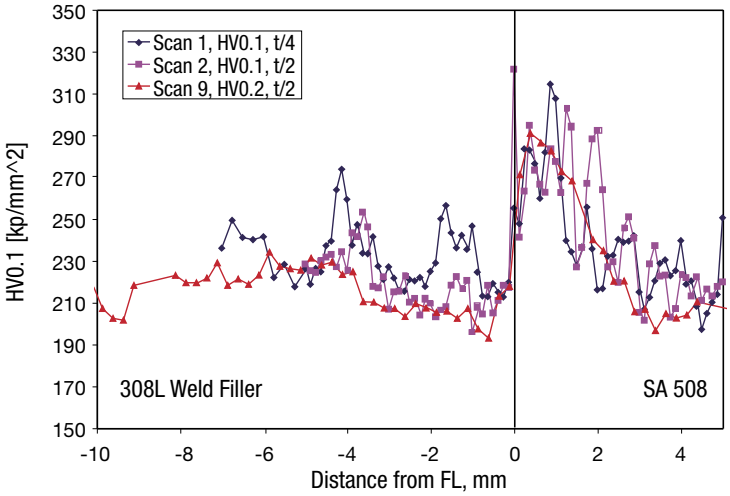

Figure 5.4: *Microhardness profiles across the fusion line at quarter (t/4) and half (t/2) wall thickness*

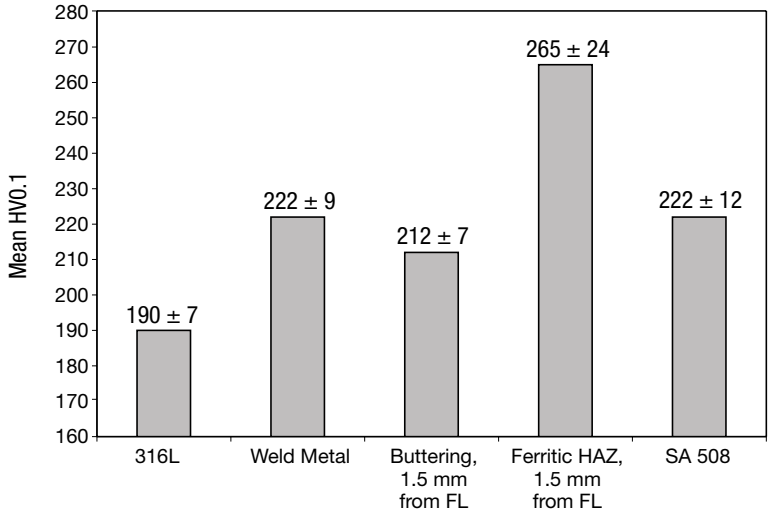

Figure 5.5: *Average microhardness values from the ADIMEW weld*

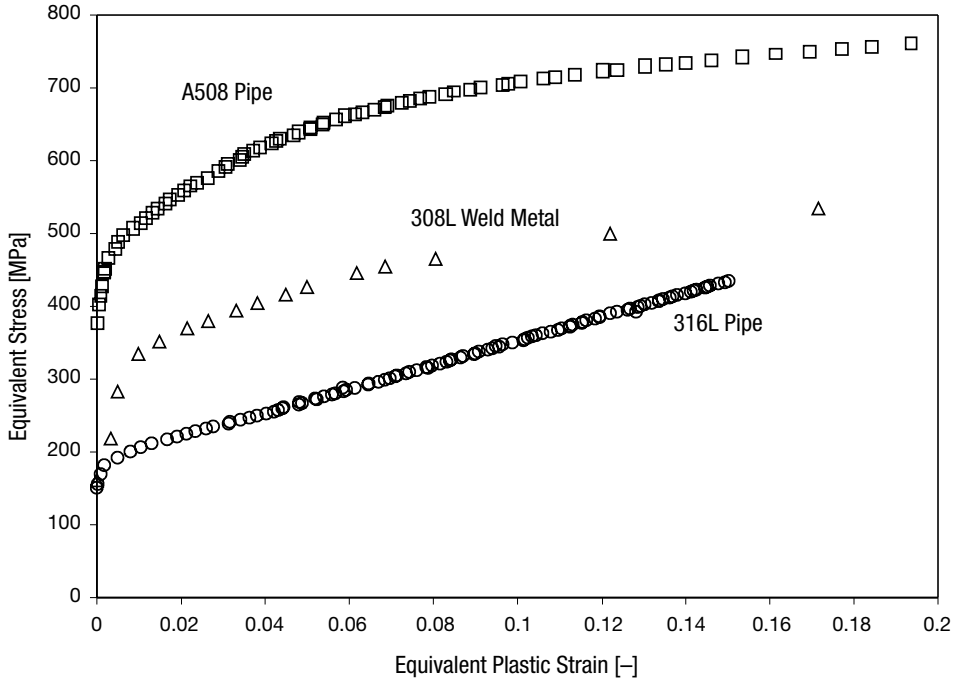

Figure 5.6: *Stress-strain data sets for the ADIMEW weld materials at 300 °C*

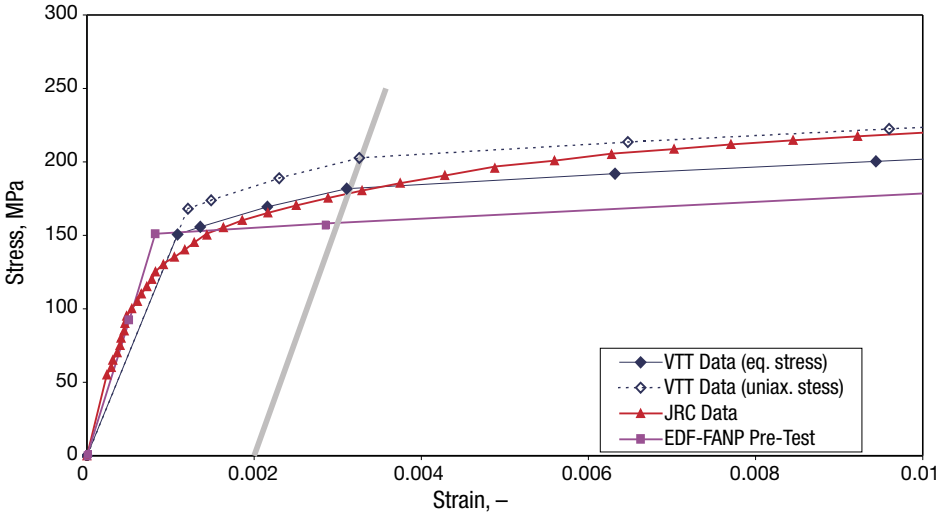

Figure 5.7: *Comparison of stress-strain curves for 316L at 300 °C: VTT data for 4 mm diameter specimens with a diametral extensometer; JRC data for 8 mm diameter specimen with an axial extensometer*

5.1.3 Instrumented indentation tests

This experimental technique uses a hard ball indenter system. By monitoring the indentation depth as a function of the load applied throughout the test, several hardness-related parameters can be derived as well as estimates of the tensile strength and the true stress–true strain curve. The latter is evaluated via determination of Meyer's constants, which are then converted into the two parameters C and n in Ludwik's stress–strain power law $\sigma = C.\varepsilon^n$. The ultimate tensile strength is directly obtained from the true stress–true strain curve. This quasi non-destructive method is particularly suitable for characterizing the mechanical properties of various (sometimes narrow) material zones at welds, which can be easily addressed by the 1 mm diameter indenter involved. It could also be potentially used on components in service to assess changes in properties due to ageing.

The ADIMEW mock-up offered an opportunity to benchmark this innovative technique with results from tensile experiments. The experimental work was performed by Mat-Tec and funded by the Swiss Federal Nuclear Safety Inspectorate (HSK). The measurements [42] were carried out on a cross section of the ADIMEW weld that had been polished and slightly etched. Figure 5.8 shows the indentation data for the base metals A508 and 316L as well as for the weld metal 308L. Figure 5.9 compares the corresponding calculated true stress–true strain curves with the results from the standard ADIMEW tensile tests. The best overall correspondence is observed for the ferritic base metal. The estimates produced for the austenitic materials seem to be less accurate with respect to tensile strength (in the case of 316L) or true stress–true strain behaviour (for E308L). It should be noted that austenitic stainless steels generally shows a rather linear stress-strain relationship at higher strain values, which is not captured by the power law as assumed in the calculation method.

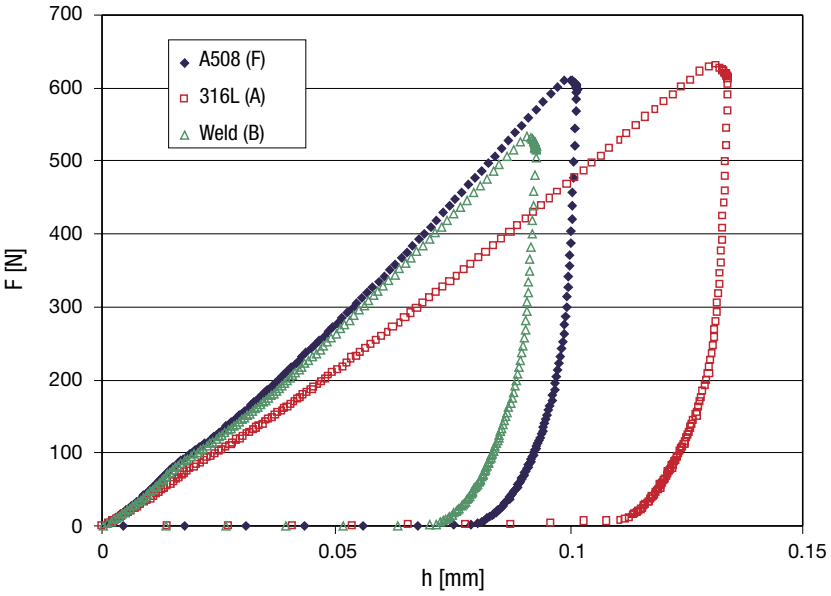

Figure 5.8: *Measured indentation curves for the base materials 316L and A508 and the weld metal*

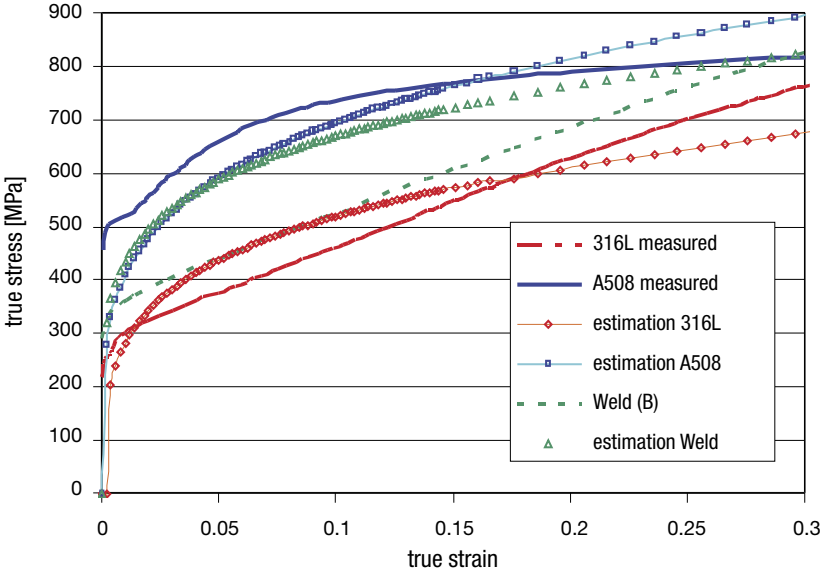

Figure 5.9: *Estimated stress-strain curves from instrumented hardness testing compared with tensile test results*

5.2 FRACTURE TOUGHNESS

5.2.1 Data Available

In dissimilar welds the fracture behaviour is sensitive to the local microstructure sampled by the crack tip and the constraint conditions due to mismatch effects. In ADIMEW several series of fracture tests were carried out both at room temperature and at 300 °C by four different laboratories. The overall aim was to determine the J-integral near the onset of stable crack propagation and to estimate the crack growth resistance curve[7]. Several series of specimens were prepared so as to study the fracture behaviour of crack tip in different material zones in the vicinity of the A508–E309L fusion line. These crack tip locations were:

a) The CG-HAZ in the ferritic A508 material: although the parent ferritic steel should demonstrate high toughness upper shelf behaviour, these tests were intended to check for any propensity to brittle fracture in the altered HAZ microstructure adjacent to the fusion line and corresponding to the region of high yield strength as evidenced in the tensile and hardness tests.

b) The fusion line (FL), on the buttering side: these tests were expected to detect and characterise any so-called "fast ductile growth" can occur in the weld metal [44], possibly leading to cleavage in hard regions of the adjacent HAZ.

c) The 1st buttering layer (BU) at 1 to 2 mm from the fusion line: these tests were intended to determine the initiation toughness and crack propagation characteristics in the 1st buttering layer. It was expected that the crack tip plastic zone would remain sufficiently contained so as not to be directly influenced by the mismatch to the stronger A508 material at the near by fusion line. This location corresponds to the position and orientation of the notch in the ADIMEW test mock-up.

d) The 309L weld metal (WM)

Several different specimen types were used: 10x10mm sub-sized SE(B) specimens, 20x40mm SE(B) bars and standard CT25 specimens. For the larger specimens this required use a weld build-up technique to allow the crack to be positioned with the same orientation as in the mock-up i.e. in the buttering, parallel to the fusion line (Figure 5.10). For most of the tests the specimens were fatigue pre-cracked to a nominal a/W value of 0.5 but, since the test mock-up used an EDM notch with no fatigue pre-cracking, the effect of notch tip radius on the fracture toughness was also assessed through a series of similarly notched C(T) specimens (also with a/W ≅0.5).

There are no specific fracture test standards for dissimilar welds and the labs followed procedures for homogeneous specimens without any correction: TWI tested SENBs according to BS 7448 [45], VTT followed the ASTM standard E1820-01 [46] for sub-size SENBs, BZF used the E1820-99 version for CT-25 specimens and Framatome-ANP used the GFR French method [47], also with CT25 specimens. Table 5.3 summarises the results. Several tests did not lead to 'valid' J initiation values (J_{Ic} for ASTM, $J_{0.2BL}$ for BS or $J_{0.2}$ for GFR), largely due to values being above the maximum foreseen for the specimen size or because of crack deviation problems. J values were calculated

[7]A series of mixed-mode tests were also performed using the sub-sized SE(B) specimen geometry. Although the raw data have been reported [43], these have not been analysed up to now.

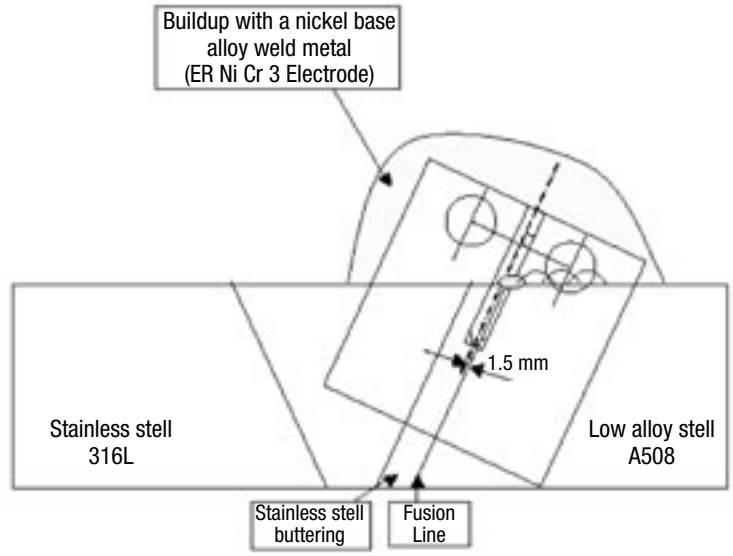

Figure 5.10: *Sampling of fracture mechanics specimens from the ADIMEW weld, illustrating the need for an weld build-up to accommodate full sizes (in this sketch a CT, but a build-up was also required for the 20 mm x 40 mm SE(B) specimen)*

from the area under the load vs. load-line displacement curves. This approach had been successful for BIMET, although a load vs. CMOD approach had previously been recommended for tests on welds [48]. The CTOD parameter was directly included in the programme, however it was measured and reported for several of the SE(B) tests performed by TWI.

Figure 5.11 shows the fracture toughness values for the 300°C temperature level in terms of the distance of the initial crack tip from the fusion line. As expected the buttering is the less tough than either the bulk weld metal or the coarse grain heat affected zone. However there is significant variability din the values reported for different specimen types. In particular the $J_{0.2BL}$ values from the SE(B) specimens (55/54 kJ/m^2 from 10 mm x 10 mm specimens and 64/67 kJ/m^2 from 20 mm x 40 mm specimens) are significantly lower than the values from the C(T) tests (156 kJ/m^2 for the single specimen test and 178 kJ/m^2 for the multi-specimen series).

The corresponding JR-curves are shown in full in Figure 5.12, while Figure 5.13 provides details of the initial growth up 2 mm crack extension. Valid *J*-R curves were obtained up to 1.75 mm for 20 mm x 40 mm SE(B) specimens and up to 2 mm for C(T) specimens. It is noticeable that the SE(B) tests at TWI (with unexpectedly low toughness values) show no experimental blunting line trend in the early part of the tests. The flattening R-curve for crack growth observed on large SE(B) specimens of more than 1 mm is not seen on pre-cracked C(T) specimens, probably due to the observed tunnelling and loss of constraint when the crack deviated out of the side grooved plane.

Table 5.3: *ADIMEW Fracture Toughness Data at 20 and 300 °C*

Specimen type	Dimensions B, W, L mm	Procedure	Temp. °C	Notch location	No. tests	Specimen	$J_{0.2BL}$ kJ/m²	Notes
SENB	10, 10, 55	BS	300	FL	2	A2-3 A3-1	50 62	
	10, 10, 55		300	$BU_{1.5}$	2	A2-2 A3-3	58 53	Crack deviation
	20, 40, 100		300	$BU_{1.5}$	3	W01-04 W01-05	63 59	
CT	CT-25	GFR	300	$BU_{1.5}$	2 4	Single spec Multiple spec.	156 178	Crack deviation and tunnelling
CT, with notch instead of fatigue pre-crack	CT-25 Radius 0,2	ASTM	300	BU_{1}	1	BZF-4	130	
	CT-25 Radius 0,2		300	BU_{2}	1	BZF-2	266	
	CT-25 Radius 0,1		300	BU_{2}	1	BZF-1	221	
SENB	10, 10, 55	BS	300	WM	3	Average	162	
	10, 10, 55		300	A508 CGHAZ	3	A3-2	137	
SENB	10, 10, 55	ASTM	20	FL	2	03 06	267 156	
	10, 10, 55		20	$BU_{1.5}$	2	03 06	173 249	
	10, 10, 55		20	BU_{2}	2	03 06	272 308	
notched CT	CT-25 Radius 0,2	ASTM	20	BU_{2}	1	BZF-5	345	
CT	CTJE25 B = 25	GFR	20	$BU_{1.5}$	2 + 1	Single spec	216 215	

Notes:
All the specimens were pre-cracked to give a/W ≅ 0.5.
$J_{0.2BL}$: this term is used to indicate the crack initiation value derived from the intersection of 0.2 mm offset blunting line with the J vs. a data, although the definition of blunting line slope varies according to the test procedure followed.
$BU_{x.x}$ indicates the notch is located in the weld buttering at a distance "xx" mm from the fusion line
FL indicates the notch is located on the fusion line tending towards the buttering side,
The pre-crack or notch orientation is parallel to the fusion line in all cases.
For the VTT tests the sectioning depth from surface (03 = 1/3 t or 06 = 2/3 t) is noted.

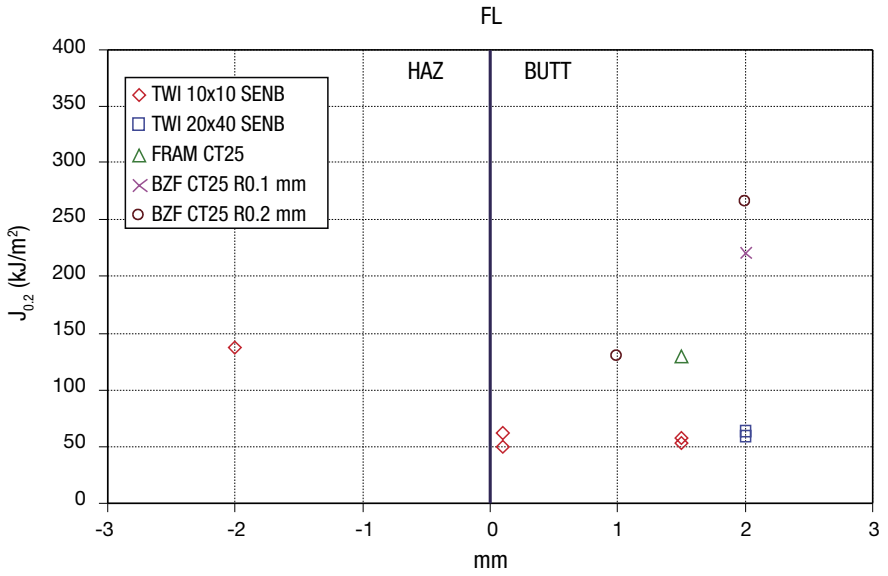

Figure 5.11: *$J_{0.2BL}$ values at 300 °C compared to the distance of the initial crack tip from the fusion line*

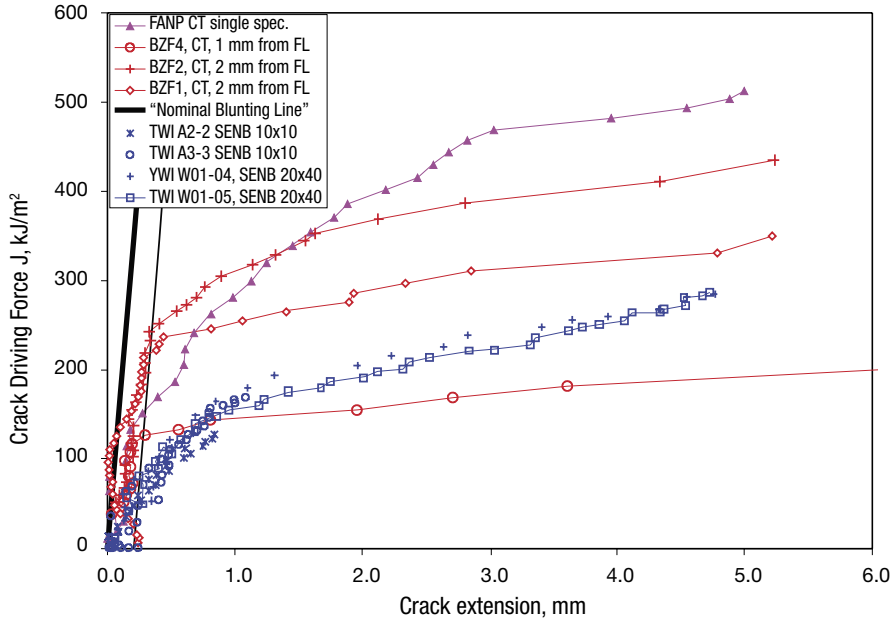

Figure 5.12: *Full crack growth resistance curves measured at 300 °C*

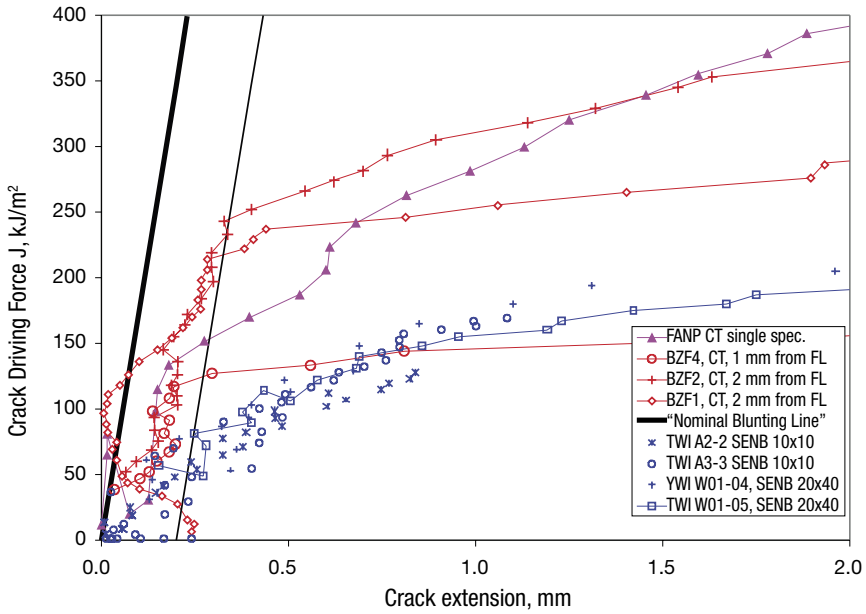

Figure 5.13: *First 2 mm of the JR curves measured at 300 °C*

The specimens with EDM starter notches instead of fatigue pre-cracks at 2 mm from the fusion line produced higher values of $J_{0.2BL}$ relative to that obtained from fatigue pre-cracked specimens, as would be expected. This difference is also likely to have been slightly enhanced by the fact that the test standard used in this case (ASTM E1820) imposed a blunting line of slope $2\sigma_Y$, i.e. two times the flow stress of the material around the crack tip. This is lower than values of $3.75R_m$ used for the SE(B) specimens tested to BS7448 and $4\sigma_f$ used for the C(T) specimens tested in accordance with the GFR procedure. The specimen with a notch 1 mm from the fusion line produced a much reduced fracture toughness and a far flatter JR curve than the other C(T) or SE(B) specimens.

Figure 5.14 provides an overview of the toughness results from the tests performed at ambient temperature. The SE(B) tests (using 10x10 Charpy-size specimens) confirmed that that the lowest toughness is observed in the first buttering layer close to the fusion line. Only in this area was a significant variation detected between the 1/3 and 2/3 through-wall thickness location, with the former providing the lowest $J_{0.2BL}$ value. For what concerns JR curves, these sub-size bend bars only produced a limited amount of crack growth (typically 1mm), from which the valid crack length data were limited to approximately 0.5 mm. Moreover the J measurement capacity was only 100 kJ/m^2.

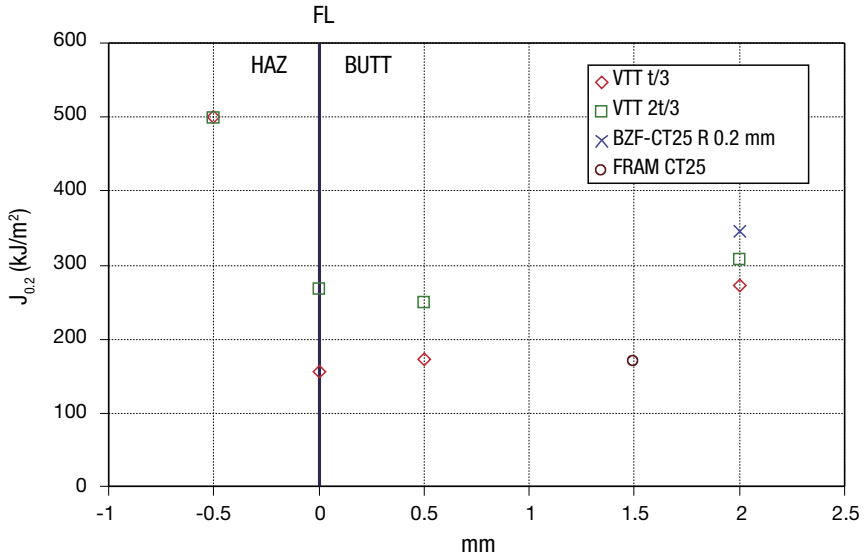

Figure 5.14: *$J_{0.2BL}$ values at room temperature (VTT used 10x10mm SE(B) bars, Framatome used CT25 specimens and BZF used CT25 specimens with a starter crack tip radius of 0.2 mm)*

5.2.2 Discussion

5.2.2.1 η factor for the experimental determination of J

When analysing the J-R test data, the plastic component of J is derived from the formula:

$$J_{pl} = \frac{\eta \times A_{pl}}{B_N \times (W - a)}$$

where U_{pl} is the area under the load vs. plastic load-line displacement curve, W is the specimen width, a is the crack length and B_N is the net specimen thickness (B_N = B if no side grooves are present). The factor η can be determined from load-line displacement data (η^{VLL}) or from CMOD data (η^{CMOD}) and is also a function of the a/W ratio. Current test standards (BS, ASTM and GFR) for homogeneous specimens with a/W=0.5 specify η^{VLL} values of 2.0 for SE(B)s and 2.261 for CTs, and these were used to analyse the ADIMEW test data, although the specimens are comprised of distinctly mismatched materials[8]. The above approach is consistent with the recommendation of Wang et al [49] that standard J estimation procedures are accurate to within 10% error if the 0.5<M<1.3. The recommendations [48, 49] that the CMOD approach should used for fracture tests on welds i.e. using η^{CMOD}, was not followed in either BIMET or ADIMEW.

[8]For the ADIMEW weld M ≅ 0.75.

Considerable work has been performed to establish the effect of mismatch on η^{VVL} and η^{CMOD} for different fracture specimen geometries. However these typically consider a symmetrical arrangement with a deep crack in the centre of a weld and asses the sensitivity of the calculated J value to weld width h, mismatch ratio M and strain hardening exponent. As such, the results are not directly comparable to the crack position in either the ADIMEW SE(B) or C(T) specimens, in particular for those with fusion line cracks. Nonetheless, the ADIMEW buttering specimens can be assessed according to these models by assuming that the weld width parameter h is given by a nominal distance to the fusion line of 1.5 mm. Kim et al's analysis [50] shows that for the SE(B) geometry with M=0.65, the η^{CMOD} rises 2.9, compared to the widely accepted value of 2.7 for homogeneous specimens [51]. For a C(T) geometry with M=0.75, η^{CMOD} rises to 2.6 compared to a value of 2.26 for a homogeneous specimen.

FE simulations provide another approach to checking the validity of η values and AREVA NP made such an analysis [52,53] for one of the two C(T) specimens tested using the partial unloading compliance method (specimen 2196-1, crack at 1.5 mm from the interface, $J_{0.2BL}$ = 156 kJ/m^2 at v_{LL} = 1.35 mm). Numerical simulations of the specimen behaviour up to initiation were conducted using small and large displacement hypotheses, calculating J from the area under the computed load-line displacement curve. Excellent agreement between computed and experimental results was obtained up to v_{LL} = 1 mm, indicating that crack growth began at about this point, which corresponds to a J = 97 kJ/m^2. On this basis the reported $J_{0.2BL}$ value appears overestimated. The J values were also computed using the Rice integral [54] and the G-Theta method [55,56]. The results were slightly lower than those obtained using the experimental or numerical load-displacement curve. This shows that for this specific specimen the η factor is 6.7% lower than the value given by the standard formula for homogenous material. This difference may be partly due to the use of a 2D model, but it is consistent with other results showing the mismatch influence on the η factor of non-homogeneous C(T) specimen to be quite low.

An FE simulation for the SE(B) geometry was also made [79]. For v_{LL} = 0.98 mm and CMOD = 0.7 mm, the G-Theta estimate of J is 83 kJ/m^2, compared to the measured $J_{0.2}$ value using the ASTM formula for homogeneous specimens of 59 kJ/m^2 This result implies that the η^{VLL} value differs from that for a homogeneous specimen (η^{VLL}=2) and that for mismatched specimens its value should ideally be evaluated based on the distance of the crack to the interface.

5.2.2.2 Crack deviation from the notch plane

The deviation of a crack out of its original plane is a risk in all bi-material specimens due to the presence of shear stresses along the interface, which are induced by the differences of material properties. In this present case in which the buttering is overmatched by the ferritic steel in both the elastic and plastic regimes, under mode 1 loading a crack parallel and close to the interface deviates away from the interface. This effect diminishes when the crack is sufficiently far away from the interface. A significant crack deviation was observed in both the SE(B) and the C(T) specimens. In all these cases, the fatigue crack deviated from the plane of the notch at an angle of 25^o to 33^o, veering away from the fusion line and further into the buttering. For the case of the Charpy-size SE(B) bend bars, the specimens were used for the actual fracture tests at 300 ^{o}C but the side-grooves were machined from the tips of the deviated fatigue cracks. The remaining buttering bend bars were fatigued in the presence of shallow side grooves, guaranteeing straight crack extension.

These were then deepened to 10% prior to the fracture test itself. This two-step procedure was also applied to the C(T) specimens tested by AREVA NP, but proved ineffective since the fatigue veered away from the fusion line in any case. Also, as the side groves machined just before the fracture experiment were positioned at the initial starter notch position and not at the actual fatigue crack tip, the crack tip constraint at the edge of the actual crack would have been reduced and the plane strain state limited to the specimen centre. Indeed crack tunnelling was observed in both the C(T) specimens Moreover, the use of a net specimen thickness of 20 mm did not reflect the actual situation during fracture testing. These two aspects together suggest that the J initiation values obtained from the pre-cracked C(T) specimens are overestimates. Combining this with a possible 7% overestimate of η (see section 5.2.2.1 above) leads to corrected $J_{0.2}$ value as low as 100 kJ/m^2.

5.2.2.3 Influence of the distance of the crack tip from the fusion line

The ADIMEW test programme has produced limited information (see Figure 5.11 and Figure 5.14) on the influence of the distance of the initial crack or notch tip in the buttering from the fusion line:

- The TWI SE(B) tests at 300 °C for crack tips at the fusion line[9] and at 1.5 mm into the buttering produced little variation in the reported $J_{0.2BL}$ values. In terms of J-R curves, the fusion line tests used sub-sized SE(B) specimens (10 mm x 10 mm section) so that the amount of valid was very limited, precluding any assessment in this respect.
- The VTT tests at room temperature showed that the lowest $J_{0.2BL}$ values were obtained either at or very close (0.5 mm) to the fusion line. Again the fact that sub-sized SE(B) specimens were used means the J-R curve data is limited. However as shown in Figure 5.15, one specimen produced a distinctly flatter J-R curve.
- The results of the BZF tests on notched CTs at 300 °C showed that the specimen with a notch 1 mm from the fusion line produced low initiation toughness and a distinctly flat J-R curve with respect to the tests with notches at 2 mm from the fusion line. However the exact crack growth path was not reported.

This evidence therefore provides some support to the hypothesis that enhanced ductile tearing can occur in the buttering very close to the fusion line. This phenomenon is likely to be influenced by the high local constraint effect due to the hard adjacent HAZ and microstructural features. In this respect Wu and Knott [44] report a high local density of inclusions in the buttering adjacent to the interface of a similar safe-end weld. Up to now such detailed microstructural investigations have not been performed for the ADIMEW weld.

5.2.2.4 Comparison to the BIMET data

Figure 5.15 compares the BIMET J-R curves for the buttering layer and the fusion line with selected results from the ambient temperature tests conducted in ADIMEW. The SE(B) tests were performed in both cases by VTT using sub-size specimens. The initiation toughness values from for the specimens with crack tips approximately 2 mm from the fusion line produced comparable results for both welds. The BIMET data also produced some evidence of reduced toughness and resistance to tearing close to the fusion line.

[9]It should also be noted that the fusion line has an inherent waviness, so that the microstructure and constraint conditions at the initial crack tip may vary from specimen to specimen.

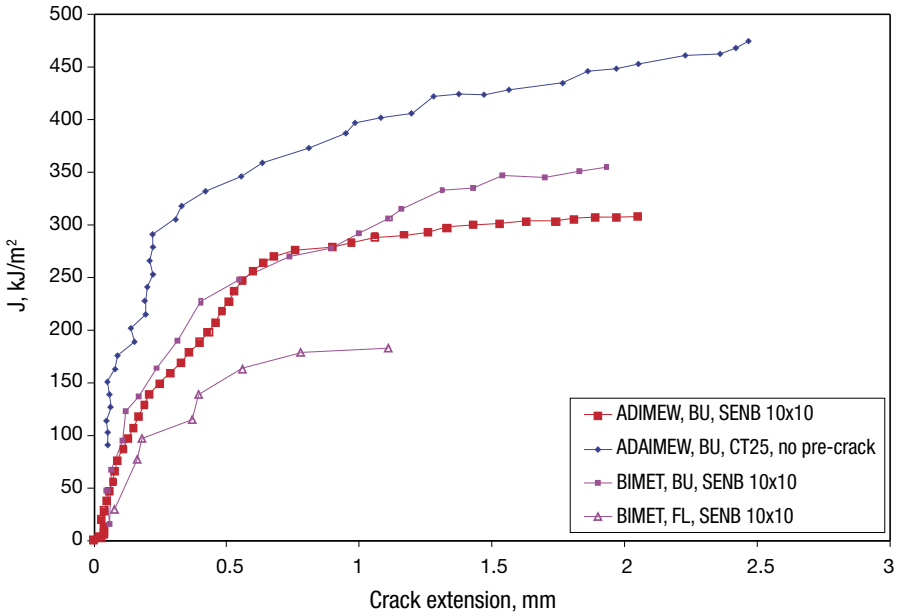

Figure 5.15: *Comparison of J-R data at ambient temperature from the BIMET and ADIMEW materials testing programs*

5.2.2.5 CTOD data

The CTOD method provides an alternative to the J-based approach and is considered relevant to situations involving inhomogeneous material where the path-independence of J may be questionable, for instance in the vicinity of a weld fusion line. It was used in the BIMET project in the form of the δ_5 parameter. As was explained above, in ADIMEW priority was given to J-R tests, on the basis that the application of the CTOD approach in BIMET was not found to have brought substantial benefits and that the transferability of CTOD data to 3-D crack geometries is not straightforward. Nonetheless for the majority of the tests on SE(B) specimens performed by TWI [57] to BS7448, the CTOD value was also reported and crack growth resistance curves are shown in Figure 5.16. Both the buttering and fusion line data produce a similar overall trend. The initiation toughness value $\delta_{0.2BL}$ is approximately 0.07 mm, which is well below the $\delta_{5,i}$ value of 0.3 for BIMET room temperature tests. This may reflect the reduced fracture resistance at the higher temperature of 300 °C used in ADIMEW, although CTOD is generally considered less sensitive than J to temperature level. Indeed, as noted above, the TWI SE(B) tests produced systemically low fracture toughness values and this appears to be again evident considering the CTOD data.

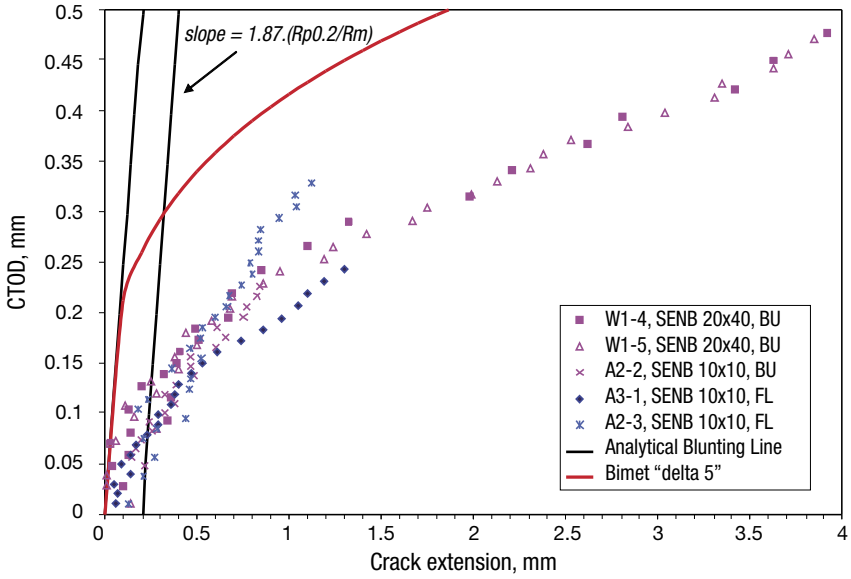

Figure 5.16: *Crack resistance in terms of CTOD as a function of crack extension Δa from the TWI tests on SE(B) specimens at 300 °C*

5.2.3 Recommendations

5.2.3.1 Crack Initiation Toughness and J-R Curve for the ADIMEW Mock-Up

Obtaining a reliable $J_{0.2BL}$ value for the test temperature of the ADIMEW mock-up proved a difficult task due to experimental difficulties in producing uniform crack growth on the desired plane and differences in results obtained from different specimen geometries and testing labs. From the data available it is considered that the $J_{0.2BL}$ value lies between 59 kJ/m² (from the 20x40 SE(B) specimen 1.5 mm from the fusion line) and 100 kJ/m² (the corrected value for 25 mm thick C(T) specimens).

The results of the fracture tests have indicated that the crack path can be strongly influenced by the mismatch at the interface and therefore the J-R curve cannot be considered as an intrinsic material characteristic. Notwithstanding this and recognising that determination of crack stability is an essential aspect of integrity assessment, for engineering purposes the J-R curve provided by the BZF-4 C(T) specimen with a notch 1 mm from the fusion line represents the lower bound of the experimental data:

$$J = 144.5\ (\Delta a)^{0.1}$$

As shown in Figure 5.17[10], although this test produced a $J_{0.2BL}$ value slightly above the range discussed above, the J-R curve is lower for crack growth values greater than 0.8 mm and is felt to best capture the enhanced ductile tearing expected at the fusion line.

[10]Figure 5.17 shows "as-reported" J-R curves, in which the data was not adjusted to account for any crack path deviations and the η factor was that for homogenous specimens i.e. without potential mismatch effects (see §5.2.2.1).

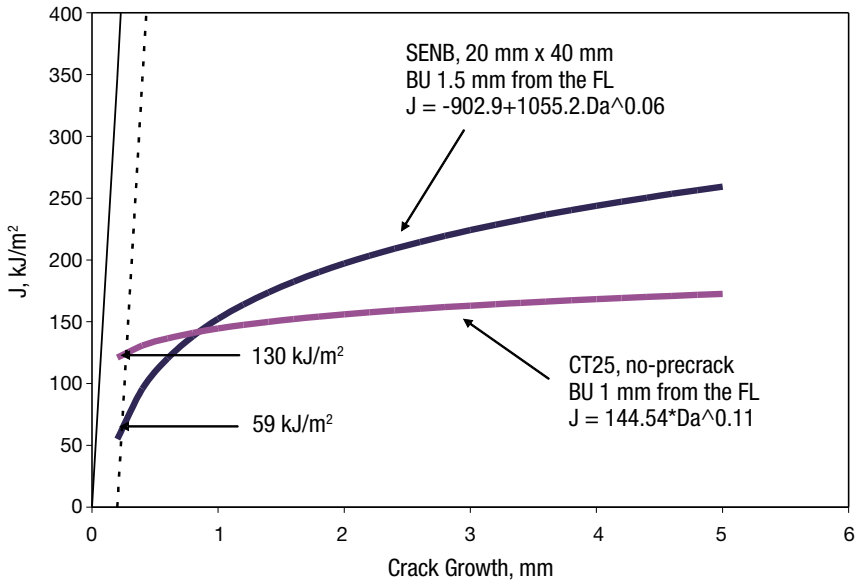

Figure 5.17: *Lower bound fracture toughness and J-R curve data 300°C in the buttering close to the fusion line*

5.2.3.2 Materials Testing Procedures

Based on the analysis of the ADIMEW data, the following recommendations are made:

- For generation of fracture toughness data the C(T) geometry is preferable to SE(B) as it is less sensitive to mismatch effects.
- For SE(B) specimens it may be desirable to use CMOD rather than in load-line displacement to calculate the plastic J component, using a suitably corrected η factor.
- CTOD measurements would avoid η factor considerations and may allow for a larger range of valid crack growth measurement
- Testing should focus on specimens with cracks on the fusion line or well into the buttering (> 2 mm from the fusion line); results from specimens with an "intermediate" crack position close to but not adjacent to the fusion line can prove difficult to interpret. For fusion line specimens it is important that the crack path with respect to the microstructure is reported with the test data.
- Pre-cracking should be done with 5% side grooves and a K_{max} of 10-12 MPa.√m; the crack tip position relative to the fusion line should be checked prior to the fracture test itself.
- For the type of weld examined, 10x10 mm SE(B) specimens did not provide reliable J-R curve information (only approx. 1 mm valid crack growth). 20x40 SE(B) and CT25 specimens provide J-R data up to about 4-5 mm crack growth, but the feasibility of extracting such specimens may be limited by the available wall thickness, so that an additional weld build-up may be required to ensure a sufficient material volume.

6 ASSESSMENT OF RESIDUAL STRESSES

6.1 MEASUREMENTS

Three different and complementary series of measurements were made of the welding residual stresses in the ADIMEW AD01 mock-up. For the ADIMEW project, JRC performed neutron diffraction measurements for each of the three principal stress components over the weld volume, while TWI made surface hole drilling measurements at the inner and outer surfaces. To complement these, MAT-TEC made also made cut-compliance measurements of the axial residual stresses using a segment of the weld. The following sections provide a summary of the results obtained.

6.1.1 Neutron Diffraction

A comprehensive series of neutron diffraction (ND) measurements were performed on AD01 at various locations within the weld, the buttering layer and base materials in the component hoop, axial and radial directions at the Petten High Flux Reactor using the Large Component Neutron Diffraction Facility (LCNDF) [58]. The measurement procedure followed internationally accepted best-practices [59]. The measurement locations were on 6 axial lines evenly distributed over the specimen thickness, i.e., 4.25, 12.75, 21.25, 29.75, 38.25 and 46.75 mm from the external surface of the pipe. The measured scattering angles for the component and the respective reference specimen were transformed to strains. The stresses were then calculated via Hooke's law using elastic constants from [40]. The resulting axial, radial and hoop stress distributions are shown in Figure 6.1, Figure 6.2 and Figure 6.3 respectively. In the axial direction half of the weld pool could not be measured due to an unfavourable texture.

Despite the challenge presented by a wall thickness of over 50 mm, a complete and reliable mapping of residual strain in the hoop direction was achieved throughout the area of interest of the weld and with small statistical error has been achieved. This forms a solid basis for the calibration of predictive numerical models. Furthermore, reliable data for residual stress in the axial and radial directions were obtained throughout the austenitic base and buttering materials, which provide additional reference data for calibration.

6.1.2 Surface Hole Drilling

Hole drilling is a standard method for measuring residual stresses at a free surface. TWI [60] made measurements at ten locations on the outside surface of the pipe and at four locations on the inside surface in the vicinity of the austenitic weld buttering to ferritic pipe fusion boundary. The results indicated that the surface axial and circumferential residual stress were predominantly compressive, on both the inside and outside of the pipe, in the vicinity of the buttering. These data contrast with the ND measurements, but it should be noted that the locations were different, i.e. the ND measurement point closest to the surface was at a depth of 4.25 mm, whereas the surface drilling holes were 2 mm depth; furthermore they are likely to have sampled material affected by the final machining of the mock-up, which was done after the PWHT.

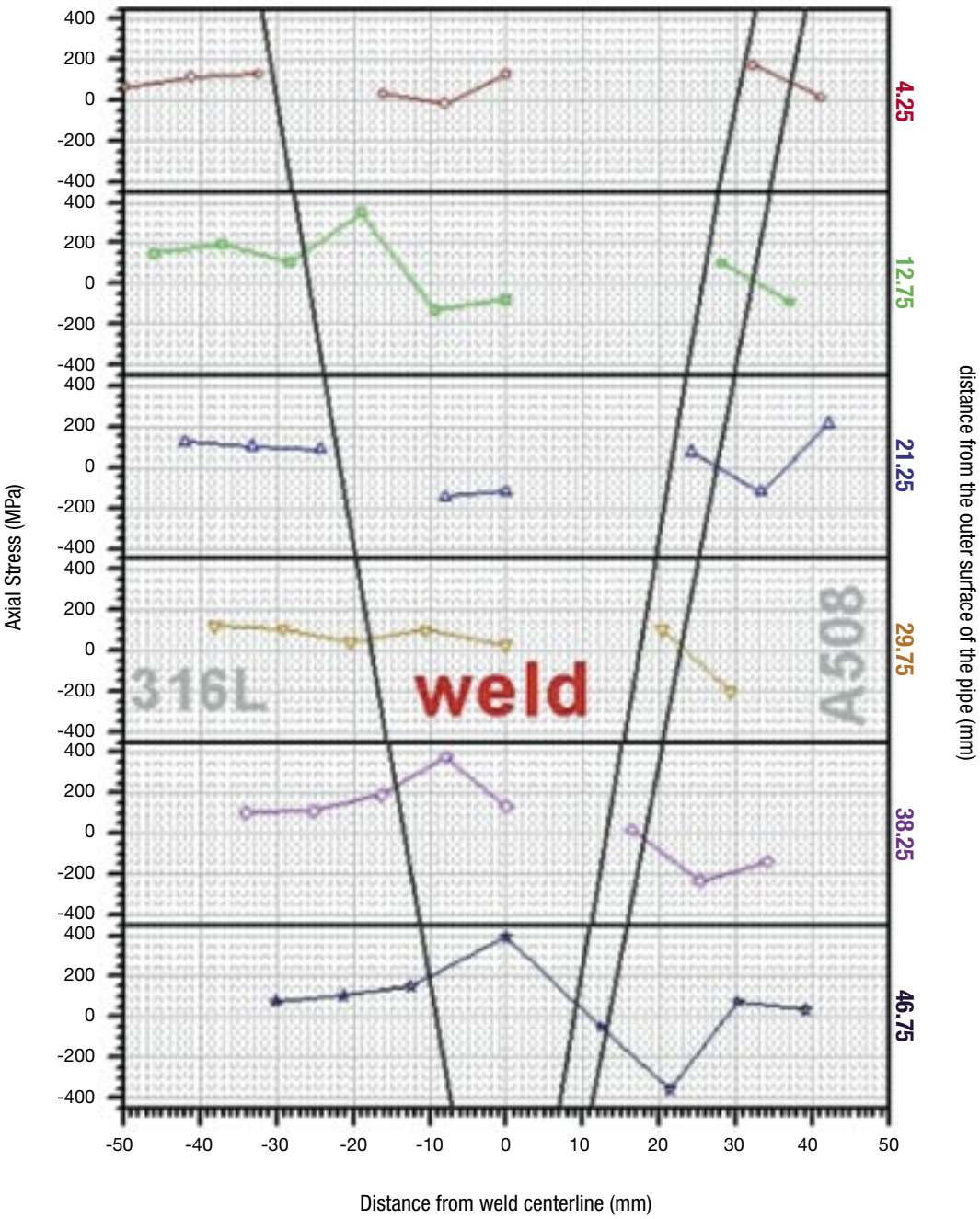

Figure 6.1: *Neutron diffraction measurements of residual stress in the axial direction, at different depths from the external surface of the pipe*

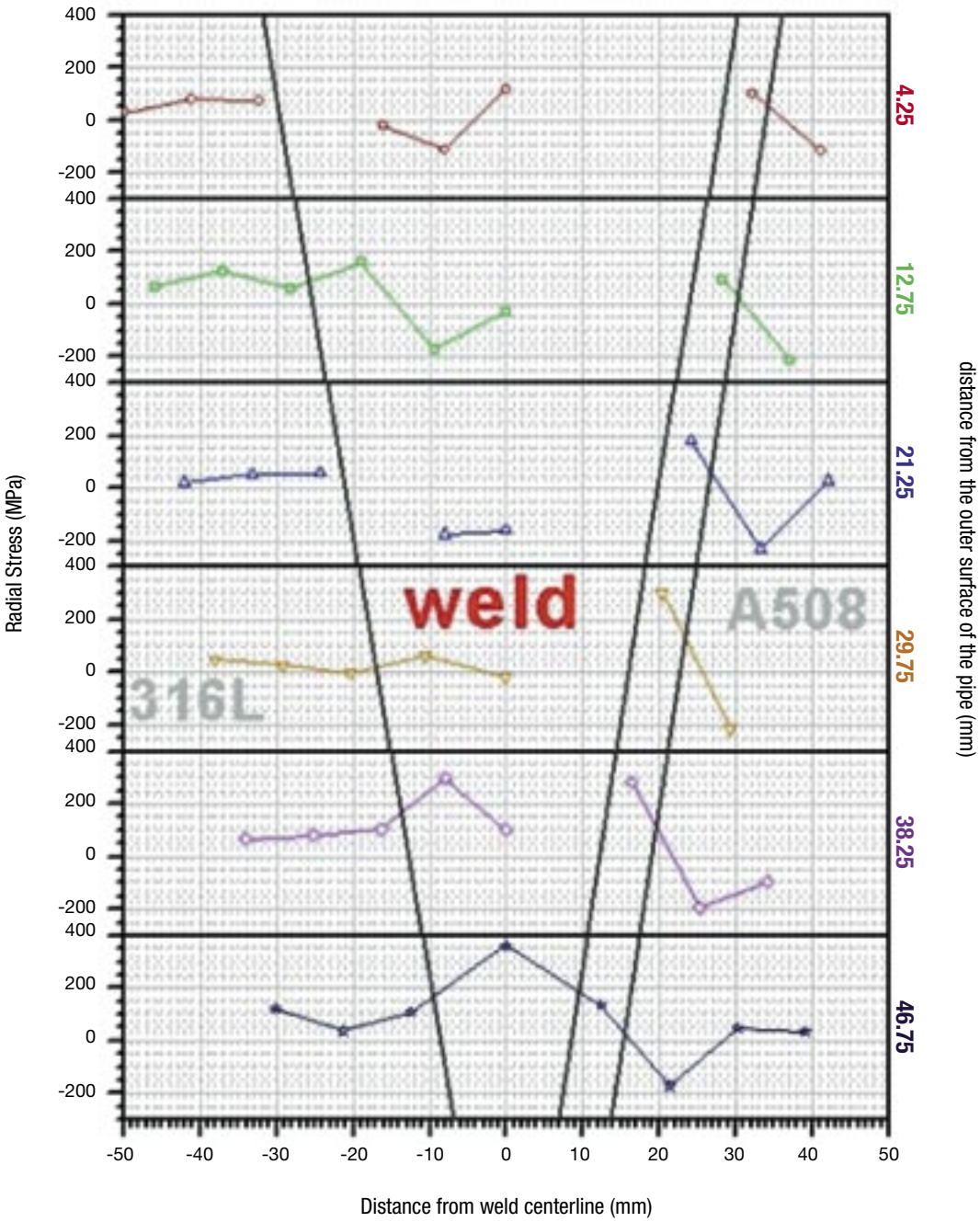

Figure 6.2: *Neutron diffraction measurements of residual stress in the radial direction, at different depths from the external surface of the pipe*

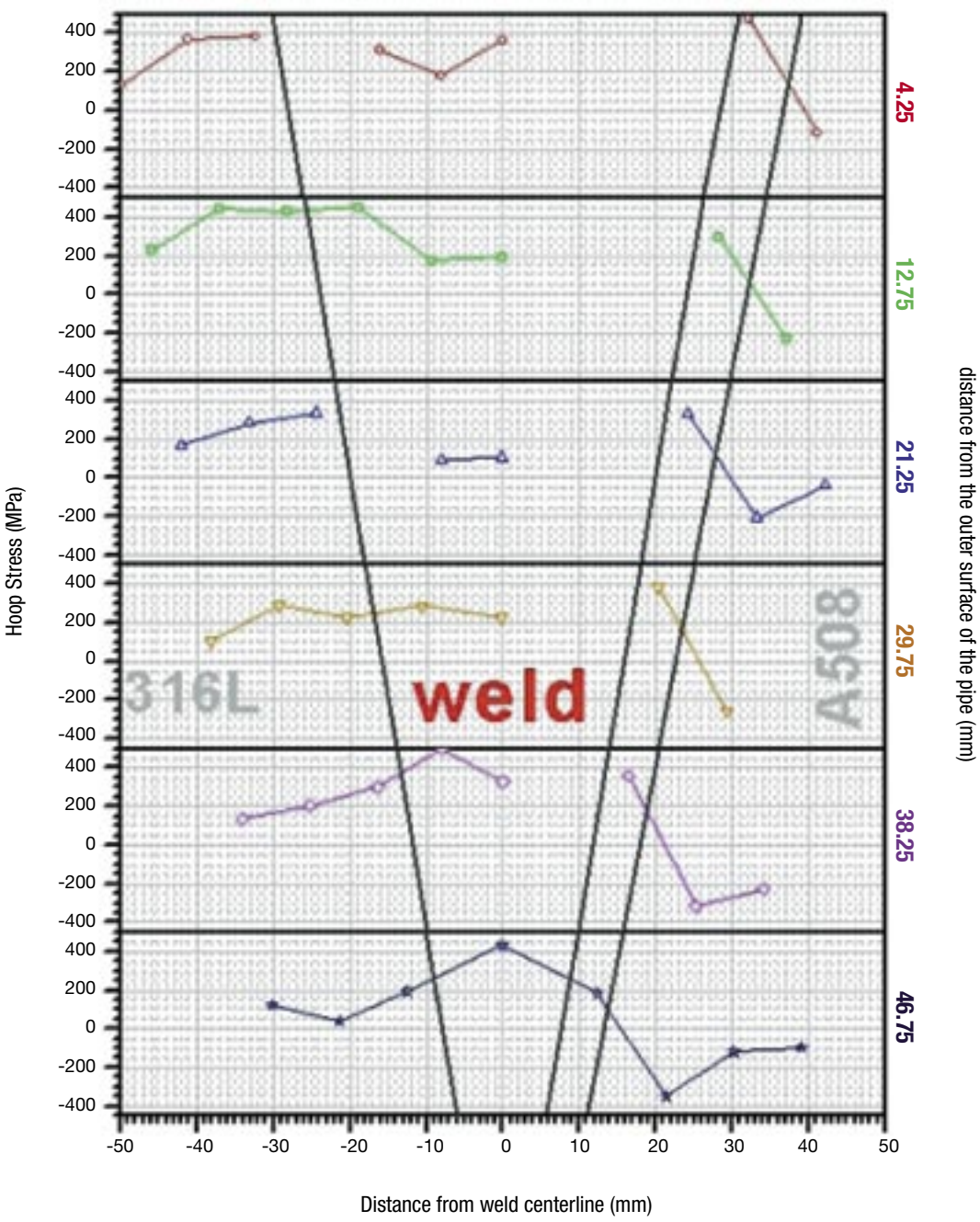

Figure 6.3: *Neutron diffraction measurements of residual stress in the hoop direction, at different depths from the external surface of the pipe*

6.1.3 Cut-Compliance Mesurements

The Cut-Compliance (CC) method was applied by MAT-TEC [61] to measure the axial component of residual stress in a 5-mm thick axial section of the AD01 weld. The CC method works as follows: Consider a plate of arbitrary shape in which the residual stresses shall be measured on an arbitrary section. A cut is progressively introduced along the plane where the residual stress is to be measured using one or two strain gages. From the changes of the measured strain as a function of the actual cut length the residual stress field released by the cut can be calculated based on principles of the theory of elasticity and linear-elastic fracture mechanics. Figure 6.4 shows the cut pattern used, while the resulting axial stresses in the centre of the weld (cuts S1 and S6) are reported in Figure 6.5, together with the ND and hole drilling measurements. The following points are noted:

- Considerable residual stresses were found in the plate segment; correspondingly even higher residual stresses are likely to be present in the full weld
- The CC data capture the high negative stress gradients near the surface, which are most probably due to the effects of machining after the PWHT.
- Significant shear/Mode-II effects exist in the HAZ/buttering region
- Given the level of residual stresses observed, it is considered that stress intensity factor at a circumferentially oriented defect on the outer surface could exceed the SCC threshold, particularly if located near the HAZ/buttering.

6.1.4 Discussion

In determining the residual stresses present in the ADIMEW weld, the different measurement techniques have proved complementary. The ND data provided a comprehensive 3-D mapping of the strains and stresses, notwithstanding the relatively high thickness of the austenitic weld. These results are

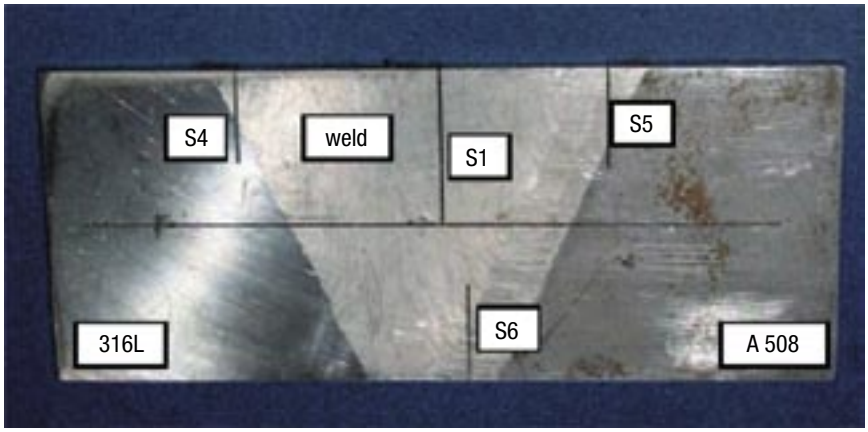

Figure 6.4: *Plate segment used for the Cut-Compliance measurements, showing the position of the cuts*

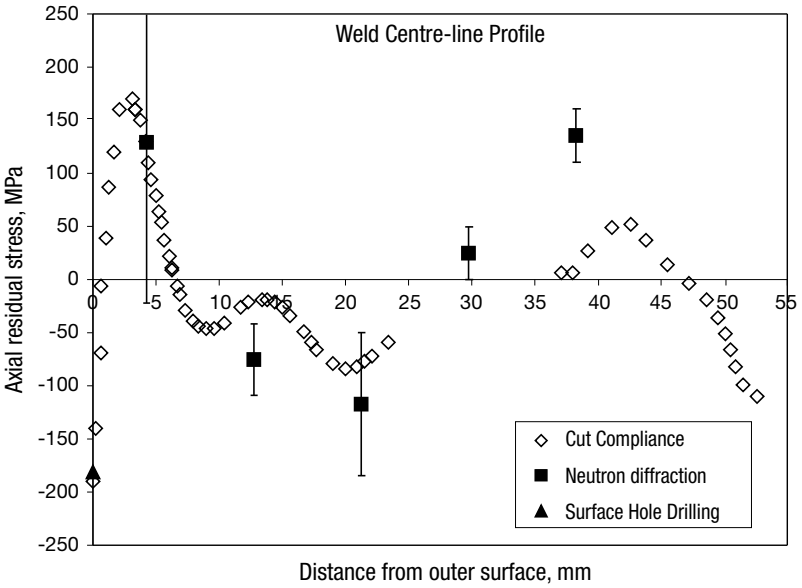

Figure 6.5: *Measurements of axial residual stress at the weld centre line*

uniquely suited for deriving profiles for input to engineering defect assessment methods and as a verification database for FE simulations of the welding process. It is noted that, in respect of statistical error, only the hoop direction data is fully reliable and any comparisons should in the first instance refer to the hoop stress data set. The ND data for both stresses and strains is provided in full in Annex 3 as a reference. A drawback of the ND technique is that it does not provide reliable information at or near free surfaces. On the other hand, the experience with the surface hole drilling technique has shown that the results of localised surface methods need to be treated with caution if they are used to infer through-section profiles. In this respect the innovative cut-compliance method proved useful in explaining apparent discrepancies between the surface and ND data, but it is limited to one directional component.

Engineering assessment methods typically require through thickness profiles of residual stresses for the specific flaw location and orientation under consideration. For their analysis of the ADIMEW test, Serco [62] fitted polynomial to the axial and radial stress components in the buttering layer. Figure 6.6 shows the measured ND axial and radial residual stress distributions at ambient temperature together with those from a smaller dissimilar weld pipe (wall thickness 25 mm) used in BIMET [63]. The values were then transformed to provide normal and shear stress components which would act on the inclined crack. The crack opening (normal) stress in MPa is given by the following polynomial expression:

$$\sigma_{yy} = 204 - 657(u/t) + 1627(u/t)^2 - 1279(u/t)^3 \quad (6.1)$$

where u is the projected depth and t is the thickness. The crack shear stress (in MPa) is given by:

$$\tau_{xy} = -18 - 221(u/t) + 1207(u/t)^2 - 919(u/t)^3 \quad (6.2)$$

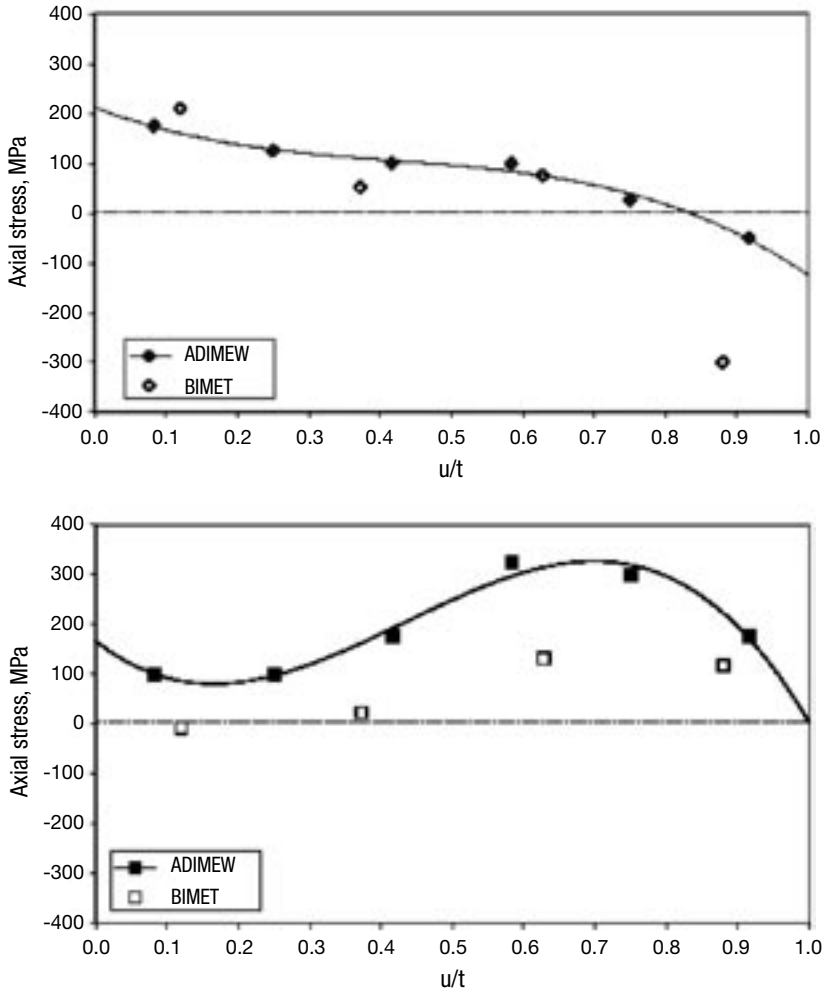

Figure 6.6: *Residual stress distributions along the buttering layer in the ADIMEW specimen compared with that in the BIMET specimen (u is the radial distance through the pipe wall)*

6.2 COMPUTATIONAL ROUND ROBINS

For Task Group 6 the participants agreed to perform three computational round robin exercises. The first two exercises considered simplified analyses of the BIMET and ADIMEW welds respectively. The main focus was however on the so-called detailed round robin was to perform a full simulation of the welding process for the ADIMEW weld. Table 6.1 summarises the calculations performed by the participants: JRC, AREVA NP SAS, AREVA NP GmbH and Inspecta. Full details, are given in the TG6 synthesis report [64])

Table 6.1: *Summary of the FE welding simulations*

Item	IE-JRC	AREVA NP GmbH	DNV	AREVA NP SAS
Round Robins	- Auxiliary - Simplified - Detailed	- Auxiliary - Detailed	- Simplified - Detailed	- Auxiliary - Simplified - Detailed
FE models	- 2D axi-symmetric - 3D solid	2D axi-symmetric	2D axi-symmetric	2D axi-symmetric
Simulation approaches	- Lump-by-lump - Layer-by-layer - Bead-by-bead	Bead-by-bead	Bead-by-bead	- Macro-bead - Bead-by-bead
Manufacturing stages analysed	- Buttering deposition - Buttering machining - Buttering heat treatment - Weld deposition - PWHT - Final machining	- Buttering deposition - Buttering machining - Buttering heat treatment - Weld deposition - PWHT - Final machining	- Buttering deposition - Buttering heat treatment - Weld deposition - PWHT - Final machining	- Buttering deposition - Buttering machining - Buttering heat treatment - Weld deposition - PWHT - Final machining
Number of buttering/weld passes	- Lump-by-lump 1/6 - Layer-by-layer 4/19 - Bead-by-bead 69/96	38/96	40/98	- macro-bead -/18 - bead-by-bead -/96
Birth & death used	yes	yes	yes	yes
Heat input model	Prescribed temperature at 1450°C with no phase change	Heat generation so that temperature at weld pool >2500 °C	- Heat generation such that temperature >1200 °C at weld pool and 800-900 °C 2mm from fusion line - Arc efficiency 0.9	Moving heat source model (3-D cylindrical source moving on a plate; source radius calculated from the fusion temperature, the bead shape and the HAZ size)
Reference temperature of born elements	1450 °C	1400 °C	1200 °C	N/A
FE code	ANSYS 8.0	- ABAQUS 6.4-1 - MSC.PATRAN	ABAQUS 6.4	SYSWELD
Computer	- Intel Pentium IV PC - 1.8GHz CPU clock - 512Mbyte RAM	- HP J6700 - 750MHz CPU clock	N/A	SGI multiprocessor
CPU time (seconds)	- 314 (simplified) - 23790 (detailed) - 39178 (3D)	45483 (detailed)	N/A	N/A
Number of elements	- 3584 (simplified) - 4307 (detailed) - 2100 (3D)	1070		2980 (macro-bead)
Number of nodes	- 3741 (simplified) - 13008 (detailed) - 9324 (3D)	3361		9023 (macro-bead)
Type of elements	- 4-node quad (simpl.) - 8-node quad (detailed) - 20-node brick (3D)	- DAXD8 (thermal) - CAX8R (mech.)		Quadratic

Item	IE-JRC	AREVA NP GmbH	DNV	AREVA NP SAS
Type of analysis	Uncoupled quasistatic thermoelasticity, small displacement	Uncoupled thermal and mechanical analysis, large displacement	Small displacement	Small displacement
Number of time steps	- 148 (simplified) - 3788 (detailed) - 968 (3D)	412 (detailed)		
Number of mechanical analyses	- 34 (simplified) - 1297 (detailed) - 299 (3D)			About 130
Materials considered	- Ferritic base - Austenitic base - Weld and buttering the same - 4 buttering layers	- Ferritic base - Austenitic base - Weld and buttering the same - 2 buttering layers	- Ferritic base - Austenitic base - Weld - Buttering - 2 buttering layers	- Ferritic base - Austenitic base - Weld and buttering the same - HAZ - 3 buttering layers
Material properties	From protocols except stress-strain curves at high temperatures, which were obtained from private database	From protocols	From protocols	From private database
Material model	Multi-linear kinematic hardening	Isotropic Hardening	Elastic-plastic	Elastic-plastic with isotropic hardening; viscoplastic model for the PWHT
Cooling	- Free convection at 5 Watt/m^2/^{o}C - No radiation	Free convection at 15 Watt/m^2/^{o}C and radiation on free-non-welded component surfaces and at the last weld layer	- Free convection - Radiation	Free convection
Supports	- Free to expand - Only rigid body motion preventive - Fitting lip considered as contact surface	- Radial at both ends on external surface - Axial on ferritic end (over whole cross-section) - Lip not considered, austenitic and ferritic pipe fused at this point	- Only axial constraint - Fitting lip considered as contact surface	Fixed end displacement is applied during the heating phase and free boundary conditions during the cooling phase
Creep/ viscoplasticity	No	No	Yes, Norton creep law fitted to in-house data	Yes, but details of the model is not available
Metallurgical phase transformation	No	No	No	Yes (as a sensitivity study)
Machining Simulation	Yes, using death of elements	Yes, using death of elements	Yes, using scaling of predicted stress profiles and death of elements	Yes, using death of elements

6.2.1 Simplified Thermal Mismatch Analyses

In the simplified approach only the cooling process from the post weld heat treatment temperature of 610°C to room temperature is simulated. It is not a real weld simulation technique, but rather provides a direct means of generating a residual stress field based on the mismatch of material properties (specifically the coefficient of thermal expansion) between the two steels that are joined together by welding. Both steels are considered stress free at 610 °C and as they cool down they contract at different rates thus producing stresses, which at some point turn plastic and thus remain at the end of the cooling process as residual.

The first exercise (referred to as the auxiliary round robin) considered the BIMET weld. The overall pipe length is 2.5 m, its external diameter 168 mm and its thickness 25 mm. The weld groove geometry and the material properties were described in a problem definition document [65]. Excellent agreement was obtained between the FE models of JRC, AREVA NP SAS and AREVA NP GmbH (Figure 6.7). However while the computational results reproduce the general trend of the ND measurements, the tensile stresses in the weld are underestimated. A contributory factor to this difference is that the BIMET pipe (on which the ND measurements were made) had not been post-weld heat treated, so that the assumption made in the analysis of a stress-free state at 610 °C is questionable.

The second exercise applied the simplified approach to the ADIMEW weld. The overall dimensions, weld groove geometry, material properties and PWHT data were described in a problem definition document [66]. Figure 6.8 compares the hoop stress values obtained by JRC, AREVA NP SAS and DNV to the corresponding neutron diffraction measurement data. As for the BIMET analysis the predictions of three models are in very good agreement. Overall they underestimate the peak hoop stress values measured close to the outer surface.

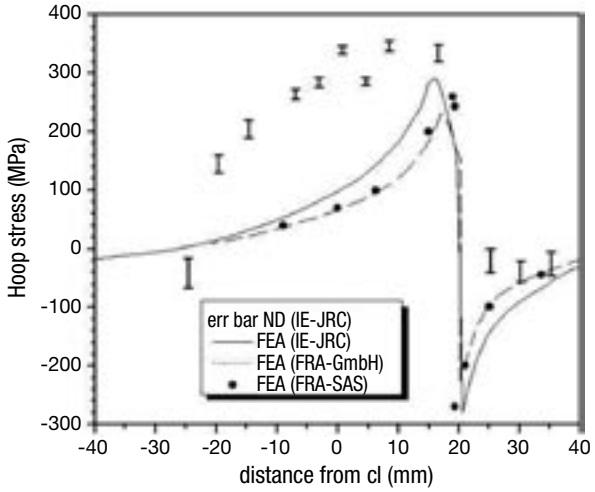

Figure 6.7: *Results of the simplified analysis of the BIMET weld, comparing the predicted hoop residual stress values with neutron diffraction data at 3 mm under the pipe external surface*

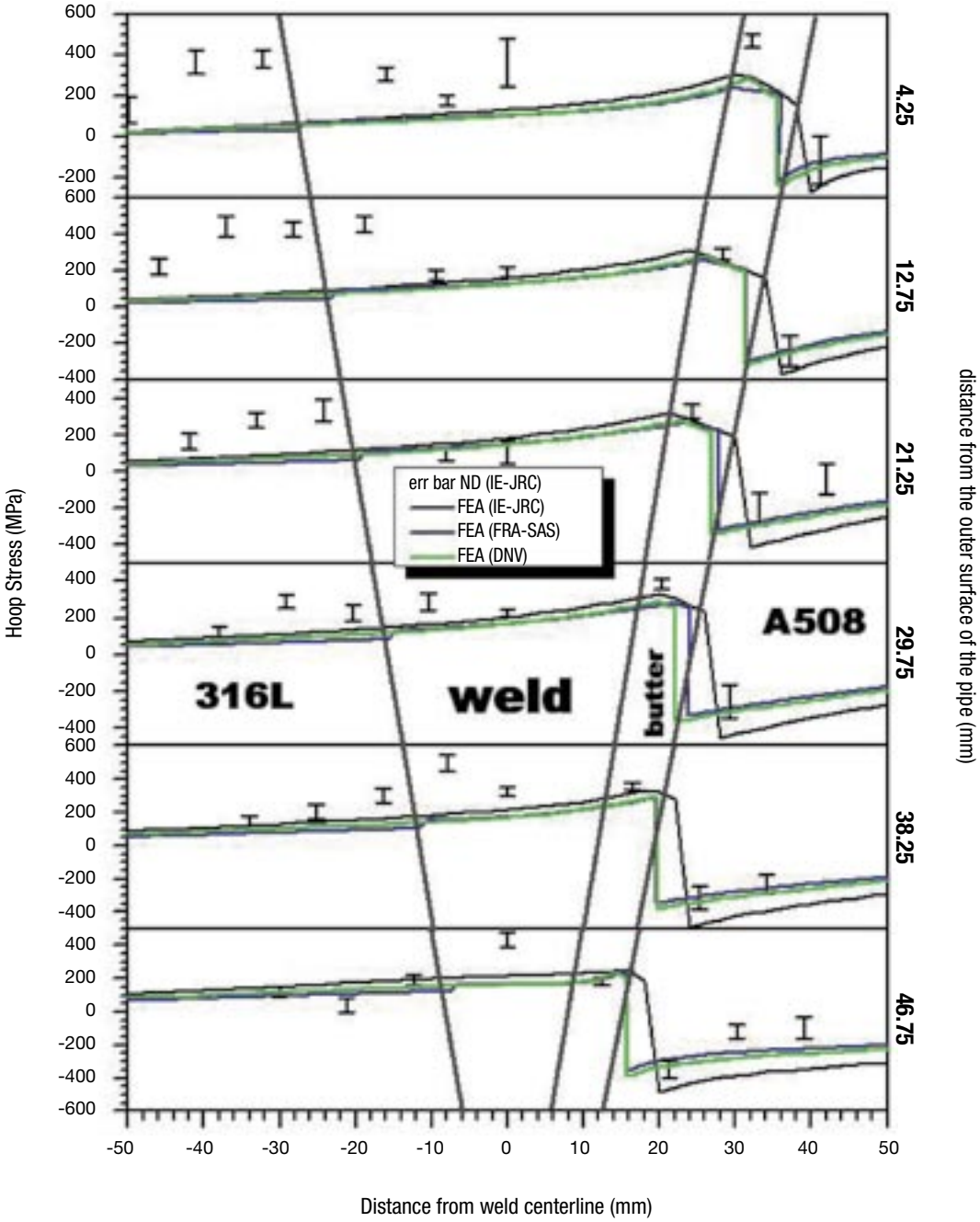

Figure 6.8: *Results of the simplified analysis of the ADIMEW weld, comparing the predicted residual hoop stresses with the neutron diffraction data*

6.2.2 Welding Process Simulation

The main TG6 round robin considered a detailed simulation of all stages of the manufacturing process. The aims were:

a) to compare the detailed approach against the simplified approach, in respect of computing time and accuracy of residual stress predictions

b) to pinpoint differences between models and methodologies used by the participants and make recommendations for best practices

c) to provide residual stress profiles for use in engineering assessment of flaws in DMWs.

The participants were asked to analyse all 5 stages of the manufacturing process, as described in §2.3.1 above (buttering deposition, buttering machining, weld deposition, PWHT and final machining). This, as well as the welding parameters (electrode travelling speed, number of passes, arc voltage, welding current, etc), was described in detail in the problem definition document [67]. Four materials were considered: the ferritic pipe, the austenitic pipe, the weld filler and the buttering. Figure 6.9 shows an example of the detailed FE mesh used to model the weld. A full set of temperature dependent material properties, as well as weld groove geometry and weld-pass sequence, was made available. Creep relaxation properties were not included, and participations were free to use their own data. The NESC-III group also arranged to have continuous temperature [68] and strain measurements [69] made during the welding of the second mock-up (AD02). Histories of temperature against time are valuable sources of information to set-up and validate finite element simulations of welding. Weld pass number and sequence, electrode travel speed and direction, inter-pass cooling rate and duration, thermal conductivity and convection coefficient, are but

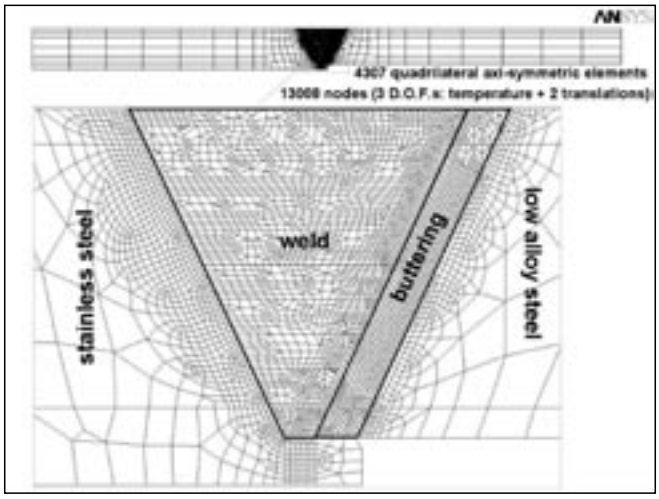

Figure 6.9: *Example of a 2-D axi-symmetric FE mesh of the dissimilar metal weld pipe joint for the weld process simulation (JRC)*

a few welding parameters that can be obtained from temperature measurements. But most importantly the heating rate, heating duration and maximum temperature are parameters that regulate the heat input during welding. The time scale extended to a total of 20 days, including idling periods. The data is available in electronic format as is available as part of the project documentation.

6.2.2.1 AREVA NP GmbH

The AREVA NP GmbH welding simulations [70] were performed with the FE code ABAQUS, the pre-processing (mesh generation) was done with PATRAN and the generation of the ABAQUS input decks was supported by specific FORTRAN programs. The actual 3D problem was treated as an axial-symmetric 2D model to save numerical effort. Large displacement theory was applied. The complete weld process was simulated taking into account the addition of the weld passes, removing of machined material and the involved heat transfer (weld energy, cooling by the environment). Any metallurgical conversion processes in the HAZ were not considered.

Basically, the welding simulation was treated as an uncoupled thermal and mechanical problem in which both kinds of analyses simulate the adding and removing of material caused by the weld processes and machining, respectively. First a nonlinear heat transfer analysis was performed to obtain the time dependent temperature field resulting from the heat input by the welding electrode and the subsequent cooling to inter-pass temperature before welding the next weld pass.

Following the heat transfer calculation a nonlinear mechanical analysis was performed as a static stress-displacement analysis with elastic-plastic material behaviour using the time dependent temperature field determined before. In this way the residual stresses and strains could be predicted at the end of the cooling down process of the completed dissimilar weld. Because of the unavailability of appropriate data for cycling hardening caused by cyclic thermal loadings from the weld passes, an isotropic hardening model was used. No creep was simulated during the PWHT phase due since the necessary input data was not included in the problem definition document

6.2.2.2 Det Norsk Veritas (DNV)

In the DNV analysis [71] an axi-symmetric FE weld simulation was made with the ABAQUS software. The welding process was simulated using a thermo-plastic analysis. First a transient thermal analysis is performed during which the time dependent temperature distribution is determined for the successive build up and heating of the weld passes. Then the stress field due to the transient temperature field and the adding of material is calculated at each time step in an uncoupled elastic-plastic structural analysis. The new material for each weld bead is added using inactive elements (element birth/death). Quiet element technique (low stiffness) could be used to achieve better deformation of the inactive mesh, but is not judged necessary in this case. 40 successive weld passes were used to two buttering layers (not four), resulting in a final buttering thickness of 7.2 mm. No machining of the buttering is modelled. The bead sequence at the manufacturing of the weld is given in the problem definition.

The assumption of rotational symmetry implies that the new material and heat is deposited at the same time around the full circumference of the pipe. Thus, the effect of heat flow in the circumferential direction is neglected. In reality the molten pool is moving and is only some 10 mm long.

These facts imply that for an axi-symmetric model some calibrations had to be made in order to simulate the effect on the temperature gradients due to the lack of heat transport in the third dimension. In the subsequent structural analysis of the thermal transient, the stresses were calculated with an elastic-plastic material model. The von Mises yield criterion with associated flow rule and bilinear kinematic hardening was used, together with small strain theory. The mechanical properties are temperature dependent. There is no exact modelling of phase transition in the carbon steel, and only one constant curve for the thermal expansion as a function of temperature is used. The multi-pass weld is modelled by activating the elements belonging to the current pass at a proper time during the transient. The structural elements are activated when all elements in the current new weld bead have reached above the melting/softening temperature (1200 ^{o}C), and the temperature has started to decrease. The elements are introduced strain-free, and the strain free temperature for the new added material is put to the melting/softening temperature. The FE analysis is done using parabolic axi-symmetric elements. The only mechanical boundary condition is constrained rigid body motion in the axial direction for the end of one pipe.

6.2.2.3 AREVA NP-SAS

AREVA NP SAS performed an extensive series of weld simulations using the SYSTUS software. The detailed analysis consisted in simulating the entire manufacturing process, from buttering stage to final machining after PWHT stage. The welding parameters were those defined in the manufacturing report. Initially a macro-bead technique was applied [72], which consists in modelling the welding operation by depositing layers of beads instead of a full sequence of bead deposit. The technique is conducted under the small displacement hypothesis and assuming 2D axi-symmetry of the joint. Although computationally more efficient, it tended to overestimate slightly the residual stresses on the interface and at the root. Hence a full bead-by-bead simulation was also performed [73,74], with 50 passes for the three buttering layers and 90 passes for the weld filling.

Three materials were considered: A508 for ferritic base metal, 316L for austenitic base metal, and 308L for weld metal. The buttering was considered as identical to the filler weld material in the present study. The yield limit and stress-strain curves at 20 and 300 °C were taken from the ADIMEW pre-test problem definition report, supplemented by the RCC-M [25] material database and private information. Creep characteristics were taken into account during PWHT stage.

The model itself was 2-D axisymmetric. The self-restraint effect of the cold parts during welding was taken into account by appropriate boundary conditions: fixed end displacement is applied during the heating phase and free boundary conditions during the cooling phase. Only 3 buttering layers (one 309L and two 308L) have been modelled; the fourth one was not considered. The mock-up was meshed using quadratic elements. These increase the size of the problem, but give much better results than linear elements (for the same number of nodes) at locations where stress gradients are high like at the interfaces. The two machining operations (reduction of the buttering thickness and final reduction of external and internal diameter of the mock-up) were modelled by reducing the element strength to a negligible value, and any effect of heating due to machining is neglected.

The results obtained showed that the 2-D multi-pass model produced good prediction of residual stresses due to welding, even with the assumption of axisymmetry. This validates the BSSN-INSA-

Framatome-EDF database used for the material properties. It was shown that the PWHT plays a critical role in reducing the level of residual stresses and is sensitive to the creep properties used in the analysis. It was also demonstrated that, if phase changes in the ferritic HAZ are considered, the model is capable of predicting the hardness variation in the different phases (coarse grain HAZ and fine-grain HAZ), as evidence by the micro-hardness measurements (Figure 5.4).

6.2.2.4 JRC & University of Patras

The JRC [75] used ANASYS software with a 2-D axi-symmetric model. A bead-by-bead buttering deposition was performed on the ferritic pipe, and after the heat treatment and machining, the austenitic pipe elements are activated. The mesh used a total of 4307 8-node isoparametric elements and 13008 nodes. The transient thermal problem is solved first and the resulting transient temperature distribution is used as temperature load in a series of non-linear static mechanical analyses, of which each one uses as initial stresses the results of the preceding one. The FE mesh used for the mechanical analysis is identical to that for the thermal analysis. It is also assumed that the thermal transient evolves much faster than the resulting changes in the displacement field, so that the process can be considered as an uncoupled quasi-static thermo-elasticity problem. Partial melting of the base material and re-melting of already deposited weld passes is not incorporated. Both parent and weld material mechanical behaviour are modelled using the multi-linear kinematic hardening law. Creep and metallurgical phase transformation effects were not considered.

For modelling the heat input due to welding, a "prescribed temperature approach" was followed instead of applying a heat generation rate per unit volume load. This allows much higher heating rates, which dominate during arc welding. Each buttering and weld pass was "deposited" i.e. the relevant elements were activated, in a predefined order, following the corrected weld-pass sequence of problem definition document. The deactivation and activation is achieved through the element "birth & death" technique. Element deactivation is achieved by multiplying their conductivity or stiffness (for thermal or mechanical analysis, respectively) by a severe reduction factor. Similarly, when elements are "born," they are not actually added to the model; they are simply reactivated.

6.2.3 Inter-Comparison of the Results

Figure 6.10 and Figure 6.11 compare the predicted residual stresses in hoop and axial directions with the neutron diffraction measurements close to the external surface of the pipe (the 4.25 mm depth corresponds to the location of the ND measurements closest to the surface). The JRC, AREVA NP GmbH and AREVA NP SAS values are from calculations without creep relaxation during the PWHT; the DNV results are shown both with and without PWHT creep relaxation. There is generally good agreement in the trends predicted by all four FE simulations.

a) Hoop stresses: since the measured ND hoop stresses are considered more reliable and complete than those in the axial and radial directions, they are particularly important for verifying the FE results. As indicated in Figure 6.10, the FE simulations reliably predict the measured transition from tension in the weld to compression in the A508L. The peak values at the outer surface are slightly above the room temperature yield stress for the weld material, 417 MPa. Considering

the through-thickness variation, the simulations tend to underestimate the stresses at the inside of the weld, as shown in Figure 6.12 for a section through the weld thickness along the centre of buttering layer.

b) Axial stresses: the predicted axial stress values are tensile in the vicinity of the outer wall and peak near the fusion line, in broad agreement with the ND measurements (Figure 6.11). For what concerns the through-thickness variations, the simulations predict substantial compressive stresses at the inside of the weld, whereas the ND measurements only become marginally tensile towards the weld root. This is shown in more detail in Figure 6.13 for a section through the weld thickness along the centre of buttering layer. The predicted axial stress are tensile close to the outer surface (at 4 mm depth the values range from 170 to 300 MPa, compared to the weld metal yield stress of 416 MPa), but then decrease in an approximately linear fashion to values between -100 and -300 MPa at the weld root. This poor agreement between the predictions and the ND data when coming closer to the root passes is of potential concern in relation to postulated flaws on the inner surface of this type of DMW. One aspect to be considered further is the effect of the layering method in modelling the buttering, since in the root area these have almost the same width as the weld.

Two of the participants reported detailed values of temperature and strain in the two pipes during the welding process, which can be compared to the measured values. Figure 6.14 illustrates temperature history during deposition of the last 9 weld passes for three locations. It can be seen that temperature peaks recorded by TC2 and TC4 are get higher as weld passes come closer to these

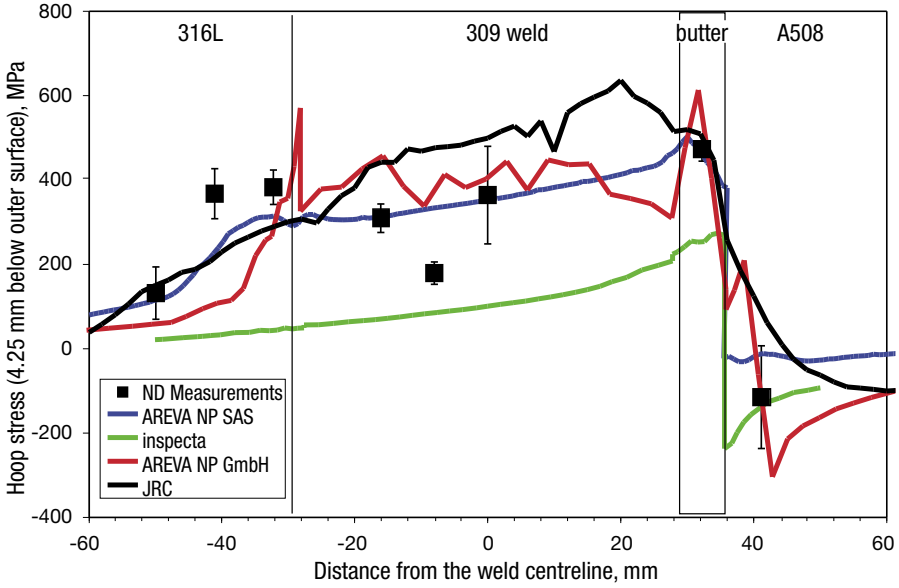

Figure 6.10: *Predicted vs. measured residual stress in the hoop direction at 4.25 mm below the outer surface*

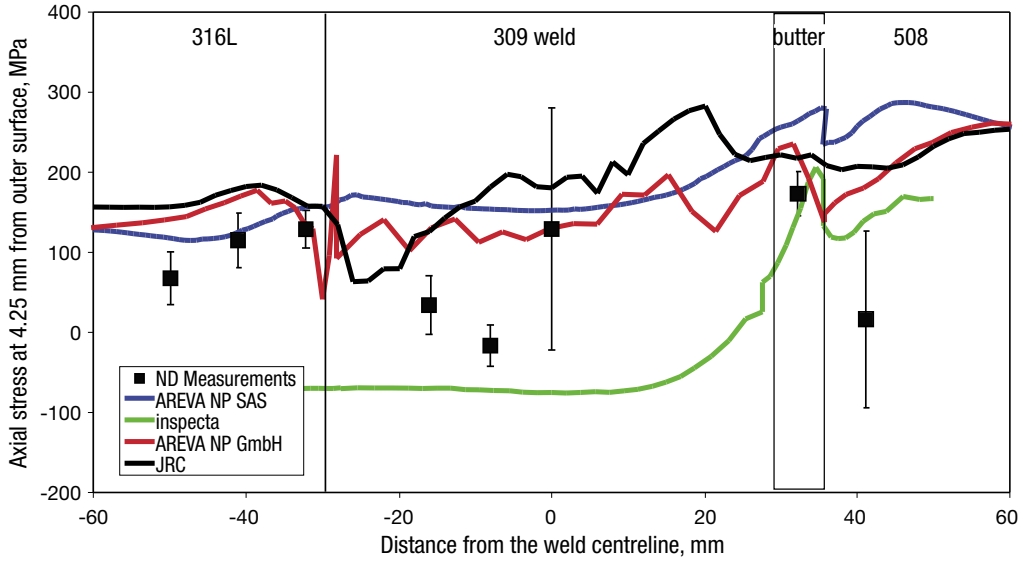

Figure 6.11: *Predicted vs. measured residual stress in the axial direction at 4.25 mm below the outer surface*

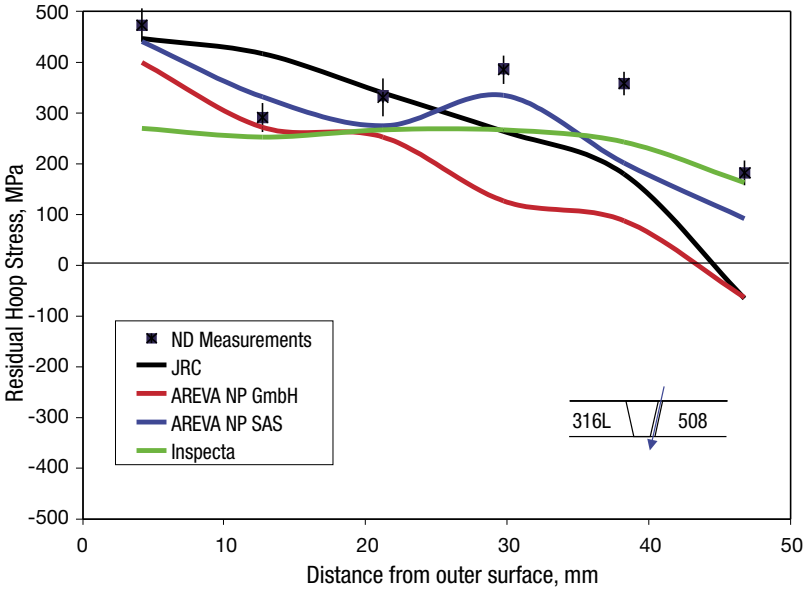

Figure 6.12: *Comparison of the predicted hoop stresses with the ND measurements at a section along the centre of the buttering layer*

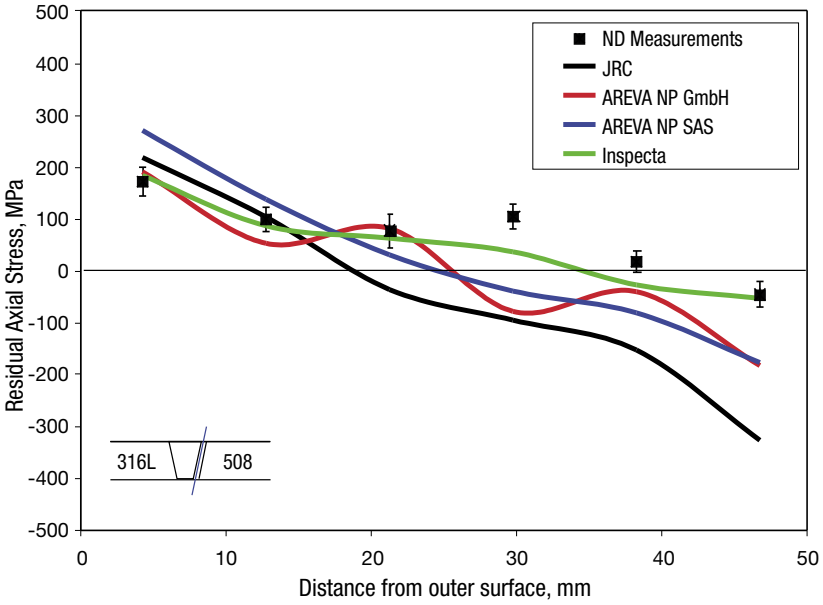

Figure 6.13: *Comparison of the predicted axial stresses with the ND measurements at a section along the centre of the buttering layer*

thermocouples, whereas the root thermocouple (TC1) records low temperatures. Between TC2 and TC4 the highest temperature peak for each day depends solely on the weld pass sequence followed during welding. Figure 6.15 shows the thermal strain history for the axial direction at the internal surface of the ferritic pipe near the buttering ferrite interface. The FE simulations capture the measured build-up of compressive strains. Similarly an accumulation of tensile strains occurs at the external surface.

In summary, the exercise has shown that the FE models can predict the measured residual stresses for most of the locations with reasonable accuracy. In this respect it is necessary to bear in mind the uncertainties associated with the material properties and the ND measurements in the welded area, which can have anisotropic characteristics due to the deposition process. Further factors that may have contributed to the observed differences include:

- The welding history data and the residual strain measurements are from two different mocks-ups; although the welding process was nominally identical, some differences were present, for instance in the bead sequence.
- Small deviations between positions of reference nodes in the FE models and the measurements locations.
- Simplifications implicit in applying a 2-D model to a 3-D welding process.

6.2.4 Model Optimisation

The evaluation of the results suggests the following factors are the most significant for model optimisation:

- Availability of reliable materials properties especially in the temperature range up to 700 °C.
- Selection of a cyclic material mechanical behaviour law to avoid excessive strain hardening, either by considering kinematic hardening or isotropic hardening with a suitable recovery parameter. When large deformation and cycling loading are present at the same time, then a non-linear kinematic hardening law, such as the Chaboche model, may be preferable (although calibration data is then also an issue).

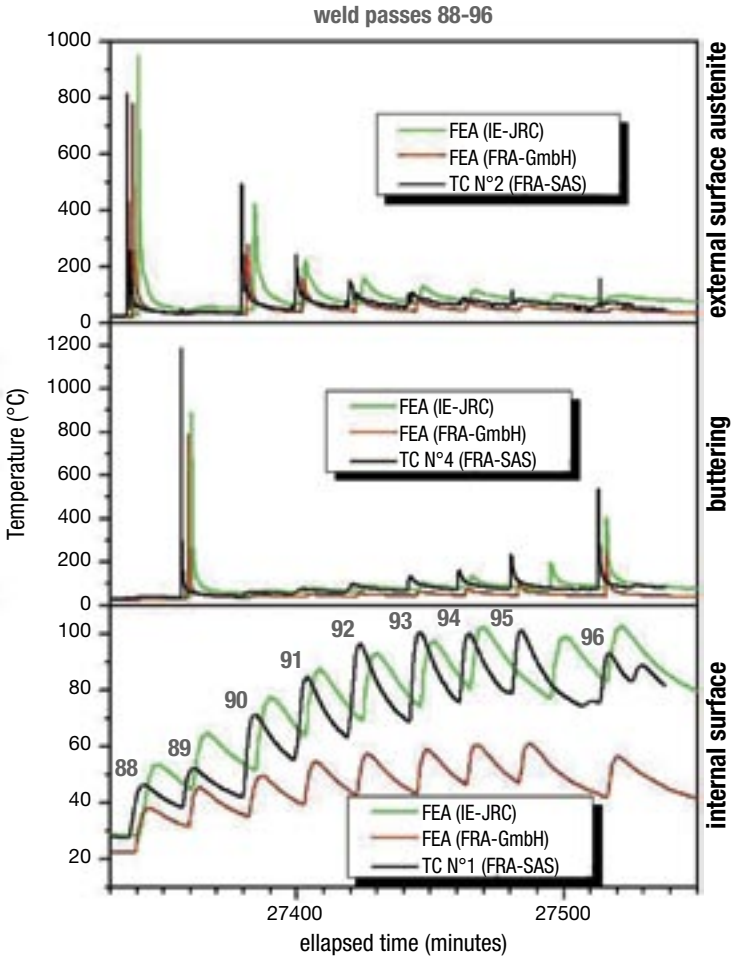

Figure 6.14: *Comparison of predicted and measured temperatures during the final 9 weld passes*

- Adequate mesh refinement needs to be ensured close to the interfaces, in particular the buttering/ferrite interface. Elsewhere mesh optimisation can reduce the analysis time considerably without significantly compromising the accuracy of predicted residual strains.

Further factors to be considered include:

- Manually controlled time stepping during the transient thermal analysis phase can be computationally efficient and comparatively large time steps may be used, as long as appropriate convergence tests are performed.
- The radiation boundary condition and phase change modelling have insignificant effects on the resulting residual stress predictions. Although their incorporation into the FE model, does not increase the computation time, they add complexity and make convergence more difficult.
- Bead-by-bead simulation of welding proved to be more accurate than the lump bead approach, but this needs to be weighed against the decreased computational efficiency (lumping of the beads reduced the CPU time by a factor of 5 comparing to the bead-by-bead analysis). However it is noted that lumped techniques are nonetheless difficult to apply since no general recommendations exist.
- Reliable welding and materials properties data are fundamental to simulations of multi-pass welds. It is recommended that the following data should be available: detailed geometry and bead sequence, supports and constraints, electrode travel speed, inter-pass temperature, cooling conditions and PWHT data (or even better, temperature recordings), stress-strain curves up to and including the melting temperature for both parent and weld materials, creep strain rate at various temperature and stress levels (only for PWHT), CCT diagram and dilatation curve (only for ferritic steels). Temperature and strain measurements from the welding itself are not essential, but certainly provide an excellent way to verify a model at an intermediate stage of the simulation.

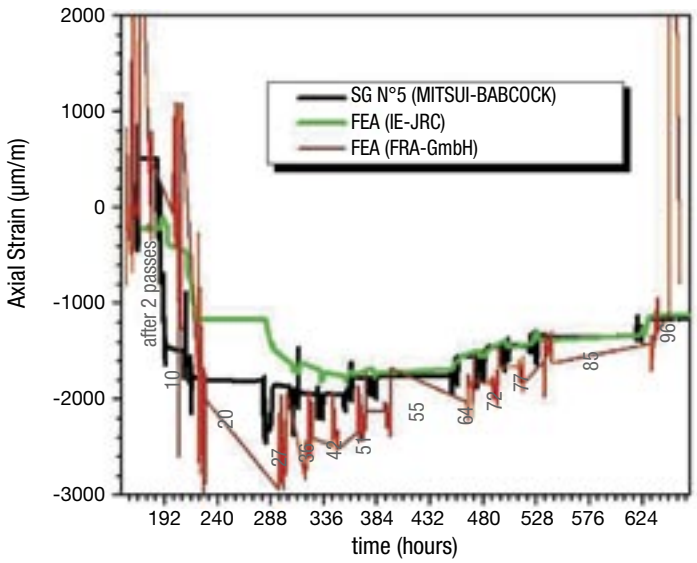

Figure 6.15: *Evolution of axial strain on the internal surface of the ferritic pipe during welding*

6.2.5 Simulation of the PWHT

During the PWHT at 610°C creep is expected to play a role in redistributing the residual stresses. Hence for meaningful simulations of the PWHT, a creep law or a suitable viscoplastic material model needs to be included in the FE simulation. Such information was not included in the problem definition document, but in the detailed round robin two participants considered this aspect using creep data from their own sources.

Figure 6.16 shows the predicted variation in axial stress in the buttering at the outer surface during the PWHT obtained by AREVA NP SAS [73,74] using the SYSWELD software. The creep properties were taken from an internal database. Introducing creep relaxation is seen to have a significant effect, reducing the final peak value of axial residual stress (at room temperature) from approximately 310 MPa to 180 MPa. It is also of interest that even without creep effects, plasticity alone produces a 10% reduction in the stress level.

Inspecta [71] also modelled creep relaxation during the PWHT with a Norton power law calibrated from literature data. In this case almost complete relaxation was predicted, so that the final ambient temperature residual stress distribution is close to that from the simplified mis-match analysis (Figure 6.17). The relaxation process can produce a strong variation in the overall stress distribution, not only in the peak values. In fact in Figure 6.17 the peak hoop stress value is shifted from the centre of the weld before PWHT to the buttering region after PWHT. Furthermore, the stresses in weld away from the buttering interface are predicted to be substantially reduced, and underestimate the values reported from the ND measurements.

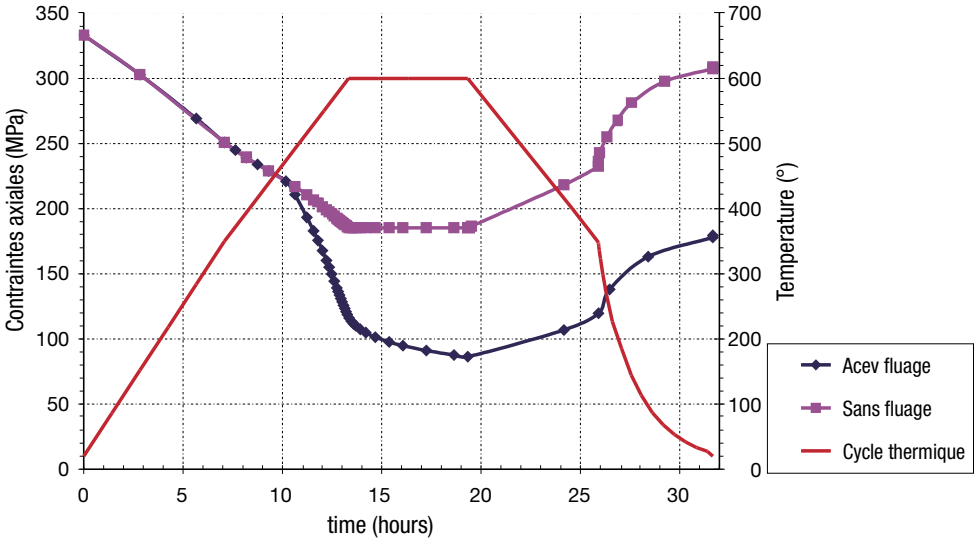

Figure 6.16: *SYSWELD predictions of the effect of the PWHT on the axial residual stress in the buttering at the outer surface a) with creep (avec fluage) and b) without creep (sans fluage)*

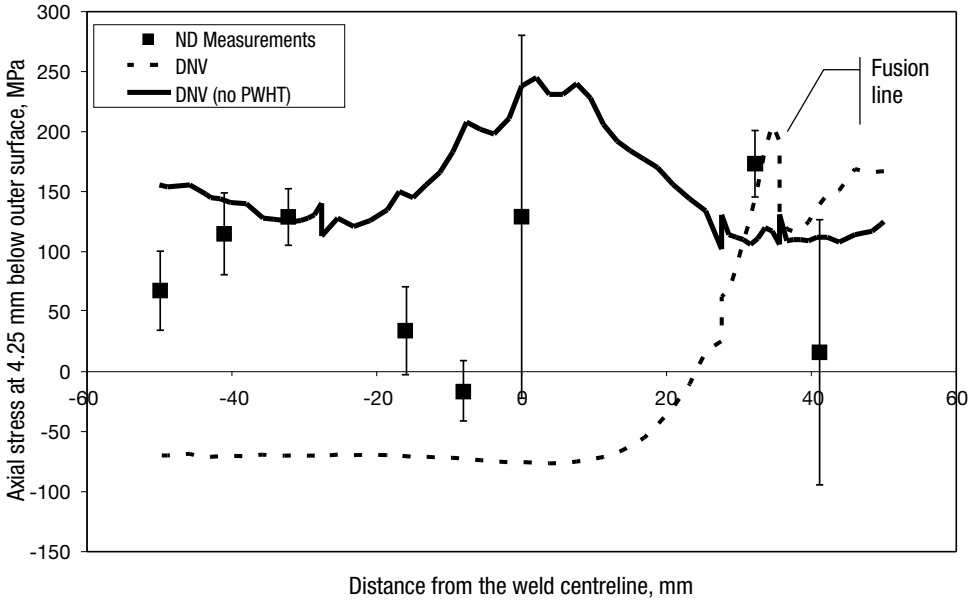

Figure 6.17: *Inspecta predictions of the effect of the PWHT treatment (including creep relaxation) on the redistribution of axial residual stress*

Since creep relaxation a critical aspect of PWHT simulation, the results here show that considerable caution is required in calibrating the creep law, and experimental verification of the resulting stress distribution (and not just of peak values) is critical.

6.2.6 Residual stress level at operating temperature (300 °C)

When the pipe is heated from ambient temperature to the nominal service temperature of 300 °C it is typically assumed that the mis-match stresses induced by the cooling from the weld process will reduce. This has been confirmed by both the AREVA NP and Inspecta analyses. For instance in Figure 6.16 is seen that as the pipe cools during PWHT from 300 down to 25 °C, the peak axial stress at the buttering increases from approximately 135 MPa to 180 MPa. Hence a corresponding reduction can be predicted on re-heating to the service temperature. In the Inspecta calculation the reduction amounts to 50% of the initial peak axial stress value.

6.2.7 3-D vs. 2-D modelling

One partner (JRC) performed a feasibility analysis for a full 3-D solid model and simulation of the DMW pipe joint, using an optimised mesh and lumping of weld beads to reduce computational costs. The results indicated a significant circumferential variation of residual strains and showed that the welding start/stop effect can be influence the axial strains and stresses. However the signif-

icance of the result is difficult to assess since there are no reference experimental measurements around the circumference. Hence while it is of interest to further explore the use of 3-D models in future, the availability of appropriate benchmark measurement data for the a range of positions around the circumference of the weld is essential.

6.2.8 Simplified Thermal Mismatch vs. Welding Simulation Models

The residual stress distributions predicted using a simplified mis-match model and a detailed weld process simulation approach are in qualitative agreement, as would be expected since the mock-up received a full PWHT. For defect location and orientation of interest here i.e. the buttering layer, the through wall profiles from both approaches are in reasonable agreement and are consistent with the ND measurements, as is apparent from Figure 6.13. In the case of the hoop stress, it appears that the simplified model underestimates the values from ND measurements at the outer surface, whereas the detailed approach appears more accurate. This is also evident if the whole weld is considered, as in Figure 6.10 and Figure 6.11.

7 STRESS AND FRACTURE ANALYSIS

7.1 INTRODUCTION

Twelve organisations[11] analysed the ADIMEW test using a variety of approaches as shown in Table 7.1. The reference documents for these investigations were the pre-test data sheet [41] and the test report [23], including the data recorded by the instrumentation. Concerning materials properties, the data sheet provided tensile stress-strain curves at 300°C for the all the pipe and weld materials. The fracture properties data from ADIMEW were made available to the other NESC-III participants on an *ad hoc* basis. Initially it was also planned to include analyses of the two BIMET tests, in particular BIMET02, which was not analysed in the scope of BIMET itself. While the relevant data sheets are now available, no calculations were performed

Table 7.1: *Overview of stress and fracture analyses of the ADIMEW test*

No.	Organisation	Project Involvement	Refs.	Scope of Analyses
1	AREVA NP SAS	ADIMEW & NESC-III	[76-79]	FE cracked body analysis, FE local approach models
2	TWI	ADIMEW	[80, 81]	FE cracked body analysis
3	CEA	ADIMEW & NESC-III	[82, 83]	FE cracked body analysis and J_i-G_{fr} engineering approach
4	Serco Assurance	ADIMEW & NESC-III	[62]	SINTAP FAD method
5	Bay Zoltan Institute	ADIMEW	[84, 85]	FE cracked body analysis
6	MAT-TEC	NESC-III	[86-89]	FE + engineering approach
7	NRI	NESC-III	[90, 91]	Modified R6 FAD analysis for tearing and stability limit
8	GRS	NESC-III	[92]	FE cracked body analysis; engineering estimate of tearing
9	VUJE	NESC-III	[93]	FE cracked body analysis
10	DNV	NESC-III	[94]	FE cracked body analysis; R6 FAD assessment
11	NRG	NESC-III	[95]	FE cracked body analysis
12	LEI	NESC-III	[96]	FE cracked body analysis

7.2 FE SIMULATIONS OF THE MOCK-UP BEHAVIOUR

As a basic step in the analysis, the majority of participants set up a FE model of the mock-up and simulated the applied loading conditions. The meshes precisely model the straight-fronted crack geometry and its orientation on a plane at 25° to the vertical and a maximum depth of 17 mm. As such they have been shown to provide more accurate, less conservative estimates of the J parame-

[11]These include several ADIMEW project participants, who agreed to include their results in NESC-III.

ter than handbook solutions, which typically describe semi-elliptical circumferential cracks, perpendicular to the outer surface. Further the material properties in the different weld materials are simulated. The calculations were all performed assuming material properties at 300 °C. The residual stresses due to welding or to thermal mismatch between the ferritic and austenitic materials were not considered.

7.2.1 Load-displacement behaviour

Figure 7.1 compares the predicted ram force vs. displacement curves from six teams with the experimental data. As discussed in section 2.3.2, the actual ram displacements in the test differed by a small constant amount and hence the ram forces were not balanced. There is reasonably good agreement between the analyses themselves. All however slightly over predict the average force once the component starts to show plastic behaviour. This yielding is largely determined by the stress-strain properties of the 316L(N) pipe section, which has the lowest yield strength. At the average displacement value corresponding to initiation (≅110 mm), the overestimation of the average ram force ranged from 4.3% to 8.6%. Extensive sensitivity analyses were performed to better understand this discrepancy, including sensitivity to material properties variations, mesh type, detailed consideration of the loading collars, and precise simulation of the individual ram displacement histories. In spite of all efforts test the calculated ram loads remain larger than the measured ones. A further point if interest is that the average ram displacement vs. load curve from models in which the rams are assumed to move exactly together e.g. the TWI data in Figure 7.1, are in excellent agreement with predictions from models which simulated the experimental offset of the ram displacements.

In Figure 7.2 the predicted CMOD vs. average ram displacement is shown. The GRS, NRG and VUJE predictions (all with a similar mesh) correspond well with the experimental measurements, while those of AREVA NP, TWI and BZF overestimate the CMOD for a given average ram displacement to varying degrees.

Figure 7.3 considers the values of CMOD vs. bending moment at the crack section. The predictions can be divided into three groups:

a) The AREVA NP, CEA and TWI predictions are all in very good agreement with the test results.
b) The GRS, VUJE and NRG predictions tend to slightly underestimate the CMOD for a given applied moment.
c) The BZF and LEI predictions are the most conservative i.e. tending to overestimate the CMOD for a given value of applied moment.

7.2.2 Crack Driving Force Estimates

FE analysis incorporating the precise crack geometry and orientation as well as the full stress-strain curves for the relevant materials is the typical route for obtaining best estimate of the crack driving force in terms of J. The contours for the J integral were confined to the buttering layer. At the centre of the crack front the path independence was (when reported) considered adequate.

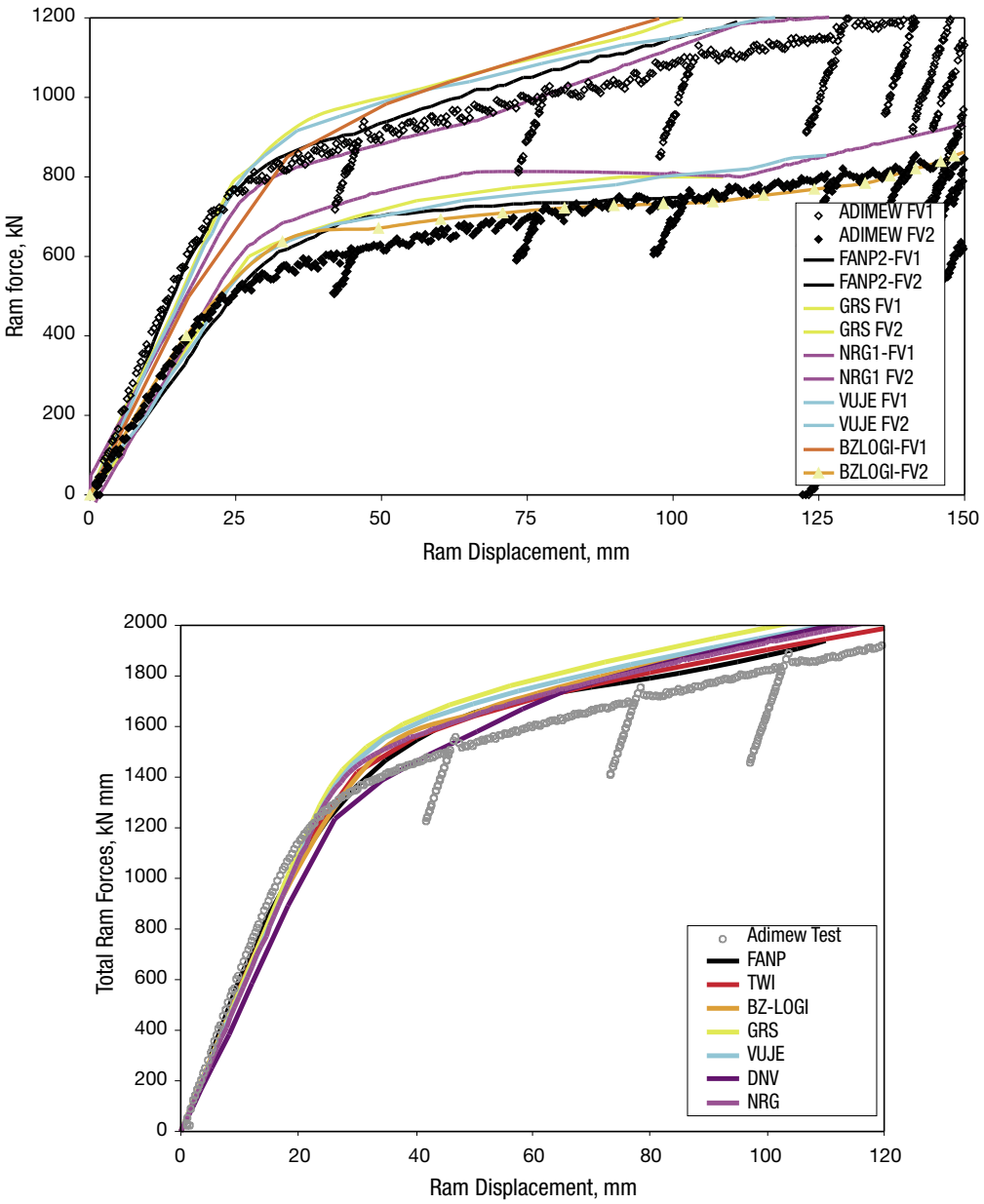

Figure 7.1: *Comparison of predicted and measured ram force vs. displacement curves: upper plot gives individual ram values while the lower plot gives average values*

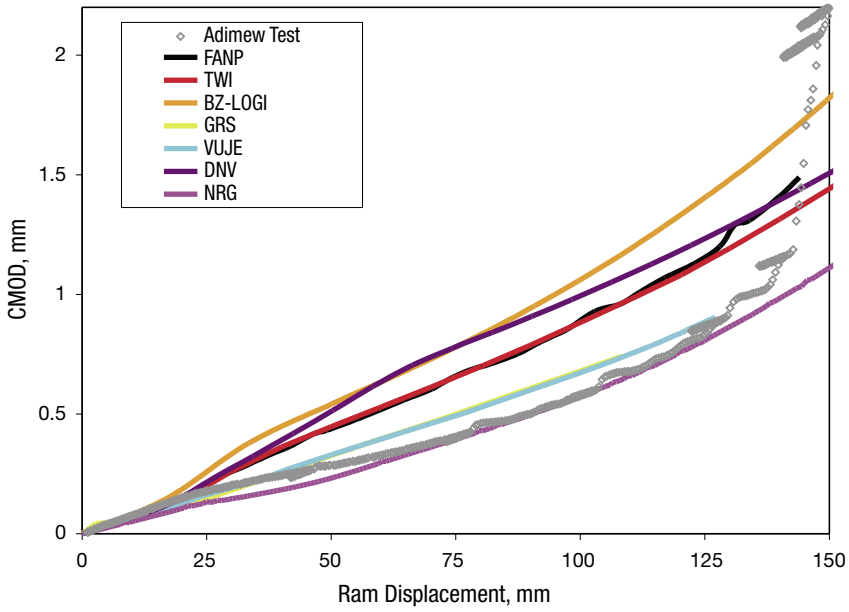

Figure 7.2: *Predictions of average ram displacement with CMOD*

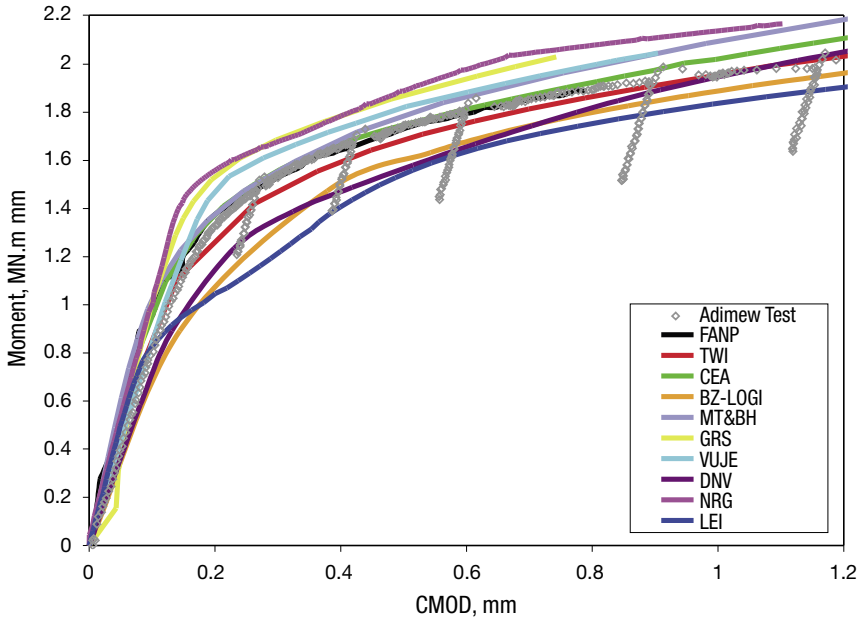

Figure 7.3: *Predictions of applied moment at the crack section with CMOD*

Figure 7.4 compares the computed J vs. applied moment curves obtained by the participants from such crack-body analyses. Although some systematic variations are present, the agreement is considered to be reasonably good. One advantage of the full 3-D cracked body models is that they provide J estimates over the full-crack front. These results confirm that J peaks at the centre of the crack front, with a significantly decrease towards the edges (Figure 7.5). This is consistent with the variation in ductile growth over the crack front in the test (Figure 2.19). All the models show that a very rapid increase in J once the applied moment exceeds 1.6 MN.m. As would be expected the simplified 2-D pipe analysis from LEI predicts distinctly higher J values than the 3-D models. The MAT-TEC values were derived from a 3-stage hybrid approach: elastic-plastic beam theory for the overall pipe, an un-cracked 3-D FE analysis of the weld region and finally a 2-D cracked-body sub-model of the defect location. The predictions are in good agreement with the full 3-D analyses.

Estimates of CTOD as a crack driving parameter have also been made, as shown in Figure 7.6. TWI derived these from 3-D FE analysis, using a 2.72 mm gauge length at the crack tip in the centre of the crack front. The MAT-TEC values were taken form the 2-D sub-model of the crack tip (the exact gauge length is not specified) and are consistent with the 3-D predictions. MAT-TEC also estimated the CTOD mode mixity. The ratio of Mode 2 to Mode 1 components is approximately 0.36 at the crack initiation load (1.8 MN.m). This compares with a ratio of 0.22 for K_{II}/K_I calculated from a 3-D model by Framatome.

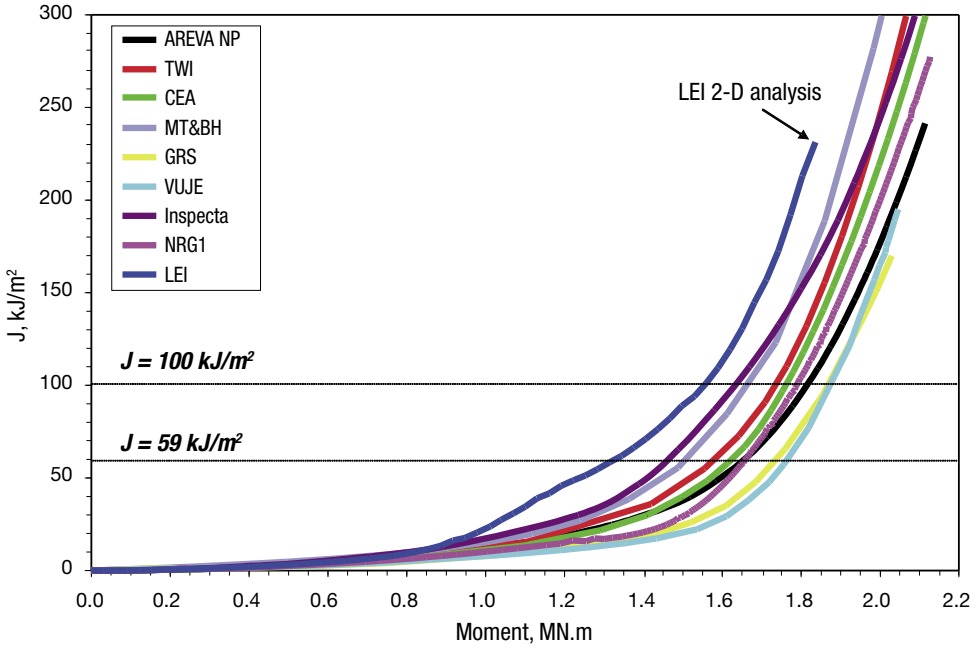

Figure 7.4: *Predictions of J for the centre of the crack*

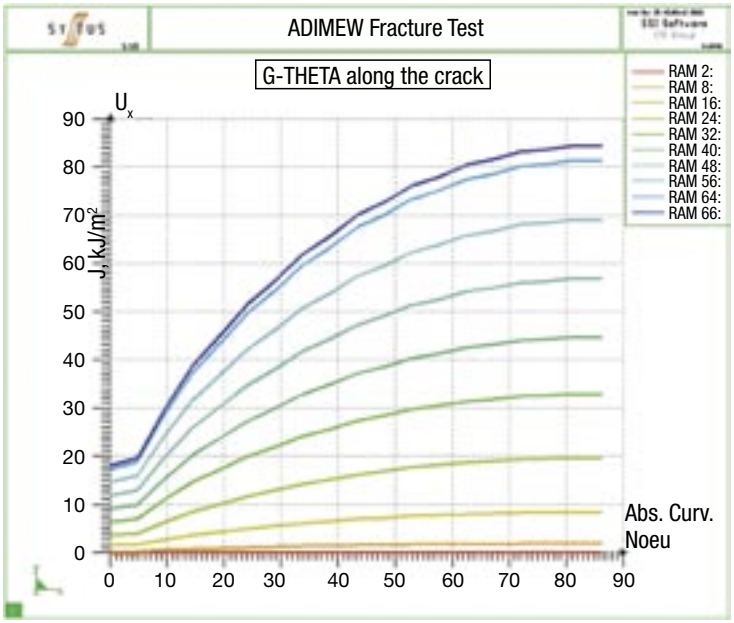

Figure 7.5: *Predicted values of J over the crack front from a 3-D cracked-body FE analysis for increasing values of ram displacement (in mms)*

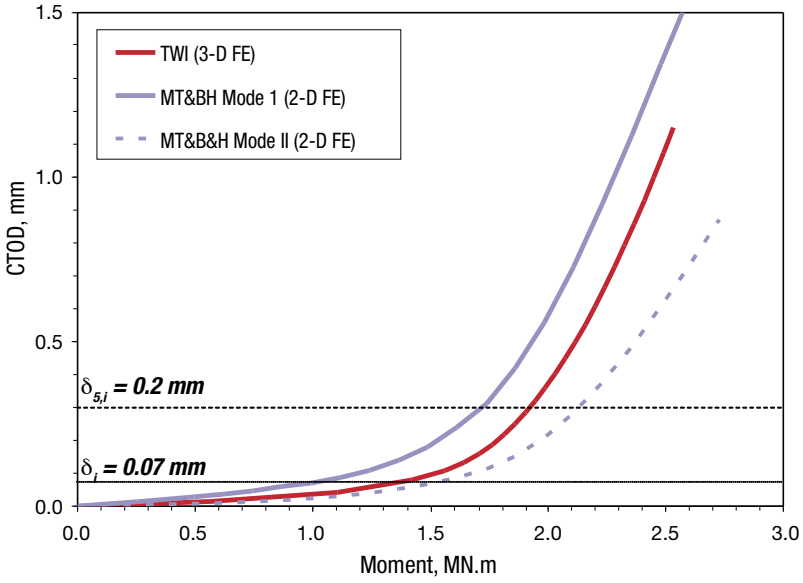

Figure 7.6: *Predicted values of CTOD at the centre of the crack front from a 3-D cracked-body FE analysis [81] and from a simplified 2-D model approach [86]*

Concerning the potential influence of the weld residual stresses (including thermal mismatch stress) on the crack tip driving force, only AREVA NP SAS [78] addressed directly in their FE model. Several difficulties were encountered. The stress transfer from the axisymmetric model to the 3D cracked structure was conducted following several steps:

- Creation of an un-cracked 3D quadratic mesh (UM2) of half of a cylinder from the axi-symmetric linear mesh (UM1) used for the weld process simulation.
- Node by node and Gauss point by Gauss point transfer of all the physical quantities on to the UM2 mesh.
- Modification of the cracked model (CM1) by setting the ferritic steel/ buttering interface at the correct location and by filling the notch, to give the CM2 model.
- Projection material by material of all the results of the UM2 model to the CM2 model by averaging stresses at the nodes.
- Restoration of the equilibrium of the structure with the projected stresses.
- Machining of the defect by cancelling the material characteristics of the relevant elements.

The restoration of equilibrium, conducted at 20 °C without any loading, reduced the stress levels in the welded zone, namely at the defect location. This problem is caused by the 3D discretization which is non uniform along the circumference. Close to the defect the element size is 0.25 mm and has a much larger value away from the crack. Therefore the large residual stress gradients in the welded zone are not always well represented in the CM model. During the simulation of the test, initially the presence of the residual stress field acts to open the crack. However once the 316L pipe section starts to yield at a moment of 1.24 MN, the predicted CMOD becomes less that given by the residual stress free model (so that the crack driving force is also less). This effect is explained by a local shell bending induced by residual stress relaxation in the yielded 316L pipe section, but it is recognised that further work needs to be done to confirm this and to validate the transfer of the residual stress field into the 3-D model.

7.2.3 Limit Load Determination

The limit load is required for several engineering assessment methods and the results of FE analyses can potentially provide less conservative values than those provided by handbook solutions. Figure 7.7 shows the moment vs. average ram displacement data from the tests together with the TWI FE prediction, which is considered representative of the 3-D pipe analyses). Table 7.2 compares the values obtained using standard graphical methods (tangent intersection and 2x elastic slope) with the handbook solution. The latter is seen to provide the most conservative estimate, which is unsurprising since the formula uses the yield strength value for the weakest material i.e. the 316L[12].

The values obtained from the FE simulation of the pipe behaviour are somewhat above those determined from the experimental curve, reflecting the problem discussed in §7.2.1 i.e. that the predicted ram forces lie above the experimental values for a given applied displacement. Overall, the experimental crack initiation load (1.8 MN.m) is above the limit load estimates in Table 7.2 although of course the critical locations are different.

[12]If the yield strength value for the weld metal (333 MPa) were to be used, the P_{lim} would increase almost 2 MN.m.

Table 7.2: *Limit load values obtained for the ADIMEW mock-up*

Source	Limit Moment, kN.m	Comments
Miller formula	1266	Assumes entire pipe is in 316L, with a yield strength of 213 MPa
FE pipe simulation	1600 1660[13]	Tangent intersection method ASME 2 x elastic slope method
Test data	1375 1500	Tangent intersection method ASME 2 x elastic slope method

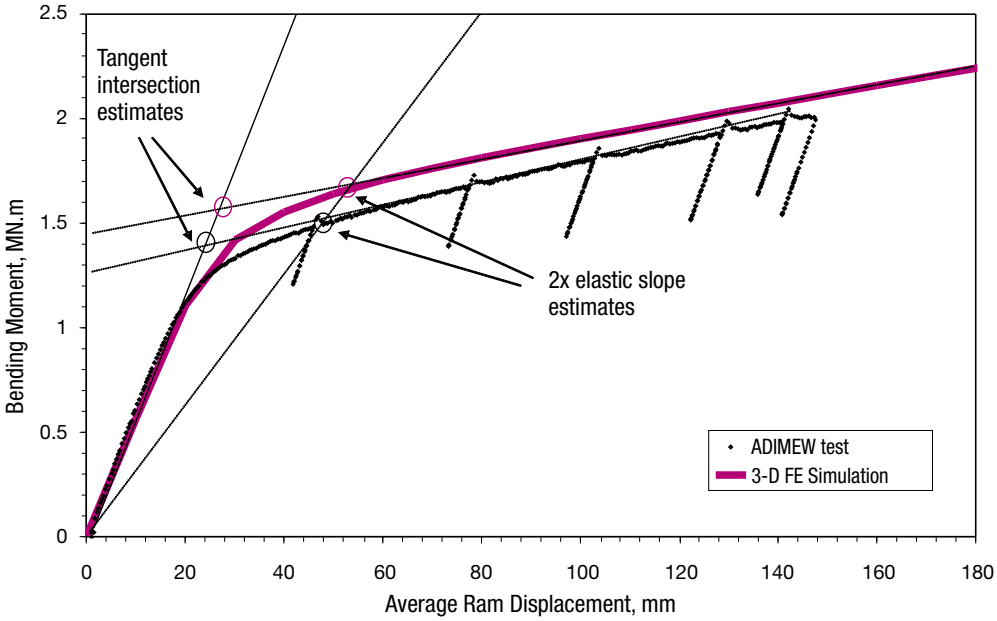

Figure 7.7: *Determination of the mock-up limit load from the load – displacement data*

7.3 ENGINEERING ASSESSMENT METHODS

7.3.1 Best Estimated J-Based Approach for Crack Initiation and Tearing Stability

The most straightforward estimate of the crack initiation moment is obtained by comparison of the predicted values of J and the centre of the crack front with the measured toughness value. As shown in Figure 7.4 the analyses successfully predicted the narrow range of load over which significant growth of the defect occurred, a consequence of the low tearing resistance of the buttering material.

[13]The DNV FAD analysis used a limit load of 1800 MN.m based a 2x elastic slope calculation from their FE results.

Considering the range of $J_{0.2BL}$ values recommended in section 5 above (59 kJ/m² to 110 kJ/m²)[14], predicted values of applied moment for crack initiation from the 3-D analyses lie in the following ranges:

$J_{0.2BL}$ kJ/m²	Predicted Moment at Initiation MN.m
59	1.45 to 1.76
110	1.67 to 1.89

For the lower $J_{0.2BL}$ value the models are seen to provide conservative estimate of bending momemt at initiation compared to the experimentally determined value of approximately 1.8 MN.m. For the higher value of 110 kJ/m², the predictions are also are within ±7% of the above value. Two further factors should be considered in relation to these comparisons:

a) The test result value 1.8 MN.m refers to crack initiation and, as will be discussed further below, if an allowance is made for blunting and a 0.2 mm crack extension a somewhat higher value will be obtained.

b) The above $J_{0.2BL}$ values refer to pre-cracked specimens, whereas the ADIMEW flaw had a finite radius of approximately 0.2 mm. As discussed in section 5 above, the test on notched C(T) specimens show that this may increase the initiation toughness. However the lowest value obtained in such tests was 130 kJ/m² (specimen BZF-4 with a notch 1 mm from the fusion line).

There is no evidence that the small mixed mode character of the crack tip driving forces had a significant influence on the crack initiation load. There is however general agreement concerning the qualitative influence on the observed crack growth behaviour.

- The crack, which is at an angle of 25° to vertical, experiences Mode I/II loading up to initiation
- Mode I dominates at initiation, as the crack grows initially towards the fusion line
- Crack deviated by low constraint (triaxiality) at the ferritic HAZ towards high constraint (triaxial plastic strains) along the fusion line/buttering under Mode I/II loading

For tearing and stability assessment the FE cracked-body approach requires combining results from a series of meshes of different crack depths together with a representative J-R curve. For 3-D models this requires considerable modelling effort as well as *a priori* assumptions about the direction of likely growth over the crack front. TWI and CEA followed this approach, assuming that the crack front remains straight during growth. Figure 7.8 illustrates tangency conditions between driving force and J-R curves. The implicit assumption of load rather than displacement controlled conditions resulted in rather low estimates of the amount of stable crack extension, almost an order of magnitude below that observed in the ADIMEW test. Furthermore the uncertainty about the tearing modulus of the J-R curve and the lack of valid experimental data for crack growth of than a few mm was reflected in the variability of the instability load estimates (Figure 7.9).

[14] $J_{0.2BL}$ values are 59 kJ/m² rom the 20x40 SE(B) specimen with a pre-crack 1.5 mm from the fusion line and 110 kJ/m² for the "corrected" value for 25 mm thick C(T) specimen.

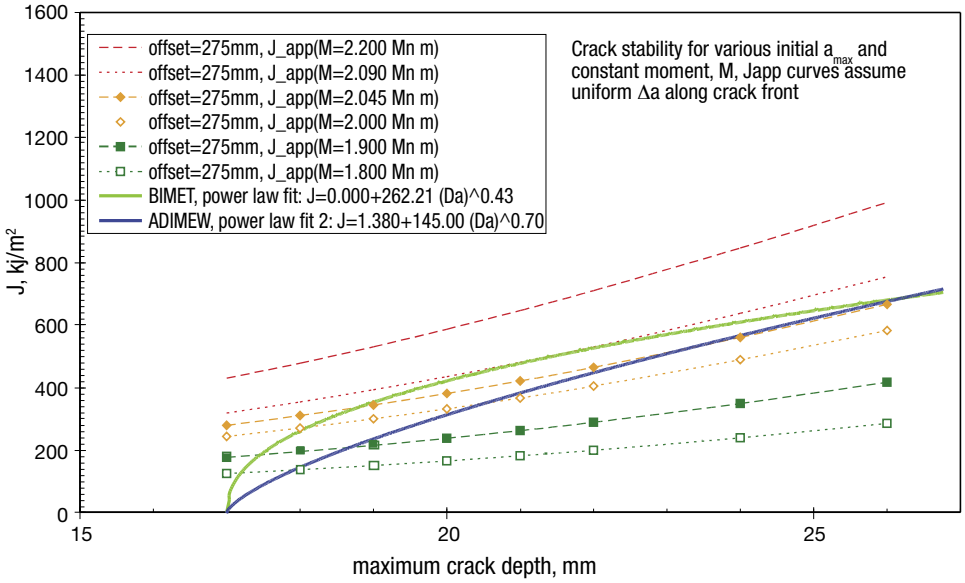

Figure 7.8: *Comparison of two buttering J-R curve fits with applied J vs. crack depth data for increasing levels of applied moment*

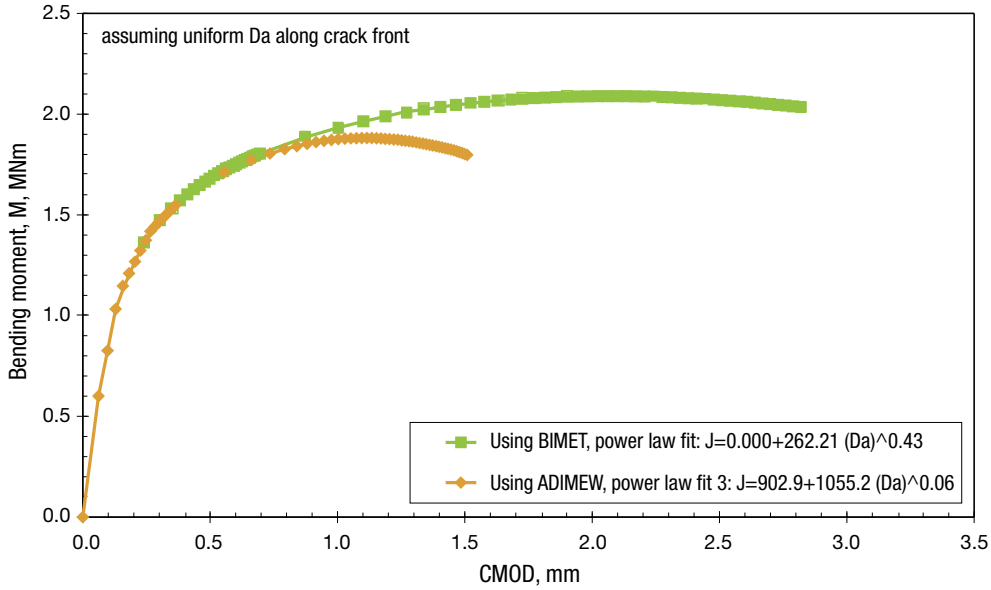

Figure 7.9: *Predicted bending moment vs. CMOD curves for two buttering J-R curve fits*

7.3.2 Failure Assessment Diagram Approach

The FAD approach as implemented in the R6 [97] and SINTAP[15] [98] procedures considers both fracture initiation and local plastic collapse modes and is designed to provide inherently conservative estimates of the critical defect size or critical load for fracture initiation. It is noted that the plastic collapse criteria is applied to the weakest part of the structure under consideration, which may not necessarily correspond to the defect location. This is the case in ADIMEW, where the 316L pipe reaches its limit load before the dissimilar weld on account of its much lower yield strength. Both Serco [62] and DNV [94] applied this approach to the ADIMEW test.

The Serco analysis followed the SINTAP procedure, using a conservative handbook calculation of the crack driving force K as a function of applied moment. For the fracture toughness two value of Jmat were considered: 67 kJ/m^2 from TWI tests and 300 kJ/m^2 from a notched C(T) specimen. The assessment of initiation is significantly influenced by the choice of limit moment. In their case as estimate of 1600 KN.m was used, derived from FE analysis. Residual stresses were also considered, using the profiles given in section 6.1.4. Figure 7.10 shows an example of the assessment diagrams. The predicted values of applied moment at initiation are summarised in Figure 7.11, showing that results from all three levels are highly conservative. Residual stresses were observed to have a marked influence on the predicted value of initiation moment. However this is considered to be due to conservatism in the SINTAP methodology rather than the high levels of residual stress used in the assessment. Firstly, the residual stress profile was that for ambient temperature rather than the reduced value expected at 300 °C (see §6.2.6 above). Secondly, in the absence of residual stresses the current assessments generally lie within the high L_r regime (see Figure 7.10), where the applied moment is either approaching, or above the moment for plastic collapse. In this regime, the development of extensive plasticity effectively "washes out" the effect of residual stresses on the crack driving force [99].

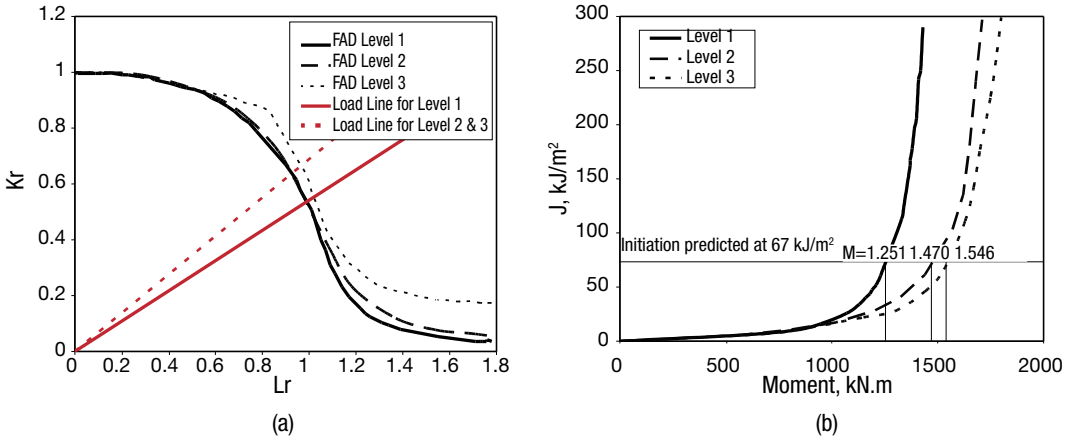

Figure 7.10: *SINTAP assessment of initiation based on J_{mat} = 67 kJ/m² using a) FAD and b) CDF approaches (the results are equivalent)*

[15]In SINTAP both FAD and crack driving force (CDF) approaches can be used and give equivalent results.

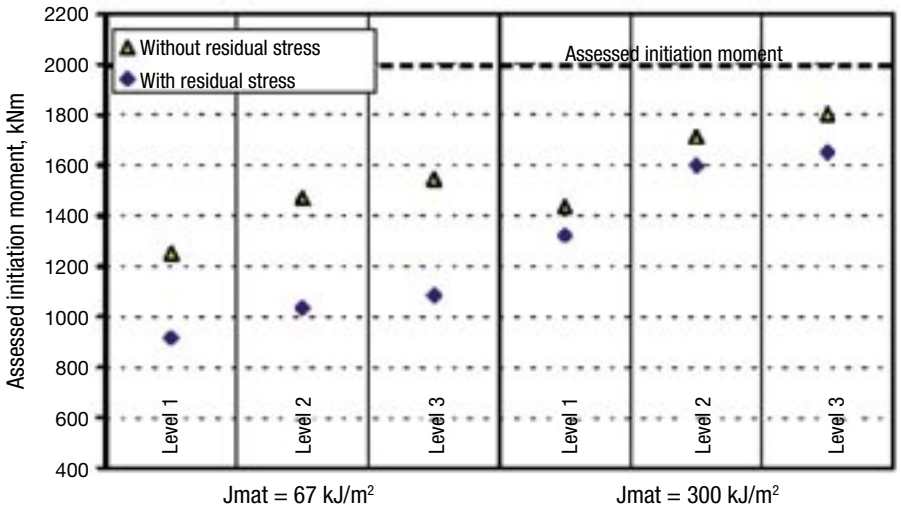

Figure 7.11: *Results of the SINTAP assessment of initiation in the ADIMEW test for two two toughness values. (Level 1: homogeneous material (316 L); Level 2: considers mismatch in the yield strengths between base and weld; Level 3: considers mismatch in the stress-strain curve between base and weld)*

Serco also used the SINTAP procedure to assess conditions for instability i.e. onset of unstable ductile tearing. Using the so-called "TWI" J-R curve, which is similar to the SE(B) curve shown in Figure 5.17, the predicted values of maximum stable tearing, Δa_{max}, and maximum applied moment, M_{max}, are 4 mm and 1.715 MN.m respectively.[16] This assumes load-control conditions, under which the attainment of a maximum load would produce unstable crack growth. In contrast the ADIMEW test was performed under displacement-control to avoid this. Careful analysis of the experimental load-displacement data suggests that maximum load was achieved at just over 2000 kNm, corresponding to a ram displacement of approximately 150 mm, i.e. slightly above the measured initiation moment. If the ADIMEW mock-up had been tested under load control, it is likely that instability would have occurred after a small amount of tearing. The calculated moment at instability is therefore shown to be conservative for the test conditions.

The DNV analysis used the R6-method (option 1) as implemented in the SACC software to calculate a critical defect size in the buttering. The assumed values of J_{mat} = 156 kJ/m² (as initially reported from the AREVA NP SAS C(T) tests) and of a limit load equal to 1.8 MN.m (based on the twice the elastic slope criterion) were somewhat higher than those in the SINTAP analysis. Also the crack driving force vs. moment relationship was taken from the handbook solution for a semi-elliptical crack perpendicular to the outer surface (see §7.2.2). The predicted critical defect size was 3.1 mm using the 316L yield strength and 18.4 using the weld metal yield strength. Introducing a weld residual stress reduced the later to 16.4 mm, which is consistent with the flaw depth of 17 mm used on the ADIMEW mock-up.

[16] If the lower bound J-R curve proposed in section 5.2.3 were to be used, the predicted extent of stable tearing would increase, while the applied moment value at instability would decrease.

To supplement the above R6/FAD analyses, NRI [91] investigated a modified J-R curve expression in which the effects of mixed mode loading, strength mismatch induced constraint and geometric constraint on the tearing behaviour can be allowed for. Determining the stability or instability of crack growth is seen as fundamental to the evaluation of piping integrity or evaluation of safety margins, whereas crack initiation is considered less critical as well as being difficult to define or measure in an unambiguous way. Such an evaluation relies on the validity of the J-R curve for the full range of ductile tearing foreseen on the component. As a baseline, the TWI 10x10 mm SE(B) specimen[17] test data were used. The form of J-R curve adopted is $J=C\Delta a^n$, in which n is fixed and C is modified by a correction factor equal to the product of three sub-factors: C_1 for mixed mode loading, C_2 for mismatch induced constraint and C_3 for "purely geometric" constraint.

- C_1 depends on strain hardening characteristics and mode mixity: for the weld metal $J_{IIc}/J_{Ic} \cong (K_{IIc}/K_{Ic})^2 \cong 0.64$, but for small K_{II}/K_I, $C_1 \cong 1$. Taking the average gives $C_1=(0.64+1)/2=0.82$.
- C_2: the effect of stress triaxiality due to mismatch (0.953) can be assessed via a local approach concept, whereby C_2 is inversely proportional to the cavity growth rate in the Rice-Tracey model; thus $C_2=1/\exp(1.5*(0.953-1/3)) \cong 0.39$.
- C_3 can be assessed with help of correlation of J-R curves of medium strength ferritic steels with the load-independent constraint parameter T_{stress}/K_I; due to the higher strain hardening exponent of the weld metal, the result $1<C_3<1.7$ is obtained, with average value $C_3=1.35$.

The product $C_1C_2C_3$ gives an overall correction factor of 0.437, which lies between that of 0.155 obtained from extrapolation of the TWI [80] "fit 1" J-R curve ($J=200.48.\Delta a$) and that of 0.497 obtained from extrapolation of the "fit 2" J-R curve ($J=145\Delta a^{0.7}$). These correction factors on the "fit 1" and "fit 2" J-R curves are obtained by seeing how much to reduce C to reproduce the experimental maximum load of 2 MN. Values of load are calculated for increasing values of crack length, with each step consisting of the following sequence: set a crack length value, calculate J from the J-R curve with a reduced C value, calculate K_{eq} and finally calculate a maximum load for instability using a R6/FAD analysis. The analysis also provides estimates of the crack length increment required for initiation of unstable crack growth under load control: "fit 1" gives 15.7 mm while "fit 2" gives 12.8 mm.

7.3.3 J_i-G_{fr} Approach

This engineering method [100] was developed at CEA to extend the conventional J-R curve approach for predicting large ductile crack propagation in components. It uses two independent parameters to represent resistance to ductile tearing. J_i is the critical value of J representing the onset of crack extension and is usually much lower than J_{IC} but is less sensitive to stress triaxiality. The second parameter G_{fr} represents the dissipated energy in the fracture process for a unit extension of crack area. Estimates of J_i and G_{fr} were determined from the notched C(T) specimens. These were combined with J values for a straight crack of increasing depth to predict the bending moment vs. crack growth curve (Figure 7.12). The best agreement was obtained with $J_i=240$ kJ/m² and $G_{fr}=11$ MPa from specimen BZF1 (notch radius 0.1 mm, notch tip 2 mm from the fusion line). However the beginning of the propagation is not correctly reproduced. Further work was proposed to integrate this method into a 3-D FE analysis with adaptive crack tip meshing to allow prediction of the non-uniform crack growth observed in the test.

[17] Specimen A2-2, initial crack in the buttering at 1.5 mm from the fusion line.

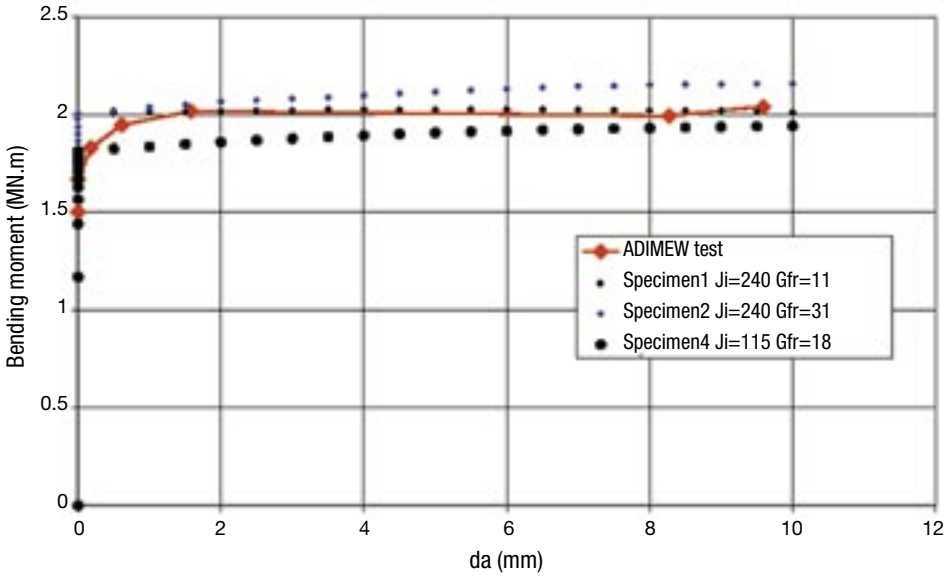

Figure 7.12: *Results of the J_i-G_{fr} approach using parameters calibrated from the notched C(T) tests BZF1, BZF2 and BZF4*

7.3.4 Engineering Analysis Based on CTOD

The Basler & Hofmann and Mat-Tec AG analyses [86] focussed on the use of simplified engineering methods, using crack-tip opening displacement (CTOD) to characterise the driving force and material toughness. The advantages of the CTOD over the J-based approach to cope with the various difficulties associated with dissimilar welds are considered to be:

- It avoids the path-independence restrictions of the J-integral at interfaces.
- Each crack opening mode can be identified and treated separately, whereas J as a scalar quantity does not distinguish between mode I and mode II loading components
- Larger range of applicability of CTOD-R-curve, which is required to determine the ultimate load by a tearing stability analysis
- Lower sensitivity of CTOD (compared with J) to temperature effects

On the other hand, fracture toughness in terms of CTOD can be more sensitive to constraint effects, although in the present case this is not a problem because a very high (saturated) level of constraint has to be assumed due to the crack path along the fusion line.

The pre-test analysis was limited to crack initiation and growth. The CTOD values were taken from the 2-D cracked body sub-model (Figure 7.6). Because of TWI CTOD data was not available until latter in the project, a J-R-curve was transformed to the required δ-R curve using the general relation: $J = m \cdot \sigma_f \cdot \delta$, where σ_f is the flow stress and m is a calibration factor and itself a function of J.

Using this approach a "best-guess" J-R-curve for the buttering was transformed to the δ-R curve. For crack growth along the fusion line, a δ-R curve is estimated to be about half of the one of the buttering layer due to constraint effects Figure 7.13. Combining the crack driving force and with the criterion that crack initiation occurs at Δa=2.0 mm, the corresponding bending moment is M_i=1.75 MNm. In principle, the crack prolongation Δa(M) can also be calculated but, since crack growth is not accounted for in the underlying simplified model, the validity of this approach is restricted to $\Delta a << a_0$=17 mm. Disregarding this restriction and assuming the crack reaches the fusion line after about 4 mm growth, the curve designated in Figure 7.14 as "best guess" resulted. In comparison with the measured curve one can see that the bending moment, at which initiation took place, M_i, was obtained surprisingly good, but that the subsequent curve of crack-growth is actually much steeper than the predicted one. Furthermore the amount of stable crack growth Δa_s (i.e. crack growth up to maximum load) was estimated to be 18 mm. These predictions were the closest to the measured ones of all the ADIMEW-NESC-III pre-test analyses, although most of them used much more sophisticated and time consuming analysis methods.

In the post-test analysis the model was extended to include tearing crack-growth and stability. Under load-control, tearing crack growth becomes unstable as the maximum load of the system is reached. Under displacement controlled loading condition, tearing can be stable even beyond maximum load. Therefore, the condition for tearing instability under load-control can be used to determine the ultimate load bearing capacity. As a first step the ADIMEW test data was re-analysed.

Figure 7.15 shows the measured rate of CTOD, d(CTOD)/dt, normalized by the ram-loading velocity v_R, as a function of the bending moment. Up to about M=2 MNm, it was more or less constant and then it dramatically increases, indicating that tearing stability was partially lost in this stage even though the test was performed under overall displacement control. This implies that the recorded maximum load of 2.04 MN.m also provides a good estimate of the collapse load. The CTOD model was applied to predict this behaviour. First the 2-D FE model was used to generate a set of M vs. CTOD curves for a series of crack depth values ranging from 17 mm to 38 mm. This data was then combined with the three possible CTOD-R curves (see Figure 7.13) to determine stable crack extension as a function of crack extension. The resulting predictions for initiation load, "technical initiation load" and collapse are given in Table 7.3 and are consistent with the experiment values from the ADIMEW test.

Table 7.3: *Comparison of predictions from the CTOD analysis [86] for three different CTOD-R curves*

		Initiation load M_i [MNm]	Deviation	Techn. initiation load $M_{0.2BI}$ [MNm]	Deviation	Collapse load M_u [MNm]	Deviation
ADIMEW Test		1.73	-	1.81	-	2.04	-
Predictions using different CTOD-R curves	Best guess	1.84	6.3%	1.91	5.5%	1.96	-3.9%
	Lower bound (fusion line)	1.56	-9.8%	1.64	-9.4%	1.88	-7.8%
	Upper bound (buttering)	1.86	7.5%	1.93	6.6%	2.28	11.8%

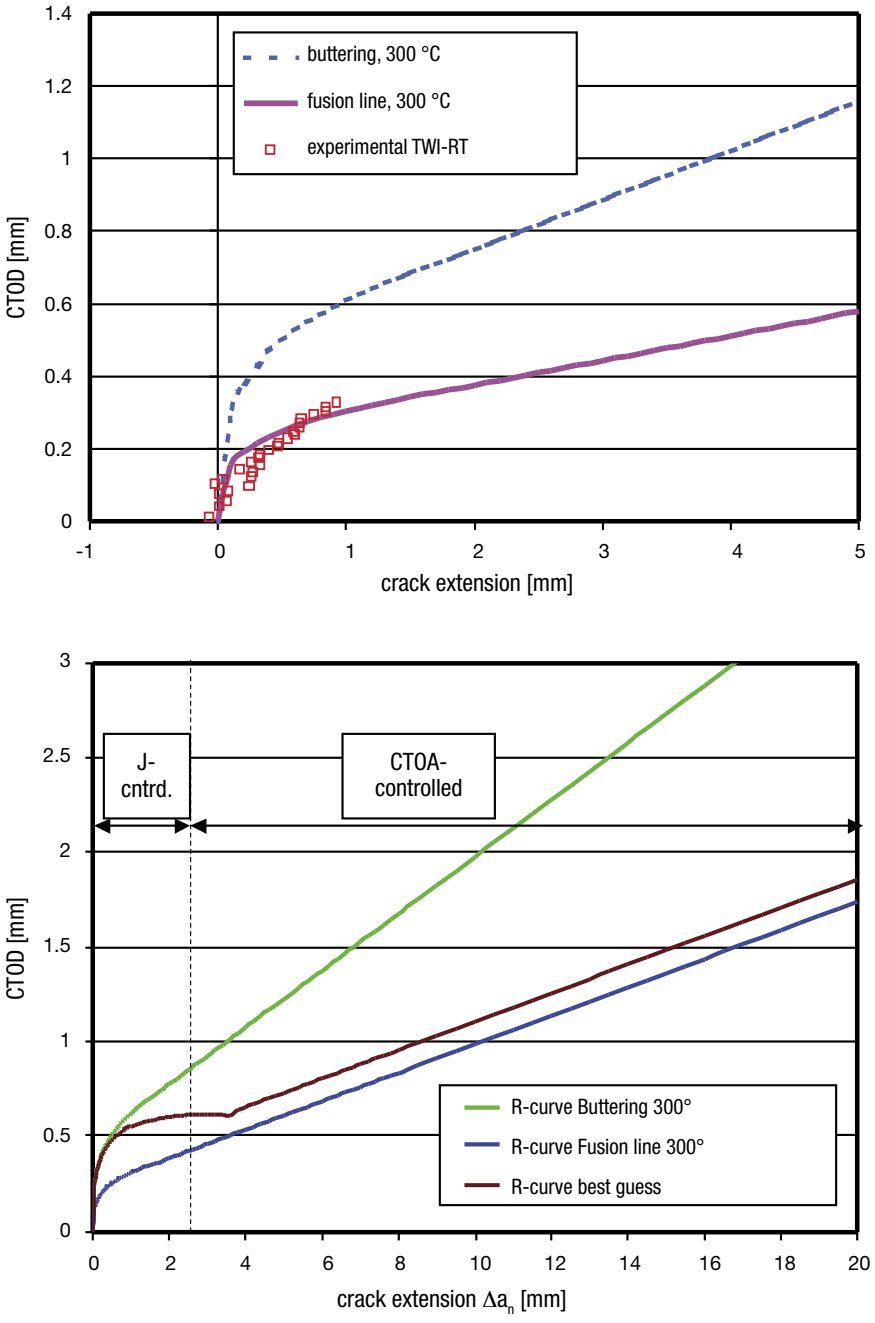

Figure 7.13: *Estimated CTOD as a function of crack extension Δa at 300 °C a) in comparison with limited experimental data and b) extended curves for large scale tearing assuming constant CTOA*

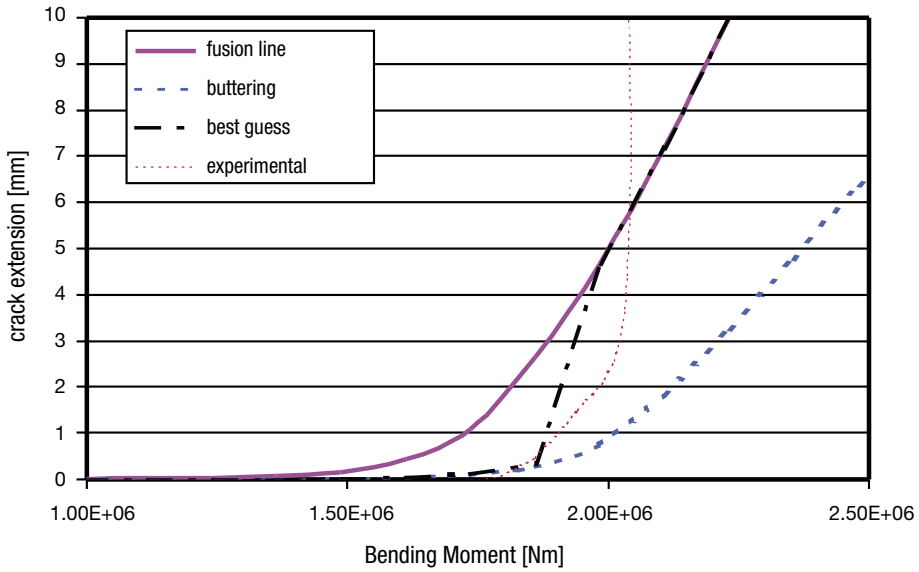

Figure 7.14: *Predicted crack extension in comparison with the measured curve from [86]; the best guess curve follows the buttering curve up to initiation and then links to the fusion line curve, mirroring the test behaviour*

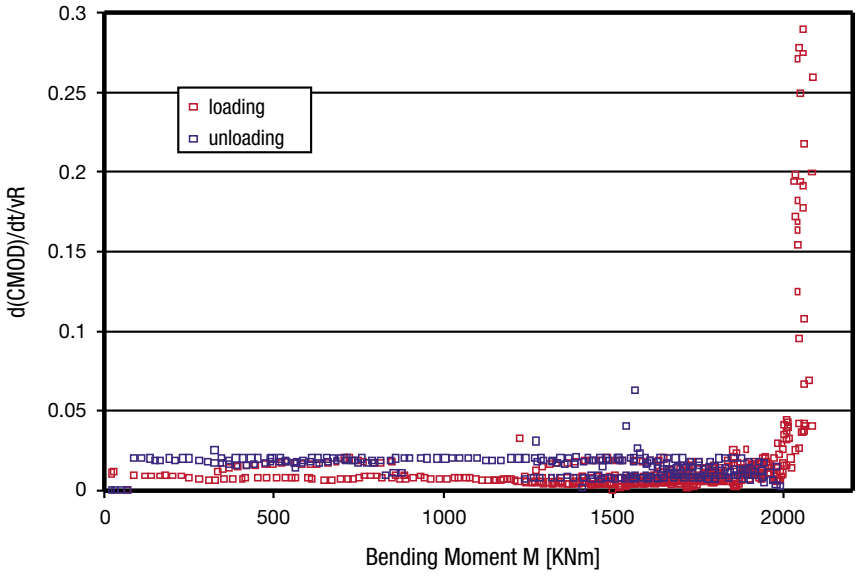

Figure 7.15: *Rate of change of CMOD normalized by the ram speed as a function of the bending moment during the ADIMEW test*

7.4 DERIVATION OF A J-R CURVE FROM THE ADIMEW TEST DATA

The possibility of combining the ADIMEW test data with J estimates to derive a "component" J-R curve[18] was investigated by two organisations.

In the CEA study [82] the first step involved a series of 3-D FE analyses for different crack depths, assuming however a straight crack front. By considering the elastic and plastic components of J, a load dependent calibration factor η was derived. Secondly a precise analysis of the potential drop and compliance measurements made during the test allowed revised estimations of tearing initiation to be made. Finally the experimental crack growth values at the centre of the defect could be combined with the crack driving force estimates to produce a J-Δa curve (Figure 7.16). The main results were as follows:

- Initiation i.e physical growth of the crack after blunting, is determined from the point at which the CMOD vs. Δa data diverge from the initial linear portion. The value obtained was J_i=146 kJ/m² at a bending moment M_i=1.89 MN.m
- $J_{0.2}$ is determined from a 0.2 mm offset of the CMOD - Δa blunting curve. The value obtained was $J_{0,2}$=230 kJ/m² at M=1.98 MN.m.
- The slope of the J-Δa curve for Δa>0.5 mm with dJ/da≈50 MPa.
- The resulting estimates of crack propagation at M_{max}=2.1 MN.m are:
  – Δa_{mean} = 9 mm for the equivalent straight defect.
  – Δa_{max} = 20 mm for the deepest point of the defect

It is noted that the J-Δa curve is a first approximation because the η-factor compendium was derived for an equivalent mean straight-fronted defect. To improve this, a series of FE calculations with more realistic crack shapes i.e. no propagation at surface point, would have to be performed.

GRS [92] performed a single 3-D FE analysis for the initial 17 mm notch depth, and adopted a more simplified approach for determining the J-R curve. This assumes that stresses and strains are constant during crack growth, so that J [a+Δa]=J[a] * (a+Δa)/a, where "a" is the original crack depth and Δa is the crack increment at the centre of the crack. By using Δa values from the unloading compliance measurements made during the test, crack growth corrected J values are calculated.

Figure 7.16 compares the two estimated "ADIMEW test" J-R curves with the data from a) a pre-cracked SE(B) specimen and b) the notched C(T) specimen BZF4. The GRS estimated curve is seen to be in reasonable agreement with the SE(B) curve, whereas the CEA predictions are somewhat higher, especially for large Δa values. In this respect it is noted that the values of J calculated by GRS for a given applied bending moment are at the low end of the range, as can be seen in Figure 7.4. Allowing for this difference would bring the two estimated J-R curves much closer. The J-R curve from the notched C-T specimen BZF4 lies well below the two estimates, and confirms its lower bound nature.

[18] It should be noted that the physical meaning of this approach for the ADIMEW defect is questionable. As is discussed in section 7.5 below, in the mock-up test the crack path deviated sharply and then followed the ferritic - buttering interface in stable tearing mode. This confirms a dominant effect of stress triaxiality on ductile tearing. The maximum normal stress criterion valid in contained plasticity predicts that the crack should extend in mode I, which in this case would be in a direction normal to the pipe axis.

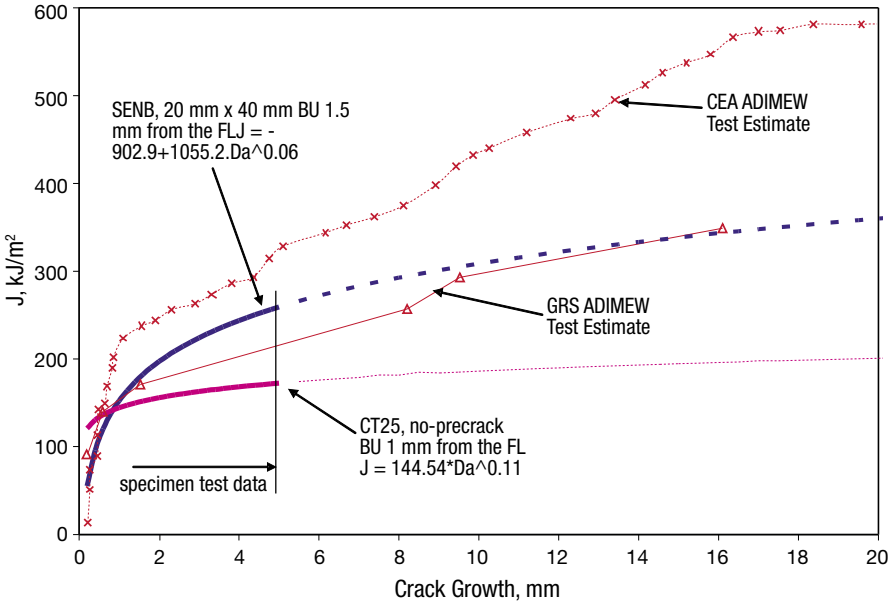

Figure 7.16: *J-R curve estimates from the CEA and GRS analyses compared with experimental data from pre-cracked SE(B) and notched C(T) specimens*

7.5 LOCAL APPROACH ANALYSES

The underlying idea of the local approach is to model the actual failure mechanism in connection with a detailed analysis of the stress and strain field. Although the J approach may be used up to initiation, it cannot predict either the extent or direction of crack growth without making some equivalence based on experimental observations.

In the ADIMEW mock-up the pipe is under bending, but at the notch location the loading is almost uniform and tensile. The notch makes a 25° angle with the pipe axis and therefore is loaded in mode I and II. Following the maximal stress criterion, established in Linear Elastic Fracture Mechanics but valid under limited yielding, the crack will deviate by an angle of –28°. The crack is predicted to propagate almost normally to the pipe axis and should therefore cross the interface.

A J value may be estimated for an equivalent crack, being the projection of the actual one on the plane normal to the pipe axis and containing the initial crack tip. J is an energy, which at yielding level depends mainly on the equivalent strain. Criteria based on maximum of J would give a path close to the line of symmetry of the directions of maximum yielding, as the direction given by the maximum stress criterion (Figure 7.17a). However ductile tearing is caused by cavity growth and coalescence and these mechanisms depend strongly on stress triaxiality. The local approach analyses show effects play a decisive role in determining the crack growth path The location of maximum triaxiality (Figure 7.17b) is influenced by constraint, deviating initially towards the ferritic

steel/buttering interface and then running parallel to it, just as observed in the experiment. This effect is independent of crack length. As a consequence of this, the tearing along the interface observed in the experiment cannot be analysed by a J based approach, and as an alternative AREVA NP SAS [76-79] have examined the calibration of three different local approach models using the SYSTUS program.

a) Rice-Tracey Model

The Rice and Tracey criterion [101] is based on an estimate of the average growth rate of a spherical cavity in a rigid plastic subjected to a remote tensile field with superposed hydrostatic stress. AREVA used a slightly different model, which accounts for strain hardening effects and is applicable to non increasing loads. The cavity growth is driven by the following formula:

$$\frac{d}{dt}\left(\ln\frac{R}{R_o}\right) = f\left(\sigma_{eq}\right)\exp\left(\frac{3}{2}\cdot\frac{\sigma_m}{\sigma_{eq}}\right)\dot{\varepsilon}^{p}_{eq}$$

Where σ_m is the hydrostatic stress, σ_{eq} is the von Mises equivalent stress, R and R_o are the actual and initial cavity radii, σ_m/σ_{eq} defines the triaxiality ratio, $\dot{\varepsilon}^{p}_{eq}$ is the equivalent plastic strain rate and *f* is a function developed by P. Lederman and implemented in the SYSTUS code [102]. The approach is referred to by the RTL acronym. Damage and yielding are uncoupled. The calibration was first performed for the C(T) specimen[19] using a 2-D model. It was found that increased computational efficiency is obtained for crack growth simulation using delocalised parameters. The model provided an excellent prediction of the observed load decrease due to crack initiation and growth. It was then re-calibrated with the 20 mm x 40 mm SE(B) specimens. The predicted initiation is at J=88 kJ/m^2. Values of critical void ratio $(R/R_o)_c$=1.3 and radius of the crack tip zone l_c=250 μm were determined.

The model was then implemented in the overall 3-D model of the mock-up. Figure 7.18 shows the predicted influence of ductile crack growth on the moment-CMOD curve. The predicted initiation is at J=89 kJ/m^2. The calculated mode mixity is approximately 80% mode I and 20% model II in terms of CMOD. A delocalization technique was used for simulating the crack extension without any pre-orientation of the mesh. It proved possible to simulate several mm of tearing and the key features of the observed crack path (first towards and then along the fusion line) and non-uniform growth (no circumferential extension), as indicted in Figure 7.19. However in spite of a careful calibration of the parameters, the model could not simulate more than 4 mm of crack growth. Overall it main advantage are: its validity for ductile tearing initiation and growth; good prediction of crack path; independence from loading conditions and its applicability to the notched structure; capability to model unloading (although the effect is negligible). Difficulties encountered include the time-consuming mesh preparation and calculation and the need for a 3-D model of the structure.

[19] The parameters are typically calibrated using data from a notched tensile specimen. A small number of such tests were performed on cross-weld specimens with the notch in the buttering layer., but the lack of direct diametral strain measurements at the root and its ovalisation during deformation meant that the results were not usable.

b) Gurson-Tvergaard-Needleman Model

More advanced models account for the macroscopic softening in the process zone due to void growth using special yield functions. The Gurson-Tvergaard-Needleman model [103,104,105] represents such a coupled approach and can be stated as:

$$\Phi\left(\sigma_{ij}, f\right) = \left[\frac{\sigma_{eff}(f)}{\sigma_{eff}(0)}\right]^2 + 2q_1 f \cosh\left(\frac{q_2 \sigma_h}{2\sigma_{eff}(0)}\right) - q_1^2 f^2 - 1 = 0$$

where f is the void volume fraction, $\sigma_{eff}(f)$ the macroscopic effective stress i.e. over several voids, $\sigma_{eff}(0)$ is the current matrix flow strength and σ_h is the hydrostatic stress. q_1 and q_2 are parameters introduced by Tvergaard to provide a better fit with experimental results. The calibration was performed for the SE(B) W40 specimen, using 250 micron square elements for the crack tip and growth zone. It was shown that the load-CMOD curve could be accurately predicted. The parameters are not de-localised. This model was then implemented for the pipe system model, using a new crack tip and ligament mesh with respect to that for the RTL model. It was found that the moment-CMOD curve is predicted with good accuracy up to a CMOD of 1.2 mm, but the corresponding maximum crack growth of 5 mm is only marginally more than that obtained using the RTL model.

c) The Wilkins model

In the Wilkins model [106] the damage parameter is given by:

$$D = \int w_1 w_2 d\varepsilon_{ep}^p$$

where:

ε_{ep}^p is the equivalent plastic strain,

w_1 is a hydrostatic pressure weighting term given by: $w_1 = \left(1 \Big/ \left(1 - \frac{P}{P_{\lim}}\right)\right)^{\alpha}$

P is the hydrostatic pressure and D= D_c when $P \geq P_{lim}$

w_2 is a deviatoric stress weighting term: $w_2 = (2 - A)^{\alpha}$, $A = Max\left(\frac{s_2}{s_1}, \frac{s_2}{s_3}\right)$ and $s_1 > s_2 > s_3$.

s_1, s_2 and s_3 are the principle stress components of the deviatoric stress tensor.

The parameters P_{lim}, α and β are calibrated from experimental results, ideally performed under multi-axial loading conditions. The delocalisation distance, called R_c is an intrinsic material property as it is linked to the inter-cavity distance. The Wilkins model parameters are associated to this distance. For 2-D modelling, delocalisation volume corresponds to a disc. In case of 3-D modelling, this volume is a sphere. The calibration of the model parameters for the buttering material resulted in the following values: D_c=0.4, α=1.5, β=0 and P_{lim}=1200 (for R_c=250 μm). The predicted initiation is at J = 102 kJ/m^2. The computation was stopped after 12 mm of growth at the centre of the crack. As shown in Figure 7.18, the flattening-out of the moment-CMOD curve is better predicted than with the RTL or GTN models. Overall the model gave excellent predictions in terms of crack opening, crack path, extension of growth through the wall, and crack shape (Figure 7.20). This is all the more remarkable since most of the growth occurs under constant moment and is attributed to the ability of the Wilkins model to account for the high hydrostatic pressure which develops between the crack tip and the interface.

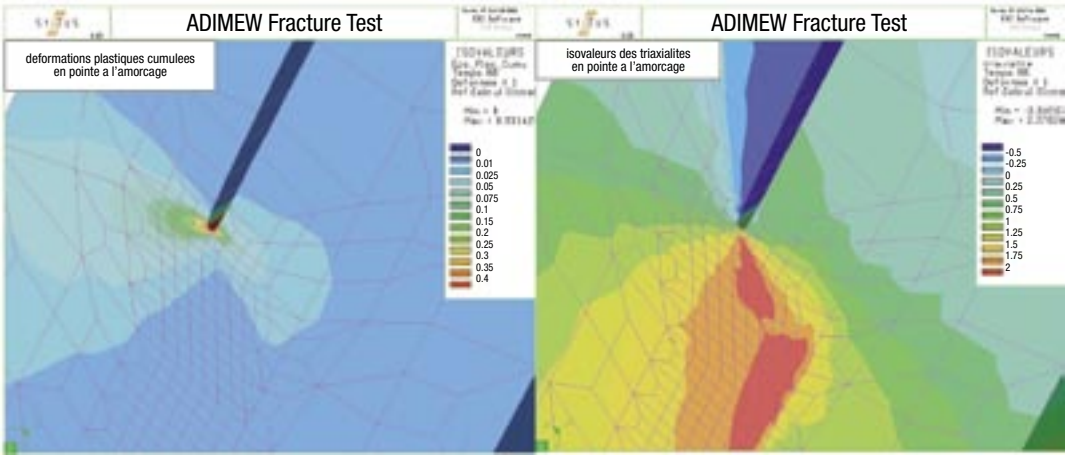

a) *b)*

Figure 7.17: *Distribution of a) the accumulated equivalent plastic strain and b) stress triaxiality field at initiation*

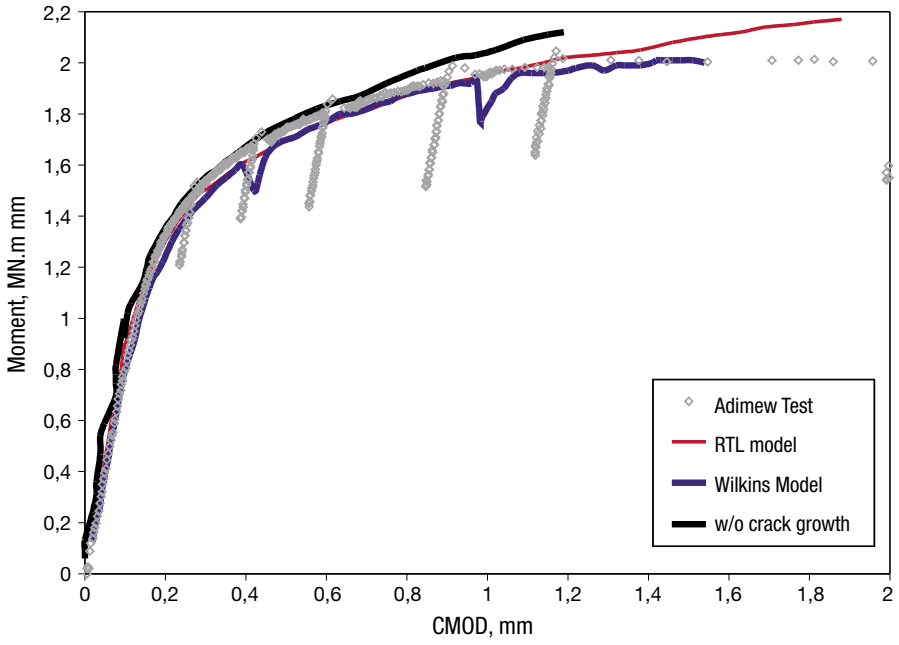

Figure 7.18: *Comparison of predicted bending moment versus CMOD for the ductile tearing local approach models, a FE model without crack growth and the ADIMEW test experimental data*

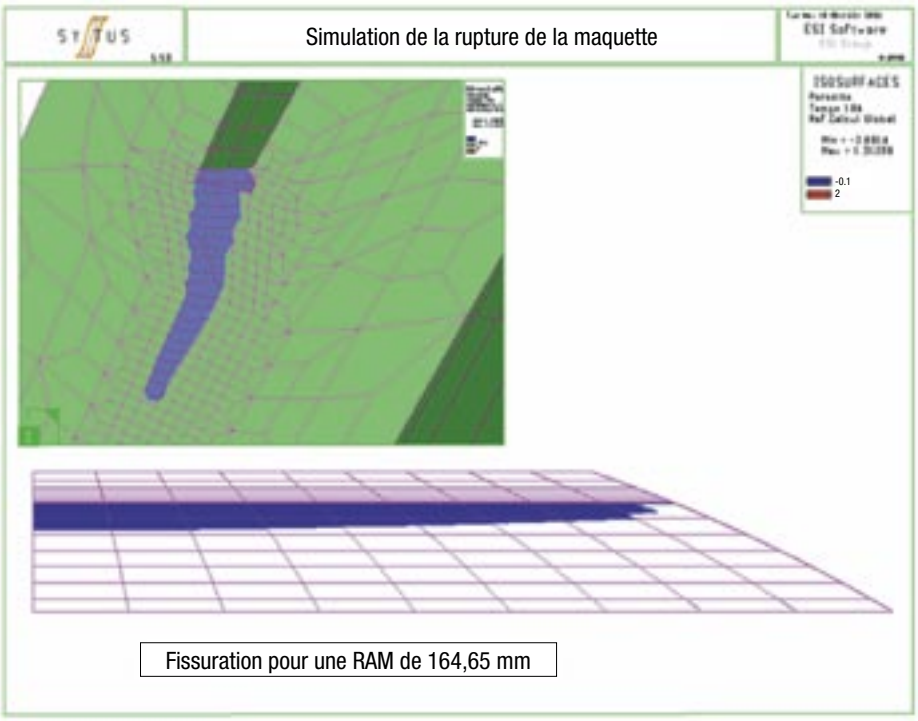

Figure 7.19: *Simulation of ductile tearing in the symmetry plane of the ADIMEW mock-up using the RTL ductile tearing local approach model*

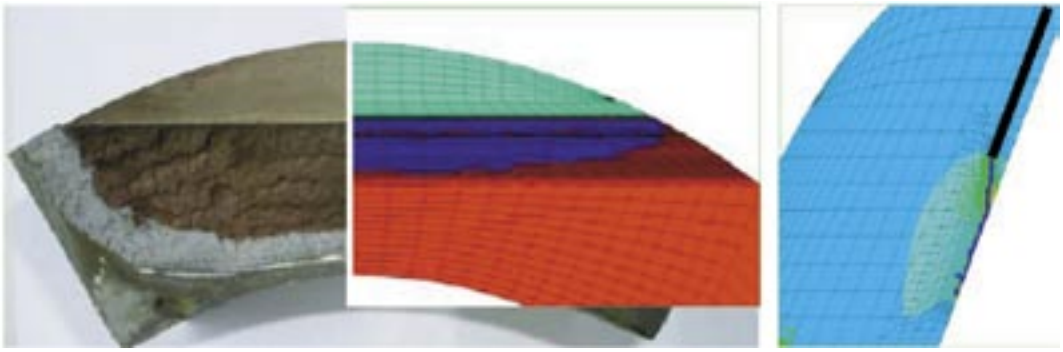

Figure 7.20: *Predictions using the Wilkins ductile tearing local approach model of a) crack front shape and b) the propagation path [79]*

8 CONCLUSIONS AND RECOMMENDATIONS

NESC-III has provided a framework for a series of investigations concerning DMW integrity assessment. These complement and extend the results of the ADIMEW project, in which a large-scale test on pipe assembly containing an artificial defect was performed. The main conclusions are as follows:

- The ADIMEW test is confirmed as a valid and important benchmark for verifying flaw assessment methods for dissimilar metal welds. It demonstrated that a real size structure with a circumferential defect in the buttering close to the fusion line can sustain bending displacements and loads above the limit level without cleavage or unstable tearing. The crack growth mechanism corresponded to that found in the earlier BIMET tests i.e. initial deviation towards the fusion line followed by extensive stable ductile tearing in the buttering along the the fusion line. Stability assessment for such tearing is considered critical to any integrity or leak-before-break assessment. The post-test analyses have shown that in the maximum applied moment in the ADIMEW was probably close to the instability limit, enhancing its usefulness for verification of calculation methods.
- Determination of a representative J-R curve for the defect location and expected crack propagation path along the buttering interface emerged as a key challenge. Despite an extensive laboratory testing programme involving several laboratories, there remains uncertainty over the crack initiation toughness. The test data available provided limited evidence that J- or CTOD-R-curve for a crack propagating very close to the fusion line is lower than that of the bulk buttering material, as would be suggested theoretically by high level of stress concentration (constraint) due to the yield-strength mismatch at this location. Recommendations for future fracture testing include: a preference for the C(T) rather than the SE(B) geometry; use of specimens with pre-cracks either on the fusion line or well (>2 mm) into the buttering, as results from “intermediate” crack positions can prove difficult to interpret; pre-cracking should be done with side grooves; specimen dimensions should be as large as possible (if necessary used weld build-up) to maximise ductile growth. With respect to the latter, CTOD rather than load line displacement measurements allow for a larger range of valid crack growth measurement.
- In characterising the residual stresses present in the ADIMEW weld, the different measurement techniques proved complementary. The neutron diffraction data provided a 3-D mapping of the strains and stresses, although the thickness of the weld and its crystallographic texture meant that only the hoop direction data is fully reliable. The surface hole drilling measurements proved susceptible to machining effects and need to be treated with caution if they are used to infer through-section profiles. In this respect the cut-compliance method proved useful in explaining apparent discrepancies between the surface and ND data, but it is limited to one directional component. The computational round robins to predict the residual stresses demonstrated that full weld process simulations produced distributions in reasonable agreement with the ND measurements. The simulation of creep effects during the PWHT proved critical, and it is recommended that creep properties should be clearly defined at the beginning of future exercises of this type.

Simplified calculations based on thermal mismatch alone were found to underestimate stresses at some locations.

- The application of FAD methods confirmed that the basic option 1 (which uses the lowest yield strength properties i.e. of the 316L(N) pipe and handbook K solutions) is highly conservative. More realistic predictions require the incorporation of better estimates of the crack driving force and limit load, for instance from FE analysis, and allowance for mismatch effects. Incorporating the measured weld residual stress profiles further reduced the predicted initiation load (or, equivalently, the critical defect size). However FE weld simulation models show that the axial weld residual stresses are small at 300 ˚C. Furthermore their effect can be neglected for crack tearing analysis (although their role in driving sub-critical crack growth processes remains important).
- The usefulness of elasto-plastic FE cracked body models for best-estimate approaches with the J-integral or CTOD parameters was demonstrated. The overall mock-up behaviour could be simulated to a good degree of accuracy, although the fact that the calculated crack tip moment values for a given average ram displacement overestimates that measured experimentally by 4 to 8% indicates that the models were slightly too stiff. The narrow load range for initiation of crack extension was predicted, despite the uncertainty in the measured fracture toughness data. At initiation the analyses show that the 316L parent pipe is subjected to extensive yielding. The small mixed mode character of the field at the inclined crack appears to have minor influence when assessing the fracture initiation load.
- The implicit assumption of load rather than displacement controlled conditions in the tearing and stability analyses resulted in rather low estimates of the amount of stable crack extension (2.5 mm), an order of magnitude below that observed in the ADIMEW test. Furthermore the uncertainty about the tearing modulus of the J-R curve and the lack of valid experimental data for crack growth for more than a few mm was reflected in the variability of the instability load estimates. The FE cracked-body approach requires combining results from a series of meshes of different crack depths together with a representative J-R curve. For 3-D models this requires considerable effort as well as *a priori* assumptions about the direction of likely growth over the crack front. Simplified 2-D sub-models were shown to provide an efficient alternative.
- Local approach models provided capable of accurately predicting the crack path for up to 5 mm of growth. Differences between uncoupled (Rice-Tracey) and coupled (Gurson-Tvergaard) models were found to be minimal. Further verification of these damage models was limited by difficulties in simulating the tearing process close to the interface, where the hydrostatic stresses are very high. The problems in accurately simulating the overall piping system response, in particular the over-estimation of the ram forces and hence the applied moment response, did not impact the moment-CMOD behaviour, which was well reproduced in the numerical analysis.
- The detection performance achieved in the ISI round robin trial was relative good, with 5 out of the 9 teams detecting all the defects larger than the detection target for the austenitic weld and 6 of the 8 teams for the Inconel weld. There no evidence that the detection performance for artificial defects types such as PISC type A defects was better than that for more realistic defect types. The sizing accuracy for through wall extent and length however showed a significant scatter for both welds.

- In view of the fact that many of the inspection teams used similar detection and sizing techniques yet obtained different results, it is recommended that the entire inspection system, including the equipment, inspection procedure and personnel, should verified by inspection qualification methodologies on appropriate test specimens and defects prior to an on-site inspection to demonstrate that it is capable of meeting the specified inspection objectives.
- The project has shown that careful application of available flaw assessment techniques in combination with the improved awareness of the likely tearing behaviour for circumferential cracks at the buttering interface can provide reliable predictions of crack initiation and stability loads for this type of dissimilar weld. Areas recommended for further investigations include:
  - assessment of the consequences of low tearing resistance in the buttering close to the fusion line for leak-before-break behaviour;
  - development and standardisation of robust experimental methods to accurately measure fracture toughness properties in heterogeneous regions of dissimilar metal welds, and verification of their suitability for assessment of component integrity;
  - clarification of the effect of long-term ageing on the fracture and tearing properties for buttering cracks;
  - application of local approach models to better understand the margins for ductile tearing instability under operation conditions involving both applied pressure and displacements;
  - further analysis of the inspection blind trial data to investigate the influence of factors such as the quality and training of the inspectors; the scanner and equipment; and the data processing equipment and software, on performance and on the influence of the different defect types.

ACKNOWLEDGEMENTS

This overview report is a synthesis of a collective effort of an international team of experts. Very sincere thanks are due to all those persons and organisations who contributed to the project, for the most part on a contribution-in-kind basis. The following list[20] hopefully leaves no one out:

P. Bredif	CEA, France
B. Brown	Mitsui Babcock Energy Ltd., UK
S. Chapuliot	CEA, France
M.F. Cipiere	Areva NP SAS (formerly Framatome ANP SAS), France
S. de Groot	NRG, The Netherlands
D. Deseruelles	Areva NP SAS (formerly Framatome ANP SAS), France
B. Dikstra	Mitsui Babcock Energy Ltd., UK
G. Dundulis	Lithuanian Energy Institute, Lithuania
B. Eriksen	European Commission, Joint Research Centre, Institute for Energy
A. Eriksson	European Commission, Joint Research Centre, Institute for Energy
C. Faidy	EDF SEPTE, France
P. Gilles	Areva NP SAS (formerly Framatome ANP SAS), France
J. Gerland	Basler & Hoffmann, Switzerland
J. Gunnars	Inspecta AB (formerly DNV Consulting), Sweden
F. Hagemann	European Commission, Joint Research Centre, Institute for Energy
F. Huckelmann	European Commission, Joint Research Centre, Institute for Energy
H. Hein	Areva NP GmbH Areva (formerly Framatome ANP GmbH), Germany
D. Heinrich	Cegelec, Germany
P. Hermansky	VUJE Trnava A.S., Slovakia
V. Horacek	Nuclear Research Inst. Rez Plc, Czech Republic
I. Iacono	European Commission, Joint Research Centre, Institute for Energy
D. Katsareas	University of Patras (formerly a grant-holder at EC-JRC/IE), Greece
J. Kayser	CEA, France
G. Lenkey	Bay Zoltan Foundation, Institute Logistics & Production Systems. Hungary
D. Lidbury	Serco Assurance, UK
M. Lorentzon	Inspecta AB (formerly DNV Consulting), Sweden
G. Martin	EDF, France
P. Minnebo	European Commission, Joint Research Centre, Institute for Energy
R. Miteva	Bulgarian Safety Authority, Bulgaria

[20] In several cases organisation names have changed or individuals have moved jobs during the project. The above list is intended to reflect both current status as well as that at the time of participation in NESC-III.

K.-F. Nilsson	European Commission, Joint Research Centre, Institute for Energy
J. Novak	Nuclear Research Institute Rez Plc, The Czech Republic
C. Ohms	European Commission, Joint Research Centre, Institute for Energy
J. Pitkänen	VTT, Finland
N. Safa	Areva NP SAS (formerly Framatome ANP SAS), France
T. Schimpfke	GRS, Germany
H.-J. Schindler	Mat-Tec AG, Switzerland
A. Sherry	University of Manchester, UK
S. Szavai	Bay Zoltan Foundation, Institute Logistics & Production Systems, Hungary
N. Taylor	European Commission, Joint Research Centre, Institute for Energy
T. Thunvik	Inspecta AB (formerly DNV Consulting), Sweden
J. Wintle	TWI Ltd. , UK
A.G. Youtsos	formerly EC-JRC/IE

REFERENCES

[1] D. Buckthorpe, C. Escaravage, P. Neri, P. Pierantozzi, D. Schmidt, Final Report of the CEC-WGCS/AG2 Study Contract on Bi-Metallic Weldments, AEAT Report C9731/TR002, Issue V02, April 1997.

[2] IAEA-TECDOC-1361, Assessment and management of ageing of major nuclear power plant components important to safety: Primary piping in PWRs, July 2003.

[3] F.W. Brust P.M. Scott and Y. Yang, Weld Residual Stresses and Crack Growth in Bimetallic Pipe Welds, Proc. SMIRT-16, 2003.

[4] C. Williams et al, The impact of fracture toughness and weld residual stress of Inconel 82/182 bimetal welds on leak-before-break behaviour, PVP2004-26459, Proc. ASME PVP 2004.

[5] J. Devaux, G. Mottet, J-M. Bergheau, S. Bhandari, C. Faidy, "Evaluation of the Integrity of PWR Bimetallic Welds". Jour. of Pressure Vessel Technology, Vol. 122, 2000, Trans. of ASME, 368-373.

[6] R. Miteva & N.G. Taylor, General Review of Dissimilar Metal Welds in Piping Systems of Pressurised Water Reactors, Including WWER Designs. NESCDOC (05) 007, 2005.

[7] PHARE Project for Nuclear Safety, NPP Kozloduy Units 1, 2, 3 and 4, Leak - Before - Break, Transfer of results, BG9311, Final report, 1996.

[8] TACIS Project R 1.2/91, Primary Circuit Integrity: Application of Leak before Break Concept for VVER 440/230 Novovoronesh 3 and 4, Kola 1, 2.

[9] TACIS Project R 2.16/93, Leak before Break (Extension of TACIS R 1.2/91).

[10] N. Taylor & D.P.G. Lidbury, "Improving Structural Integrity Assessment Techniques", 1st Symposium - Nuclear Pressure Equipment Expertise and Regulation, International Conference, Dijon, June 2005

[11] L. Debarberis, Role of international networks on structuring nuclear safety research and disseminating results, Proc. FISA 2003, EUR 21026, 2004.

[12] R. Bass, J. Wintle, R.C. Hurst, N. Taylor, NESC-I Project Overview, EUR 19051EN, 2001.

[13] L. Stumpfrock et al, NESC-II Final Report, EUR 20696EN, 2003.

[14] N. Taylor et al, NESC-IV Project: An investigation of the transferability of Master curve technology to shallow flaws in reactor pressure vessel applications, Final Report, September 2005, EUR 21846 EN.

[15] N. Taylor, K.F. Nilsson, M. Dahlberg, C. Faidy, A procedure for thermal fatigue damage assessment due to turbulent mixing in nuclear piping systems, Proc. Int. Conf. "Fatigue Design", Senlis, November 2005.

[16] D.R. Tice et al, Evaluation of techniques for assessing corrosion cracking in dissimilar metal welds, Final Project Report, AEAT-4717, December 1998.

[17] Structural integrity of bi-metallic components, BIMET Final Summary Report, BIMET(02)P001, June 2002.

[18] Chas G, Faidy C and Hurst R C: 'Structural integrity of bi-metallic components program (BIMET): fracture testing of bi-metallic welds', Paper 8585, Proc. ICONE 8, April 2000, Baltimore USA.

[19] K.-H. Schwalbe, A. Cornec, D.P.G. Lidbury, Fracture mechanics analysis of the BIMET welded pipe tests, Int. J. Pressure Vessels and Piping 81 (2004) p. 251-277.

[20] C. Faidy et al, ADIMEW "Assessment of aged piping DIssimilar MEtal Weld integrity", DG-RTD Contract FIKS-CT-2000-00047, Synthesis Report, Revision 1, June 2005.

[21] C. Faidy et al, *Assessment of aged piping dissimilar metal weld integrity* (ADIMEW), FISA-2003, EU Research Conf. in Reactor Safety, Luxembourg, 10-13 Nov. 2003.

[22] C. Faidy, et al., 'Assessment of Aged Piping Dissimilar Metal Weld Integrity: ADIMEW', Proceedings of FISA 2001 Conference, Luxembourg, EUR 20281, 2001.

[23] G. Martin, A. Ménard, 'Experimental four points bending test on a real size bimetallic welded pipe: European project ADIMEW', ASME Pressure Vessel and Piping Conference, PVP2004, San Diego, 2004.

[24] C. Faidy. "Structural integrity of dissimilar welds: ADIMEW project overview. ASME, Proc. Pressure Vessels and Piping Conf., 25-29 July 2004, La Jolla, USA, Paper PVP-2004-2542.

[25] RCC-M Class 1 (French Nuclear Piping Code), AFNOR.

[26] "Evaluation of the inspection results of PISC III safe-end assembly No 20", PISC III Report No 20, 1993, EUR 15558 EN.

[27] "Evaluation of the inspection results of PISC III safe-end assembly No 24", PISC III Report No 24, 1993, EUR 15369 EN.

[28] "Evaluation of the inspection results of PISC III safe-end assembly No 25", PISC III Report No 25, 1993, EUR 15370 EN. "PISC III Report No 25.

[29] S.R. Doctor. "Overview of V.C. Summer hot leg loop a nozzle to pipe dissimilar metal weld". Proc. SMiRT 2001, Washington, 2001.

[30] L. Skånberg. "PWSCC observations in Ringhals 3 and 4 safe ends". Proc. SMiRT 2001.

[31] B. Eriksen et al, Analysis of the Inspection Results Obtained in the NESC-III Blind Round Robin Trial on Dissimilar Metal Welds, EUR xxx EN, June 2006.

[32] Input information relevant to the NESC-III blind RRT on dissimilar metal welds, NESC Report NESC.TG1(03) 01.a, JRC, June 2004.

[33] Guidelines for reporting of the inspection data for the NESC-III blind RRT on dissimilar metal welds, NESC Report NESC.TG1(03)01.b, JRC, June 2004.

[34] R.A. Murgatroyd, B. Eriksen, R. Houghton, P. Lemaitre. "Final Report of NESC-I Inspection Task Group - Analysis of the inspection results from the pre- and post-test round robin trials". EUR 19653/I EN, 2000.

[35] I. Iacono, B. Eriksen, J. Mendes, L. Metten, F. Lofaj, T. Seldis, M. Wallendorf, "Destructive Examination Report NESC III RRT Dissimilar metal weld component, NESCDOC(05) 12, September 2006.

[36] L.R. Rawsthorn, R.A. Murgatroyd, T. Bann, The effects of austenitic stainless steel double-layer strip cladding on the propagation of ultrasound parallel to the cladding strips. AEAT Report ND-R-889, 1984.

[37] Y. Beurdeley, Effect on cladding on UT testing with 60º angle beams - PISC II Parametric Studies, PISC Report Number 9, 1985.

[38] Technical Justification for the ENIQ 2nd Pilot Study, ENIQ report 26, December 2005, EUR 22208 EN.

[39] R.A Murgatroyd & G.M. Worrall, Effect of human factors on the reliability of routine inspections. AEAT report AEA-RS-4509. PISC III Action 7.

[40] C. Faidy et al, ADIMEW Final Report "Assessment of aged piping Dissimilar Metal Weld integrity", EC DG-RTD Contract FIKS-CT-2000-00047, rev.1, 2005.

[41] C. Faidy, "ADIMEW: Pre-test data sheet (revision 3)", AGE-ADIMEW(02)-M006, EDF-SEPTEN, January 2003.

[42] P. Tipping, P. Bertschinger, H.J. Schindler, Characterisation of local material behaviour of a welded pipe by instrumented indentation test using Meyer's approach, 9th Int. Conf. Mechanical Behaviour of Materials, May 2003.

[43] A. Laukkanen, H. Keinänen, P. Nevasmaa, Mixed-Mode Small-Specimen Fracture Tests of the "AD01" Component, VTT Research report No. TUO72-033350, December 2003.

[44] S-J. Wu and J.F. Knott, Fracture Mechanisms in Mis-Matched Transition Welds, Proc. 2nd Int. Symp. On Mis-Matching of Interfaces and Welds, ISBN 3-00-001951-0, GKSS, 1997, pp. 587-598.

[45] BS 7448-4: 1997, 'Fracture mechanics toughness tests. Method for determination of fracture resistance curves and initiation values for stable crack extension in metallic materials'.

[46] ASTM standard E1820-01, Standard Test Method for Measurement of Fracture Toughness. Annual Book of ASTM Standards, Vol 03.01.

[47] 'Recommandation d'essais de mesure de la résistance à la déchirure ductile des matériaux métalliques (essais J-Δa)'. Commission Fragile Rupture de la Société Française de Métallurgie (GFR SF2M) - Juin 1990.

[48] K.H. Schwalbe, R.A. Ainsworth, C. Eripret, C. Franco, P. Gilles, M. Koçak, H. Pisarski and Y.Y. Wang, 'Common views on the effect of yield strength mismatch on testing and structural assessment'. *Proc. 2nd Int. Symp. On Mis-Matching of Interfaces and Welds*, GKSS, 1997, ISBN 3-00-001951-0.

[49] Y-Y. Wang et al, Recommended practice for fracture toughness testing of weldments with strength mismatch, *Proc. 2nd Int. Symp. on Mis-Matching of Interfaces and Welds*, ISBN 3-00-001951-0, GKSS, 1997, p. 281-293.

[50] Y-J. Kim et al, Numerical investigation on J-intergral testing of heterogeneous fracture toughness testing specimens: Part 1 - weld metal crack, Fatigue Fract Engng Mater Struc, 26, 2003, pp. 683-694.

[51] M.T. Kirk and R.H. Dodds: 'J and CTOD estimation for shallow cracks in single edge notched bend specimens', *Journal of Testing and Evaluation*, Vol 21, No 4, 1993.

[52] P. Gilles, M. Borrego Puche, G. Martin, Fracture Mechanics analysis of a 16" PWR dissimilar weld metal pipe junction, in "Mathematical Modelling of Weld Phenomena 7", Eds. H. Cerjak et al, 2004, ISBN 3-901351-99-X.

[53] P. Gilles, J. Devaux, M.-F. Cipière, ADIMEW Project: Ductile Tearing Prediction of a Cracked 16" Dissimilar Metal Weld Junction, *Proc. ASME/JSME Pressure Vessels and Piping Conf. 2004*, PVP-Vol. 479, ASME, 2004.

[54] J.R. Rice, 'A Path Independent Integral and the Approximate Analysis of Strain Concentration by Notches and Cracks', Journal of Applied Mechanics, 35, 1968, pp. 379-386.

[55] Ph. Destuynder and M. Djaoua, 'Sur une interprétation mathématique de l'intégrale de Rice an théorie de la rupture fragile', Math. Methods Appl. Sci. 3, pp. 70-87, 1981.

[56] Ph. Gilles, Ph. Mourgue, C. Lienard and C. Bois, 'Efficiency and accuracy of the G-θ method for elasto-plastic crack driving force computations'. Proc. ICES 1992.

[57] J. Wintle, B. Hayes, M. Goldthorpe, ADIMEW Project: Fracture toughness testing of AD01 dissimilar metal weld, TWI, Report 13219/2/03, November 2003.

[58] C. Ohms, D.E. Katsareas, R.C. Wimpory, P. Hornak & A.G. Youtsos, "Residual Stress Analysis in Thick Dissimilar Metal Weld based on Neutron Diffraction", Proc. ASME/JSME Pressure Vessels and Piping Conf. 2004, PVP-Vol. 479, ASME New York, p. 85, July 25 2004.

[59] G.A. Webster (ed.), "Polycrystalline Materials - Determination of Residual Stresses by Neutron Diffraction", ISO/TTA 3, ISO, Geneva, 2001.

[60] J. Wintle, ADIMEW: Residual stress measurements by hole drilling, TWI Report No: 13219/3/03, 2003.

[61] H.J. Schindler, NESC III Residual Stress measurement in Window-Piece AD01 by the Cut-Compliance Method: Preliminary Report, Technical Report No. TB03-401, 2003.

[62] A. Sherry and D. Beardsmore, Post-Test Assessment of the ADIMEW dissimilar weld test, Serco Report SA/EIG/12428/R002, December 2003.

[63] S. Bhandari, A.G. Youtsos & V. Robin, "DG XII PROJECT BIMET - Final Report TG3: Residual Stress Determination in an RPV Bi-metallic Weld", *Report EER/99.1532*, December 1999.

[64] D.E. Katsareas et al, NESC-III Project Task Group 6 Synthesis Report, NESCDOC TG6 (05) 01.F, September 2005.

[65] D.E. Katsareas, NESCIII Project TG6: 1st (Simplified) Computational Round Robin, *NESCDOC TG6 (02) 03*, IE-JRC, May 2002.

[66] A.G. Youtsos & D.E. Katsareas, NESCIII Project TG6: Auxiliary Computational Round Robin, *NESCDOC TG6 (01) 02*, IE-JRC, December 2001.

[67] D.E. Katsareas, NESC-III 2nd (Detailed) Computational Round Robin, NESCDOC TG6 (04) 01, Rev. 2, February 2004.

[68] D.E. Katsareas, M.F. Cipiere, NESC-III TG6 Temperature monitoring during welding of AD02, Report NESCDOC TG6 (03) 02, 2003.

[69] G. Vinas, T. Dauda & D.E. Katsareas, NESCIII TG6: Strain Evolution Monitoring during Welding of AD02, *NESCDOC TG6 (02) 04*, IE-JRC, November 26th 2002.

[70] H. Hein, Finite Element calculations with ABAQUS for the NESC-III/TG6 Computational Round Robin on residual stresses, *NGTM/2004/en/0209 Rev. A*, Framatome ANP GmbH (Germany), September 23rd 2004.

[71] J. Gunnars & M. Andersson, Residual Stresses in Heat-Treated Bi-metallic Pipe Weld NESC-III/ADIMEW, *RSE R&D Report No. 2004/07 Rev. 0*, DNV, March 4th 2004.

[72] N. Safa & P. Gilles, ADIMEW WP3 Deliverable D3.2: Residual Stress Analysis Report, *NFPMR-DC-93 Rev. A*, Framatome ANP SAS, November 27th 2003.

[73] P. Gilles, L. Nouet, ADIMEW Project Framatome-ANP Post-Test Analyses, Pass-by-Pass Welding Simulation of a 16" Dissimilar Metal Weld Junction, Annex 9, Minutes of the 7th NESC-III Meeting, October 2004, NESCDOC-04-10.

[74] P. Gilles, L. Nouet, Residual stress numerical simulation of two dissimilar metal weld junctions, Proc. ECF-16, Alexandroupolis, Greece, July 2006.

[75] D.E. Katsareas & A.G. Youtsos, NESCIII Project TG6: Finite Element Simulation and Residual Stress Prediction of a Dissimilar Metal Pipe Welded Joint, *NESCDOC TG6 (04) 03*, IE-JRC, November 2004.

[76] P. Gilles, Framatome ANP Post-Test Analyses: Part 1 Specimen Analyses, Part 2 Adimew Pipe Analyses, Presentations to the 6th NESC-III Meeting, NESCDOC (04)04, March 2004.

[77] P. Gilles, Ductile tearing analyses of a cracked 16" dissimilar weld junction, presentation tp 8th NESC-III Meeting, NESCDOC (05)009, Erlangen, September 2005.

[78] P. Gilles, M.F. Cipiere, Residual stress influence on dissimilar material weld junction fracture, Proc. ECF-16 Conference, Alexandroupolis, Greece, July 2006.

[79] P. Gilles, V. Robin, J. Devaux, Ductile Tearing Behavior Near a Bimetallic Interface, Proc. Euromech-Mecamat Conference (EMMC-9), Local Approach to Fracture, Moret-sur-Loing, France, May 2006.

[80] J. Wintle, B. Hayes and M. Goldthorpe, ADIMEW Project: Finite Element and Fracture Mechanics Analysis of the Dissimilar Metal Weld Test, TWI Rep[ort 13219/4/03, November 2003.

[81] J. Wintle, B. Hayes and M. Goldthorpe, ADIMEW: Fracture Assessment and Testing of An Aged Dissimilar Metal Weld Pipe Assembly, Proc. 30th MPA Seminar, Stuttgart, October 2000.

[82] Y. Kayser & S. Chapuliot, Post-Test analysis of the ADIMEW Program by Analytical Methodologies, CEA Rapport DM2S, Ref. SEMT/LISN/RT/03-041/A, November 2003.

[83] S. Chapuliot, Y. Kayser, Complement of the interpretation of the ADIMEW test on a cracked pipe containing a bimetallic weld, CEA Rapport DM2S, Ref. SEMT/LISN/RT/04-016/A, June 2004.

[84] S. Szavai & G. Lenkey, FE and Sensitivity Analysis of C(T) Specimens, ADIMEW Report D4.2.3, May 2003.

[85] S. Szavai, Report on Post-Test and Sensitivity Analyses, ADIMEW Report D4.2.4, October 2003.

[86] H.J. Schindler & G. Kerland, Fracture Behaviour of Dissimilar Welds: ADIMEW Pre- and Post-Test Analysis, Mat-Tec and Basler & Hofmann Report No. B3210.40-2 Rev.0 for HSK, October 2005.

[87] G. Kerland, H.J. Schindler, A semi-analytical CTOD approach, Minutes of the 6th NESC-III Meeting, NESCDOC (04)04, March 2004.

[88] H.J. Schindler & G. Kerland, Capabilities of Engineering Models and Failure Assessment Procedures, Minutes of the 7th NESC-III Project Meeting, NESCDOC (04) 10, October 2005.

[89] H.J. Schindler & G. Kerland, On crack extension and tearing stability, Minutes of the 8th NESC-III Project Meeting, September 2005, NESCDOC (05) 09.

[90] J. Novak: Preliminary Post-Test Analysis of Experiment ADIMEW, Minutes of the 6th NESC-III Meeting, NESCDOC(04)04, March 2004.

[91] J. Novak: Two Types of Parameters Characterizing Constraint for Constraint Correction of J-R Curves and their Mutual Relation, Minutes of the 7th NESC-III Meeting, NESCDOC(04)10, October 2004.

[92] T. Schimpfke, P. Bachman and J. Sievers, 3D Finite Element Post-Test Calculation of the Adimew Test, Presentation to the 6th NESC-III Meeting, NESCDOC (04)04, March 2004.

[93] P. Hermansky, Post-test Calculation of the ADIMEW Bending Test, Minutes of the 7th NESC-III Meeting, NESCDOC(04)10, October 2004.

[94] T. Thunvik et al, Defect Tolerance Analysis of Dissimilar Metal Weld - Fracture Mechanics post-test analysis of the NESC-III/ADIMEW Test, DNV RSE R&D Report No. 2004/08.

[95] S. de Groot, NRG Contribution to Pre- and Post-test Analysis of the ADIMEW Test, NRG Report 21399/05.66997/C, May 2005.

[96] G. Dundulis: Performing the assessment of the crack initiation and limit loads for ADIMEW test.

[97] "R6 Revision 4, Assessment of the Integrity of Structures Containing Defects", British Energy, April 2001.

[98] SINTAP: Structural Integrity Assessment Procedures for European Industry, Brite-Euram Project BE95-1426, Contract BRPR-CT95-0024, Final Report September 1999.

[99] J K Sharples, C C France and R A Ainsworth, "Experimental validation of R6 treatment of residual stresses", American Society for Mechanical Engineers, Pressure Vessels and Piping Conference, ASME PVP-Vol. 392, pp. 225-238, 1999.

[100] S. Chapuliot, S. Marie and D. Moulin, 2001, An Energetic Approach for large Ductile Crack Growth in Components, Fatigue and Fracture Mechanics: 32nd Volume.

[101] J.R. Rice and D.M. Tracey, 1969, 'On the ductile enlargement of voids in triaxial stress fields', J. Mech. Phys. Solids, 17, p. 201.

[102] SYSTUS User's Manuals, ESI-group. User's manual, Version 2003, 99 rue des Solets SILIC 112 94513 Rungis Cedex, France, 2003.

[103] A.L. Gurson, 1977, Continuum Theory of ductile rupture by void nucleation and growth Part I: Yield criteria and flow rules for porous ductile materials, *J. Eng. Mat. Tech*., **99**, 2-15.

[104] V. Tvergaard, 1981, Influence of voids on shear band instabilities under plane strain conditions. *Int. J. Fracture*, **17**, 389-407.

[105] V. Tvergaard and A. Neddleman, Analysis of cup-cone fracture in a round tensile bar, Acta Metallurgica, 32, 157-169, 1984.

[106] M.L. Wilkins, 'Computer Simulation of Dynamic Phenomena', Springer Publication, 1999.

European Commission

EUR 22510 EN - DG JRC - Institute for Energy
Assessment of Dissimilar Weld Integrity: Final Report of the NESC-III Project

Editors:
N. Taylor, European Commission Joint Research Centre, Institute for Energy, The Netherlands
C. Faidy, EDF SEPTEN, Lyon, France
P. Gilles, AREVA NP SAS, Paris, France

Luxembourg: Office for Official Publications of the European Communities
2006 – 128 pp. – 17 x 24 cm
EUR - Scientific and Technical Research series; ISSN 1018-5593

Abstract:

Dissimilar metal welds are a common feature of light water reactors in connections between ferritic components and austenitic piping systems. Inspection difficulties, variability of material properties and residual stresses all combine to create problems for structural integrity assessment. The NESC-III project was organised by the Network for Evaluating Structural Components (NESC) as a complementary activity to the European Commission sponsored ADIMEW project, with the following objectives:

- Quantify the accuracy of structural integrity assessment procedures for defect-containing, dissimilar metal welds in aged PWR Class 1 piping.
- Utilise results of the ADIMEW large-scale test to determine the actual behaviour of a defect in a DMW of industrial scale.
- Address critical issues including: inspection performance, laboratory-scale fracture testing on welds and potential benefits of advanced fracture modelling.
- Use the results to promote best practice and the harmonisation of international standards.

This final project report summarises the main results and conclusions.

EUROPEAN COMMISSION
DIRECTORATE-GENERAL
Joint Research Centre

The mission of the Joint Research Centre is to provide customer-driven scientific and technical support for the conception, development, implementation and monitoring of EU policies. As a service of the European Commission, the JRC functions as a reference centre of science and technology for the Union. Close to the policy-making process, it serves the common interest of the Member States, while being independent of special interests, whether private or national.

Publications Office
Publications.eu.int